String Theory and Relativistic Heavy Ion Collisions

Joshua J. Friess

A Dissertation

Presented to the Faculty

of Princeton University

in Candidacy for the Degree

of Doctor of Philosophy

Recommended for Acceptance

by the Department of

Physics

January, 2007

Abstract

It has long been known that string theory describes not only quantum gravity, but also gauge theories with a high degree of supersymmetry. Said gauge theories also have a large number of colors in a regime with a large effective coupling constant that does not depend on energy scale. Supersymmetry is broken in nature, if it is present at all, however the gauge theory described by string theory shares many common features with QCD at temperatures above the quark deconfinement transition. It is generally though not entirely accepted that collisions of gold nuclei at the Relativistic Heavy Ion Collider (RHIC) produce a thermalized Quark-Gluon Plasma (QGP) at temperatures distinctly above the transition temperature as determined from lattice simulations. Hence, we might hope that a string theoretic description of gauge dynamics can elucidate some otherwise intractable physics of the strongly coupled plasma.

Here we use string theory to calculate the outgoing energy flux from a RHIC process called "jet quenching", in which a high-momentum quark or gluon traverses a large distance in the QGP. Our setup is in the context of the highly supersymmetric string dual gauge theory, but we nevertheless find that the gross features of the resulting stress-energy tensor match reasonably well with experimental data. We will furthermore discuss the technology behind computations of the leading-order corrections to gauge theory observables that are uniquely string-induced, and we will describe a potential solution to string theory that could resolve a number of discrepancies between the traditional highly supersymmetric setup and QCD—in particular, a significant reduction in the amount of supersymmetry, and a finite effective coupling that is still greater than unity but does depend on energy scale.

Acknowledgements

I am extraordinarily grateful to any number of people who have helped me in numerous ways on my journey to complete this work.

It goes without saying that I am seriously indebted to my advisor, Steve Gubser, from whom I learned a tremendous amount. He has been a truly great advisor during my five years here, and I am constantly impressed by his devotion to his research and his students. I have been extremely fortunate and honored to be able to work with him for several years.

Herman Verlinde has been another mentor to me—I will always greatly appreciate the conversations we have had about physics, careers, and life, and I will always wish that we could have found the time to collaborate more.

My great experiences working with Lyman Page in my first few months at Princeton gave me a fantastic appreciation for the joys of experimental physics. I truly feel honored to have had the opportunity to work with such an amazing experimentalist.

I also have to thank Paul Steinhardt for his very early guidance, and his later collaboration.

Many other Princeton faculty have been great teachers and friends over the years—Curt Callan, Joe Fowler, Ed Groth, Igor Klebanov, Chiara Nappi, Sasha Polyakov, and Liantao Wang in particular.

I am very grateful to all my fellow student collaborators over the years: Indrajit Mitra for his teaching and advice before, during, and after our time as collaborators. Georgios Michalogiorgakis, a great friend, with whom I consulted with on literally every project I worked on at Princeton. Silviu Pufu, who never let his undergraduate status get in the way

of making incredibly significant contributions to advanced research projects. And Daniel Baumann, with whom I had two near-collaborations.

I have also learned a lot from many current and former Princeton postdocs: Oliver DeWolfe, Liam McAllister, and John McGreevy. There have also been a number of other graduate students who have been integral to my time here, as friends and colleagues: Asad Aboobaker, Chris Beasley, Matt Buican, Tolya Dymarsky, Diego Hofman, Lewis Hyatt, Justin Kinney, Ken and Meredith Kroenlein, Judy Lau, Mike Leung, Dima Malyshev, Mike Niemack, Glen Nixon, Brian Patton, Meredith Safran, Gasper Tkacik, Scott Washington and Ben Zwiebel. Also, a number of friends from the TASI 2005 summer school: Ben "Tex" Dundee, Mohammed Edalati, Nadir Jeevanjee, Peter Shepard, and Amanda Weltman.

There have also been a number of people affiliated with my undergraduate days at the University of Wisconsin. Peter Timbie and Tao Han devoted a considerable amount of time to teaching me experimental and theoretical physics, respectively. Though we did not overlap in our time there, I have since had a number of interesting physics conversations with Gary Shiu. Dan Hooper, my first physics T.A. and now one of my best friends, had an incredible passion for particle physics that largely inspired me to enter the field. Chris O'Dell, whose breadth of science knowledge demonstrated for me on a daily basis what it takes to be a great scientist. Dan Swetz and Zak Staniszewski were two of my great friends as an undergraduate, and I am continually grateful for their friendship to this day. Dafna Abelson, Kristen Looney, Dani Goldenholz, Shira Yuchtman, Steve Lederman, and Paul Litvak have provided me much wisdom.

A number of people from high school and before have continued to be great friends and mentors: Eric Lavender and Brian Smith have been tremendous friends for nearly as long as I can remember. Jan Lennon, my high school debate coach, and Tammy Dentice and Robert Lipsky, former teachers, were all great positive influences on me.

Finally, my family has been of the utmost importance to me. My father Jim, mother Pam, and brother Jon, who always offer great advice, and often remind me of the important things in life. It goes without saying that the huge amounts of time they spent teaching

and raising me are more responsible for my achievements than anyone else, myself included.

And Jessica Burrows, who makes my life great, and whose love and support made the hard work of this thesis that much easier. She shares greatly in the success of this work. I am always grateful for the advice and support of her family: Dan, Carol, Scott, and Mandy Burrows.

Contents

List of Figures

List of Tables

Chapter 1

Introduction

In its attempt to incorporate quantum field theory and Einstein's theory of gravity into a single framework, the essence of "string theory" boils down to one rather simple additional assumption: The fundamental degrees of freedom in nature are not point-like particles, but rather are line segments or loops moving through space. It is from this one claim—combined with the idea that strings should dynamically "prefer" to minimize their area as they propagate—that a host of more substantial claims follow, such as:

- Nature must be supersymmetric, i.e., every fermionic particle must have an otherwise identical bosonic partner
- Spacetime, if flat, must have ten dimensions
- Hypersurfaces called "D-branes" exist as locations on which open strings (e.g., line segments) can end, and that furthermore these D-branes are dynamical entities in their own right
- D-branes naturally serve as a residence for gauge theories, in which open strings connecting two D-branes act as the "gluons" of the gauge theory

But perhaps the most famous and important claim of string theory is that it is a *finite* theory of quantum gravity, providing a unified framework for quantum mechanics and Einstein's theory of gravity, general relativity. This again follows from the simple postulate of

string-like fundamental objects, and fails to be true for gravity in a field theoretic framework. The quanta of gravity are called "gravitons", and they propagate at the speed of light.

To see why field theory fails to be a finite theory of quantum gravity, suppose we wanted to naively introduce gravity using field theory techniques, and compute a simple scattering amplitude, such as two initial-state gravitons scattering into two final-state gravitons. The rules of quantum mechanics tell us that the total amplitude for such a process comes from summing the amplitudes for all such graphs with any intermediate state. Clearly one such graph contains a single graviton being exchanged between the initial and final state gravitons.

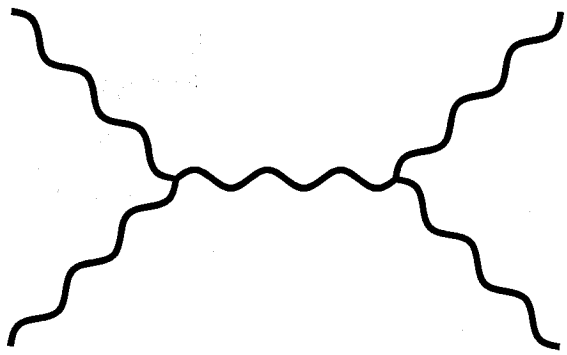

Figure 1.1: Two gravitons interact by exchanging a single graviton between them.

However, in addition to this graph, there must also be graphs where the initial and final states are separated by loops of gravitons, where the loops come in all shapes and sizes. In graphs where the loops are smaller, the graviton in the loop covers a short distance due to its high momentum. Ordinarily, high momentum particles are "more difficult" to produce, hence the amplitudes of these graphs are power-law suppressed. However, gravity is stronger in the presence of larger masses, and Einstein tells us that mass is interchangeable with energy, which by a Lorentz transformation is interchangeable with momentum. Consequently this exchange of high-momentum gravitons is significantly enhanced due to the gravitational coupling, and the amplitude for the process approaches infinity as the size of the loop approaches zero.

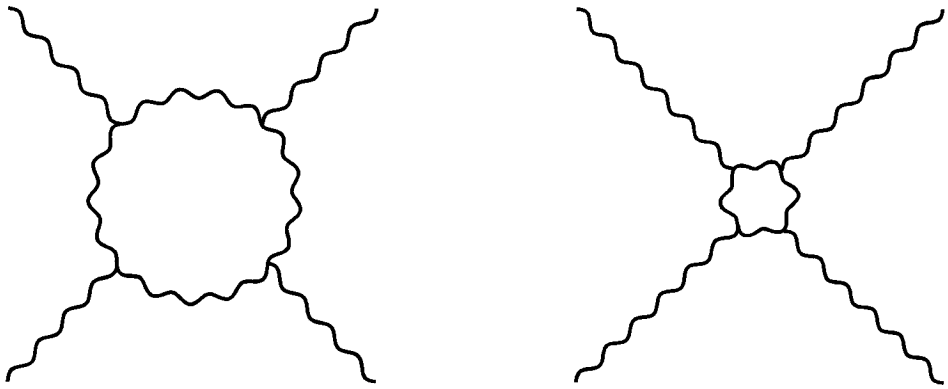

Figure 1.2: Two graphs involving two to two graviton scattering, separated by a loop of gravitons. The loop of gravitons on the right has higher momentum than the loop of gravitons on the right.

This same phenomenon does not happen in string theory. Heuristically, the width of the string provides a natural short-distance cut-off, beyond which graviton loops can not shrink. To see how this works, imagine the analogous graphs with strings instead of point particles. Each line essentially "fattens" out to make a string. Note that here the graviton loop can not shrink to smaller than a string width without overlapping with the other side of the graph. Hence the very high momentum graphs that render the field theory amplitude infinite simply do not exist in string theory a priori.

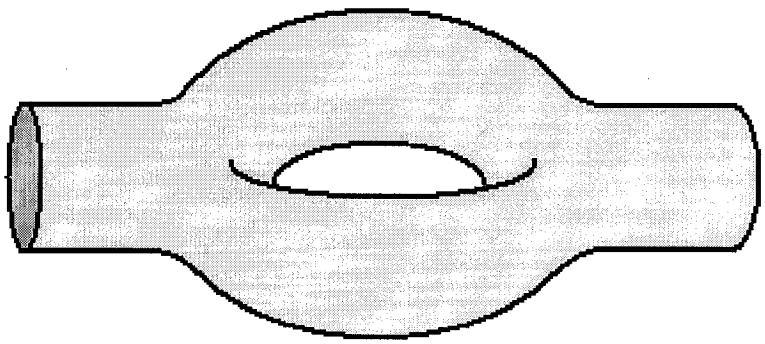

Figure 1.3: A graviton enters on the left, splits into two gravitons, which recombine into a graviton that exits on the right. The finite width of the string prevents the loop from ever having zero size.

Though the finiteness of string theory has been a great success, if string theory is to be a theory of quantum gravity, then the relevant length scale at which strings resolve themselves

as such must be roughly the Planck scale, which is about fifteen orders of magnitude smaller than the minimum length scale achieved in today's particle accelerators. Absent certain extreme and arguably unlikely assumptions about the way ten-dimensional strings appear to four-dimensional observers [1], a terrestrial experiment of stringy quantum gravity effects is highly unlikely. There is some hope that the signatures of stringy physics might be seen in observations of the very early universe, where the Planck scale energy densities were commonplace [2]. However, even the most optimistic advocates of this approach would probably agree that such an outcome is unlikely, and some authors disbelieve in this possibility entirely [3].

The difficulties in experimentally testing string theory have lent it to considerable criticism, in spite of its mathematical success. However, there is a common thread for this difficulty: The extreme separation between our everyday energy scales and the scale of quantum gravity. But string theory is no longer just a theory of quantum gravity.

In the late 1990's, it was observed that string theory and its natural embeddings of gauge theories via D-branes provides a simple means of computing physical quantities for gauge theories when the effective coupling constant is *large* [4, 5, 6, 7]. In traditional field theory techniques for computing scattering amplitudes, one typically relies on the presence of a small coupling constant that allows one to neglect graphs that contain a large number of vertices, or equivalently, a large number of loops. However, if the coupling is bigger than one, graphs with many loops dominate the total amplitude for a given process, yet they are also practically impossible to calculate. This is precisely where string theory is uniquely useful as a computational tool—the large coupling from a field theory perspective becomes a small coupling from a string theory perspective. This scenario has the potential to test string theory, since it is known that QCD, the theory of strong interactions between quarks and gluons, has a large effective coupling constant at low (and hence more easily accessible) energy scales.

This thesis discusses one such experiment that has the potential to test string theory: the Relativistic Heavy Ion Collider, or RHIC. RHIC accelerates gold nuclei around a large ring,

and collides them. After the collision, it is generally believed that the gold nuclei produce a short-lived "Quark-Gluon Plasma" (QGP), a new state of matter in which quarks and gluons are free from their hadronic containers, yet the coupling between them remains larger than one. Conventional Feynman diagram techniques are therefore unreliable, and string theoretic techniques are arguably our best tool for analyzing the physics. Indeed, first attempts at matching string theory calculations to experimental observables have been moderately successful.

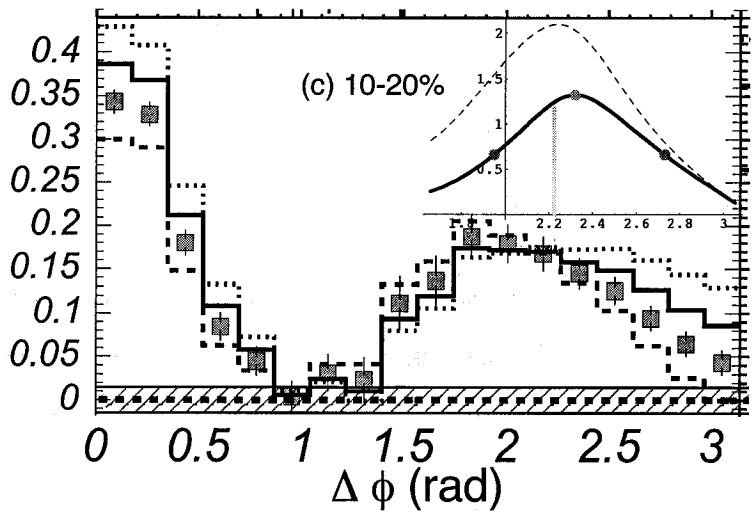

Figure 1.4: Data from the RHIC experiment, overlayed by the string theory's expected value for the same data in the upper right corner. The solid line in the upper right is numerical data to be described, whereas the dashed line is an analytic approximation that is most valid at lower energies. The vertical scale is offset in the two plots, but the horizontal scale is identical. The essential thing to note is the broad peaks in each plot.

However, the story is not ideal. First, the string theory construction is strictly valid when the effective coupling is not only large, but formally infinite. Of course, this is not the case in nature. Second, it is known that QCD is not a supersymmetric theory—it consists only of massive fermionic quarks in the fundamental representation of the gauge group (*i.e.*, carrying a single color charge) and massless bosonic gluons in the adjoint representation (*i.e.*, carrying a color charge and anti-charge, essentially). The setup in string theory does not describe QCD, but rather a theory consisting only of gluons and a large number of

supersymmetric partner particles. Third, it is known that QCD exhibits the phenomenons of confinement and asymptotic freedom, i.e., at nuclear length scales, the effective coupling is large, keeping quarks stuck to each other, whereas at much shorter length scales, the effective coupling is very small. In string theory, however, the coupling constant does not depend on the length scale, but rather is a parameter you can choose.

That said, these remarks only apply to one string theory background, in which spacetime takes on a particularly simple form. This spacetime is a solution to the "supergravity" equations of motion resulting from string theory. Strictly speaking, supergravity is the minimal supersymmetric extension to Einstein's general relativity—minimal in the sense that it contains fermionic spin-3/2 gravitinos as the supersymmetric partner particles of the gravitons, however the gravitational part of the action is simply a higher dimensional analog of Einstein gravity. In the context of this work, the fermionic components of the supergravity action will not be directly relevant, and one can understand "supergravity" as interchangable with "general relativity in higher dimensions".

We might hope to use alternative backgrounds whose field theory description is much closer to reality. Such spacetime configurations require an understanding of the gravitational dynamics of string theory beyond the leading correction to supergravity. We will develop that understanding here, and apply it to a specific background in which the effective coupling constant of the field theory is finite and depends on the energy scale. One might then think to ask RHIC-like questions with respect to this new background.

This thesis is structured as follows. In Chapter 2, we review the basic physics of interest—an explanation of the RHIC experiment, and the correspondence between string theory and strong interactions. In Chapter 3, we present the state-of-the-art in applying string theory to an analysis of RHIC physics. In Chapter 4, we discuss the technology behind higher-order corrections to Einstein gravity in string theory that could be used to determine uniquely-stringy effects at RHIC. We conclude in Chapter 5.

Chapter 2

Background

2.1 The Relativistic Heavy Ion Collider

The recent review by Müller and Nagle [8] provides an up to date account of experimental results from RHIC and their interpretation. We present here an abbreviated account aimed at introducing three aspects of the quark-gluon plasma:

- There is good reason to believe that the QGP thermalizes at a temperature significantly above the deconfinement transition of QCD.
- In non-central gold-gold collisions, the QGP undergoes a particular kind of collective motion called elliptic flow, in addition to its longitudinal expansion. Measurements of these collisions indicates that the shear viscosity of the QGP is small.
- Hard partons lose energy quickly when they pass through the QGP, a phenomenon known as jet-quenching.

An authoritative account of results through 2005 can be found in [9, 10, 11, 12].

2.1.1 The experimental setup

The primary physical process investigated at RHIC is the collision of beams of gold nuclei in moving opposite directions. The main beam ring is roughly 3.8 km in circumference, and

has four separate experiments (BRAHMS, PHENIX, PHOBOS, and STAR) with complementary capabilities situated at four of the six beam intersection points. The beam energy is 100 GeV per nucleon. In addition to gold, RHIC can handle other species, e.g. copper. The essential number is $\sqrt{s_{NN}} = 200\,\text{GeV}$, which refers to the total center of mass energy per nucleon pair.

Gold nuclei have 79 protons and 118 neutrons, and are fairly spherical with a radius R of about 7 fm. With respect to the center of mass frame, each nucleus moves with a Lorentz contraction factor γ of about 100, and consequently the front-to-back length of $2R/\gamma \approx 0.14\,\text{fm}$. The inelastic cross-section can be estimated *roughly* as $\sigma_{\text{tot}} = 4\pi R^2$. This is just the geometric overlap of the nuclei.

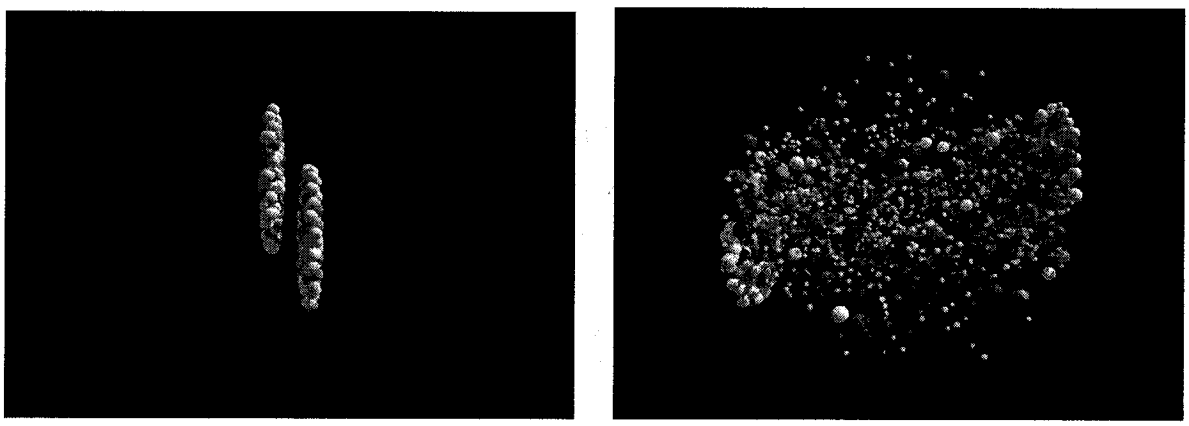

Figure 2.1: Ultra-relativistic quantum molecular dynamics simulation of a gold-gold collision [13], with view before (left) and after (right). Species are probably: protons (red), neutrons (white), meson (green), and excited baryons (blue).

RHIC's design luminosity is $2 \times 10^{26}\,\text{cm}^{-2}\text{s}^{-1}$. To date, they have achieved a total integrated luminosity in the ballpark of $4\,\text{nb}^{-1}$. An idealized version of RHIC detectors is the ability to assign p_T, ϕ, η (pseudorapidity), and particle identity (e.g. π, K, p, $\bar{p}$, Λ, Σ, Ξ, Ω, ϕ, J/ψ, D, etc.) to all hadrons coming out of the collision region, as well as to electrons, photons, and in restricted circumstances (i.e. high rapidity) muons. In reality, acceptance in η and ϕ varies: e.g. STAR accepts $|\eta| < 1$, while PHENIX accepts $|\eta| < 0.35$ with incomplete ϕ coverage. Most particles come out with $p_T < 1\,\text{GeV}$, but the high-momentum tails reach up to $p_T \sim 10\,\text{GeV}$.

2.1.2 The quark-gluon plasma

When gold nuclei collide, about 400 nucleons go in, and about 7500 come out. Clearly a lot of entropy gets produced. A more interesting and non-trivial claim is that a thermalized quark-gluon plasma (QGP) is formed with a temperature as high as 300 MeV. After formation, the QGP cools approximately isentropically and then hadronizes.

Part of the evidence for a thermalized QGP is that hadron yields at mid-rapidity can be fit to a thermal model: even multi-strange hadrons fit. See figure 2.2. The temper-

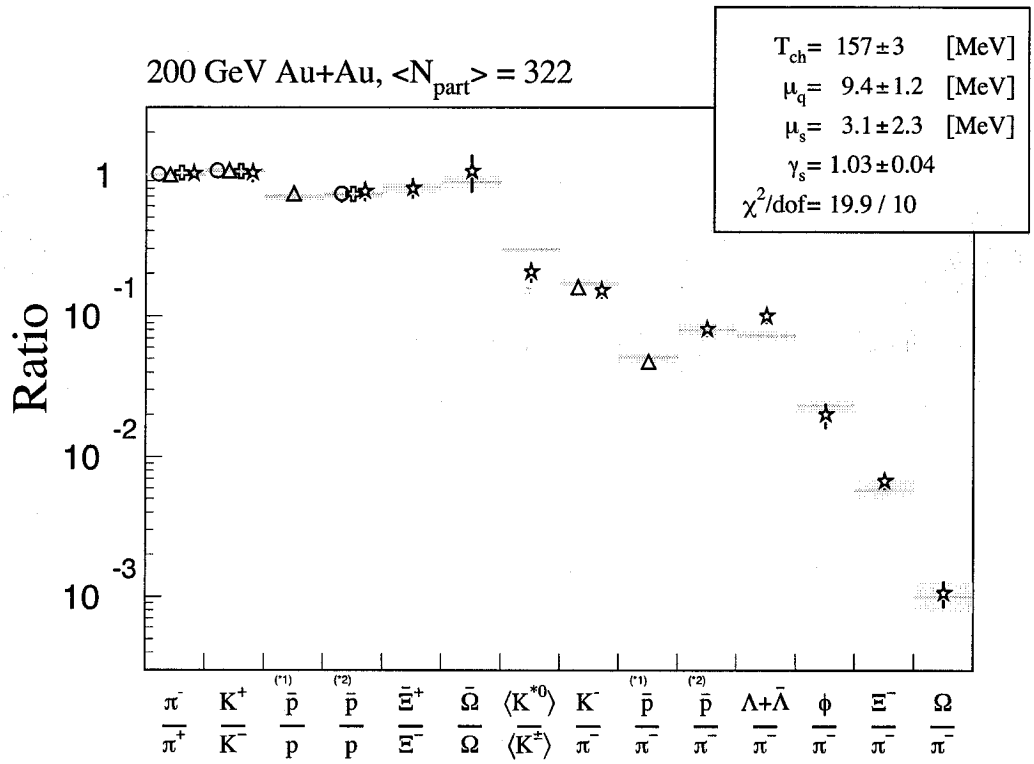

Figure 2.2: Ratios of hadron yields observed near mid-rapidity. The lines are the predictions of the thermal model. Note that the chemical potentials for light quarks and strange quarks are *small* compared to the temperature. From [14].

ature $T_{\rm ch} \approx 157\,{\rm MeV}$, which is determined by fitting hadron yields to thermal occupation numbers (i.e. Bose-Einstein or Fermi-Dirac statistics) is slightly lower than the estimated temperature for the confinement transition, $T_c \approx 170 - 190\,{\rm MeV}$, as determined through lattice calculations: see for example [15, 16]. In fact, deconfinement and chiral symmetry

restoration are believed to occur not through a true phase transition but through a rapid cross-over, above which the energy density is given approximately by

$$\epsilon \approx 6.3\,\mathrm{GeV/fm^3}\left(\frac{T}{250\,\mathrm{MeV}}\right)^4 . \tag{2.1}$$

See figure 2.3. The validity of (2.1) seems to extend to several times T_c. It is notable that

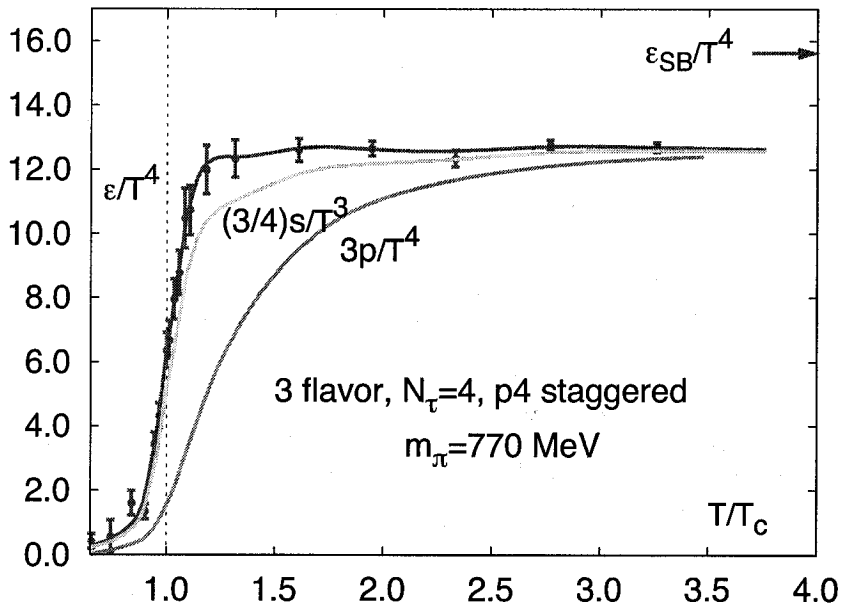

Figure 2.3: Lattice results for the equation of state of QCD. From [15].

the value of ϵ/T^4 in (2.1) is about 80% of the free-field value.

Rapidity distributions of protons in central collisions indicate that 28 ± 3 TeV of the total 39 TeV of energy winds up in heating the newly created medium (putatively the QGP) and in its collective motion [17]. If 28 TeV were entirely concentrated in the Lorentz-contacted sphere of the gold nuclei at full overlap, the result would be an energy density of roughly $2000\,\mathrm{GeV/fm^3}$. This is almost certainly a substantial overestimate of the peak energy density: simple phenomenological models (with some support from experiment) indicate that energy densities in gold-gold collisions may reach $30\,\mathrm{GeV/fm^3}$ and thermalize by the time $\epsilon \sim$ 5-9 $\mathrm{GeV/fm^3}$ [9]—well above the QGP threshhold of $1\,\mathrm{GeV/fm^3}$. See figure 2.4.

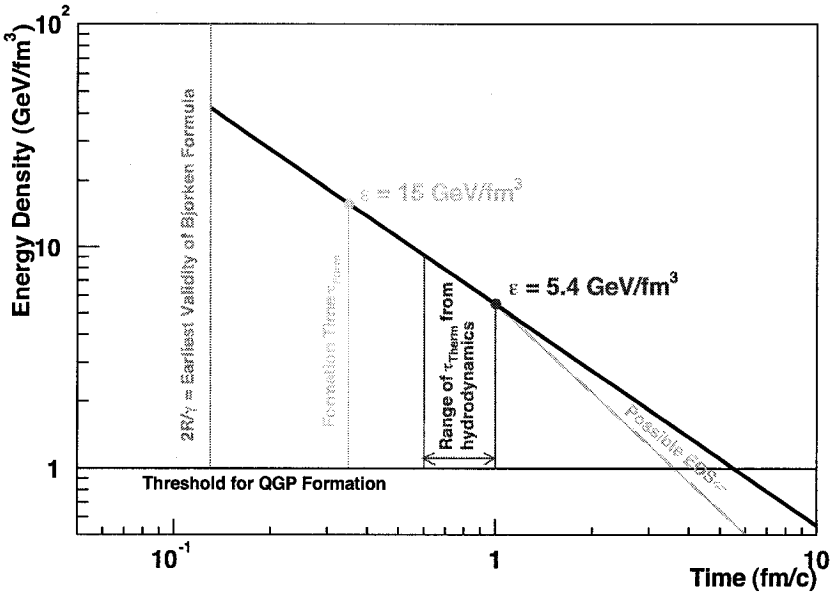

Figure 2.4: Energy density as a function of time in a central gold-gold collision, according to an elaboration of the phenomenological Bjorken model. From [9].

2.1.3 Centrality, elliptic flow, and jet-quenching

An important way to classify collisions of nuclei is the impact parameter of the collision. As described above, a crude approximation for collision rates comes from geometric overlap. *Centrality* refers to the extent of the overlap. A central collision is one where the gold nuclei hit head-on, whereas a peripheral collision is one where they almost missed.

Experiments at RHIC are capable of making an event-by-event determination of centrality, as well as the reaction plane defined by the beam line and the impact parameter. In other words, they can measure the impact parameter $\vec{b}$ as a vector: See figure 2.5. In order to avoid referring to a specific model of the cross-section, centrality is described in percentile terms. The 10% of all events that have the smallest values of b are described as having centrality of 0 to 10%. Note that this is somewhat reversed from what you might expect—head-on collisions have zero centrality. In the sphere-overlap model of the inelastic cross-section, the impact parameter corresponding to 10% centrality is evaluated as [18]:

$$0.1\ \sigma_{\rm tot} = \int_0^{b_{10}} dr\ 2\pi r \qquad \text{so} \qquad b_{10} = 2R\sqrt{0.1}\,. \tag{2.2}$$

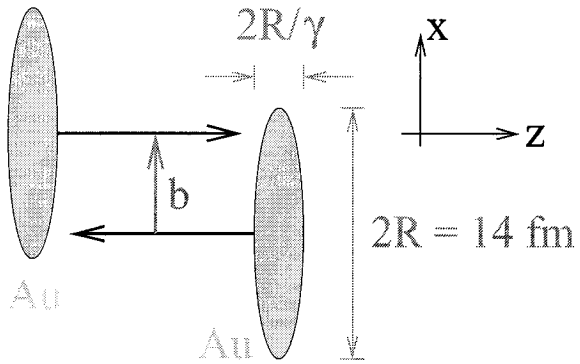

Figure 2.5: A gold-gold collision of intermediate centrality. The reaction plane is the plane of the page, in which the centers of mass of both gold nuclei are assumed to lie.

In non-central collisions, an important process called *elliptic flow* occurs. The overlap region is roughly ellipsoidal with all axes unequal (biggest in y, smallest in z). The distribution of observed particles is parametrized as

$$\frac{dN}{p_T dp_T dy d\phi}(p_T, y, \phi; b) = \frac{dN}{p_T dp_T dy}\left[1 + 2v_2(p_T, y; b)\cos 2\phi + \ldots\right], \tag{2.3}$$

Here, v_2 is experimentally measured for different particle species, and $\phi = 0$ refers to emission in the reaction plane, so $v_2 > 0$ means this is preferred. The sizable observed

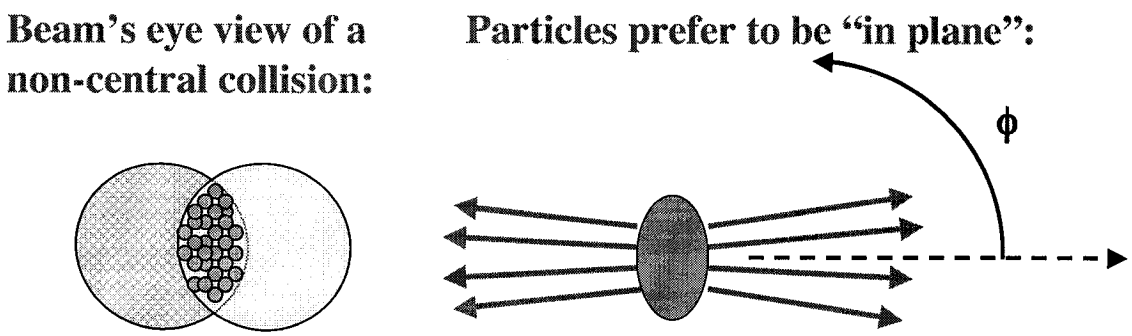

Figure 2.6: Cartoon of elliptic flow. From [19].

values of v_2 are in line with non-viscous hydrodynamic models of collective flow:

$$\frac{D}{Dt}(\epsilon\vec{v}) = -\nabla P \tag{2.4}$$

with ∇P bigger at $\phi = 0$ than $\phi = \pi/2$ because the ellipsoid is shorter at $\phi = 0$ and longest at $\phi = \pi/2$.

Jet-quenching refers to the rapid loss of energy of a hard parton propagating through the hot dense matter created in a gold-gold collision. The prima facie evidence for jet quenching is the the suppression of high p_T jets (more precisely, high p_T hadrons) relative to expectations from "binary collision scaling." In binary scaling arguments, one replaces each gold atom by an equivalent flux of nucleons, each carrying 100 GeV of energy, which do not interact with one another, but which collide with nucleons going the other way. The number of collisions that would occur in this way is denoted $\langle N_{\text{binary}} \rangle$. Thus a single gold-gold collision is replaced by $\langle N_{\text{binary}} \rangle$ independent nucleon-nucleon collisions. To obtain an expected yield for a given particle species in a gold-gold collision, one scales up the yield measured in proton-proton collisions by the factor $\langle N_{\text{binary}} \rangle$. The ratio of this theoretical quantity to the observed outgoing particles is called R_{AA}:

$$R_{AA} \equiv \frac{dN(\text{gold-gold})/dp_T d\eta}{\langle N_{\text{binary}} \rangle dN(\text{proton-proton})/dp_T d\eta} \,. \tag{2.5}$$

Binary scaling is a successful predictor of the flux of outgoing photons with $p_T > 4\,\text{GeV}$: $R_{\gamma\gamma} \simeq 1$ for most p_T. This indicates that the QGP is fairly transparent to photons. For hadrons, however, the detected flux is considerably less than what is expected: $R_{hh} \approx 0.2$. The interpretation is that when an energetic scattering event occurs, the hard outgoing partons tend to lose a large fraction of their energy while plowing through the QGP. Curiously, this suppression only occurs in gold-gold collisions – collisions of proton-gold or deuterium-gold do not exhibit jet quenching. Hence there is something special occurring in the thermalized plasma.

2.1.4 Summary of experiment

The essential aspects of the experiment that we have discussed are as follows:

- In central gold-gold collisions with 200 GeV per nucleon center-of-mass energy, a thermalized QGP forms as early as $t \sim 0.6\,\text{fm}/c$ with T as high as 300 MeV. It expands and cools isentropically with $\epsilon \propto 1/t$ (or maybe $1/t^{4/3}$) and hadronizes at about $t \sim 6\,\text{fm}/c$.

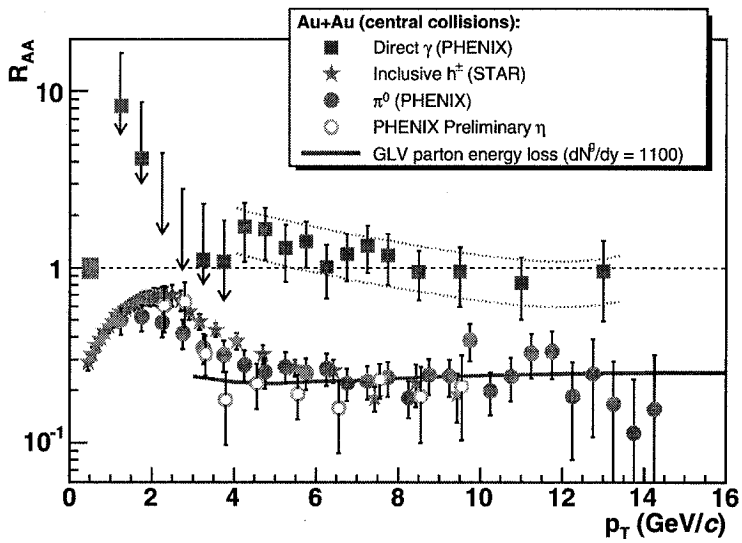

Figure 2.7: Nuclear modification factor R_{AA} for photons and hadrons in 0 to 10% central gold-gold collisions. From [8].

- Sizable anisotropy v_2 indicates elliptic flow of the QGP: a collective hydrodynamic motion which can be successfully modeled via inviscid hydro. Significant viscosity spoils the agreement: $\eta/s \ll \hbar$ seems to be a consensus from RHIC.

- Measurements of R_{AA} show that the QGP is approximately transparent to high-energy photons, but remarkably opaque to hadrons.

Lattice simulations are quite good at predicting the equation of state, the transition temperature, etc., but transport properties, e.g. v_2 and R_{AA}, are hard. Furthermore, the low viscosity indicates that the plasma is strongly coupled, spoiling the applicability of standard Feynman diagram techniques. But perhaps string theory can come to the rescue.

2.2 String Theory and Gauge Theories at Strong Coupling

As was alluded to in the introduction, calculations of physical observables in gauge theories at strong coupling are particularly simple in a string theoretic framework. In this section we detail precisely how this connection is made.

2.2.1 Planar diagrams and the 't Hooft expansion

In the early 1970's, 't Hooft had a remarkable idea that simplified calculations of QCD processes considerably [20]. Suppose we are interested in computing scattering amplitudes in Yang-Mills theory, *i.e.*, pure $SU(N)$ gauge theory with coupling constant $g_{\rm YM}$. This is simply QCD, but with no quarks, and with N colors instead of three colors. In $SU(N)$ gauge theory, gluons essentially carry one charge and one anti-charge, and hence come in N^2-1 combinations of colors. Roughly speaking, one may think of each gluon as being a "double line", in which an arrow placed on each line represents a color current. This color current is conserved—pictorially, this means that if a particular color is specified on some line in the graph, that same color persists on any connected line segments.

We are interested in specific color indices on the initial and final state gluons. However we are not interested in the specific color content of any intermediate state gluons, and hence we sum over all graphs with any intermediate state gluon colors, subject to the constraint of color current conservation.

Consider first the set of "planar diagrams"—by this we mean those diagrams that can be continuously drawn "inside" a sheet of paper. There are numerous kinematic integrals that need to be done to evaluate this graph, however we can ask a simpler question: How does a given graph depend on the number of colors N and the coupling constant $g_{\rm YM}$?

Because we sum over all N colors for each closed loop of color, a planar diagram picks up a factor of N for each loop. Furthermore, the definition of the coupling constant means that the diagram is proportional to $g_{\rm YM}^V$, where V is the number of vertices in the graph. Take a simple planar diagram as an example.

Figure 2.8 has three closed internal loops of color, and four vertices. Hence it must be proportional to $g_{\rm YM}^4 N^3 = g_{\rm YM}\lambda_t^3$, where we have defined

$$\lambda_t = g_{\rm YM}^2 N\,. \tag{2.6}$$

It is easy to convince oneself that for a planar diagram, the number of loops and vertices is

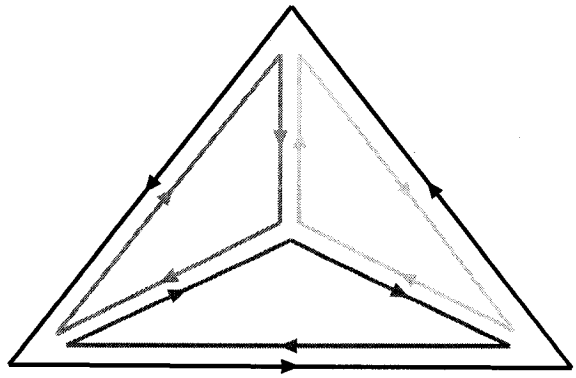

Figure 2.8: A simple planar diagram with no external lines. The red/green/blue lines indicate three disconnected intermediate loops of color current, and one must sum over the N^3 graphs found by placing one of N colors on each internal loop. Color currents on the black exterior line are not summed over, since the appropriate colors would be fixed by whatever color-specific external gluons one attaches to this graph via color conservation.

related in Yang-Mills theory by

$$V = 2L - 2\,. \tag{2.7}$$

Hence a generic planar diagram will have an amplitude proportional to

$$g_{\rm YM}^{V} N^{L} = g_{\rm YM}^{2L-2} N^{L} = g_{\rm YM}^{-2} \lambda_t^{L}\,. \tag{2.8}$$

Consider instead now a non-planar diagram, such as the one in figure 2.9. The small arc in the middle is meant to come out of the page, not in contact with the straight line.

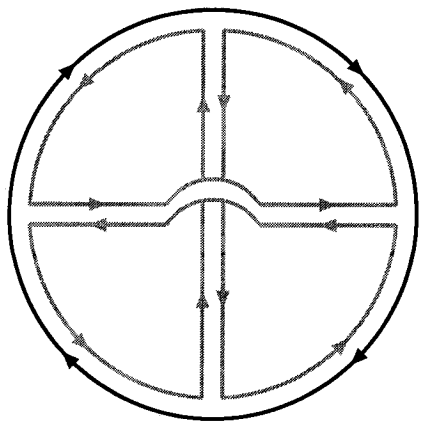

Figure 2.9: A non-planar diagram. One should view the graph in "3-dimensions", where the two gluons in the middle pass by each other without interacting at a vertex. Consequently the entire internal line is connected, and we sum only over N colors.

Note that the entire interior line is now connected, since the lines do not meet in the middle, and hence by color current conservation, the same color must propagate on the inside of the diagram. Thus this diagram picks up only a single factor of N, yet it contains four vertices, and is consequently proportional to $g_{\rm YM}^4 N = g_{\rm YM}^2 \lambda_t$. This diagram is therefore suppressed by a factor of $g_{\rm YM}^4$ relative to a planar diagram.

't Hooft's key insight was as follows: If we take the number of colors $N \to \infty$, and the Yang-Mills coupling $g_{\rm YM} \to 0$ keeping the 't Hooft coupling $g_{\rm YM}^2 N$ fixed and finite, then the non-planar diagrams are suppressed by powers of $g_{\rm YM} \to 0$. We need therefore compute only planar diagrams with an effective coupling λ_t for each loop in the diagram. Corrections due to the finiteness of N and $g_{\rm YM}$ will come in powers of λ_t and $1/N^2$.

This observation led to incredible progress in the analysis of Yang-Mills theory. In principle, it has the potential to simplify QCD calculations considerably, since QCD has $1/N^2 \approx 0.1 \ll 1$, and higher order $1/N$ corrections will be small. However, $\lambda_t \gg 1$ at everyday energy scales, and consequently the diagrams with many loops will dominate the amplitude for the process, in spite of the fact that the corresponding computations are also highly intractable.

2.2.2 The physics of D3-branes at zero temperature

D-branes are extended objects in Type II string theory [21]. They are essentially hypersurfaces that are simultaneously dynamic objects in their own right. They have some associated tension, *i.e.*, mass per unit volume, and therefore will locally warp spacetime.

"D-brane" is short for "Dirichlet-brane", since D-branes also have the essential property that strings can have Dirichlet boundary conditions at the location of the D-brane, *i.e.*, they can end on the D-brane. Without D-branes, Type II string theory would have only closed strings with periodic boundary conditions.

It is interesting to ask what happens if we have a series of N coincident D-branes stacked on top of each other. Open strings could then stretch between any two D-branes in the stack. There are therefore N^2 different open string configurations, since each string endpoint can

end on any one of the N branes. Open strings also have some associated orientation, which can be designated by an arrow going from one end of the string to the other. Strings interact by splitting and joining at their endpoints, and this orientation must be preserved across the interaction. Let us label a given string by $(i, \bar{j})$, signifying that the string stretches from the ith brane to the jth brane. For each brane, we can count the *net* number of strings on a given brane, by counting the number of strings starting on that brane and subtracting the number that end on that brane. Since string orientation must be preserved across string splittings, the *net* number strings on a brane must be a locally conserved quantity. But if we identify each brane as a "color", then the local conservation of color with N^2 degrees of freedom description implies that the open strings are effectively *gluons* of a $U(N)$ gauge theory living on the stack of D-branes! This gauge theory is $U(N)$ rather than $SU(N)$ because there are N^2 degrees of freedom for the string endpoints, rather than $N^2 - 1$.

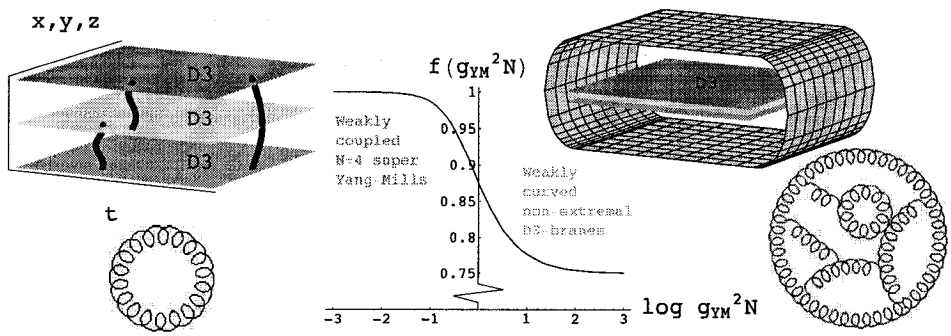

Figure 2.10: Left: Gluons with red, green, and blue colors end on one of three D-branes. The brane separation is artificial and pedagogical, not physical. Right: At strong coupling, the effective description of the gauge theory is given in terms of a weakly-curved gravitational background.

As mentioned, D-branes also have some mass, and we can calculate the spacetime metric resulting from our stack of N D-branes. The result is [22, 23]

$$ds^2 = H^{-1/2}(r)\left[-h(r)dt^2 + d\vec{x}^2\right] + H^{1/2}(r)\left[h(r)^{-1}dr^2 + r^2 d\Omega_5^2\right], \tag{2.9}$$

where

$$H(r) = 1 + \frac{L^4}{r^4} \qquad h(r) = 1 - \frac{r_0^4}{r^4}. \tag{2.10}$$

Here we have specialized to D3-branes, *i.e.*, branes with three dimensions of spatial extent, spanned by the coordinates $\vec{x}$. This solution has two integration constants: L and r_0. It is easiest to see the physical significance of r_0. This metric has a coordinate singularity at $r = r_0$, and a horizon at that location as well. The existence of a horizon implies that the solution is a "black brane" solution, an extended, higher dimensional analog of the familiar black hole. Just like black holes, black branes have an associated temperature, defined by

$$T = \frac{1}{4\pi}\sqrt{-\partial_r G_{tt}(r = r_0)\partial_r G^{rr}(r = r_0)} = \frac{1}{\pi r_0}\frac{1}{\sqrt{1 + L^4/r_0^4}}\,. \tag{2.11}$$

For $r_0 = 0$, the horizon disappears, and the temperature goes to zero as well. This particular limit is called the "extremal brane". On the other hand, finite r_0 corresponding to a finite temperature will add energy to the system. In the absence of a temperature, the only contribution to the tension should come from the D-branes themselves, and hence should be simply N times the tension of a single D-brane [24]:

$$\tau = N\frac{g_{\rm str}(2\pi)^4\alpha'^2}{16\pi G_N}\,. \tag{2.12}$$

On the other hand, one can calculate the tension of the system based on how an asymptotic test mass gravitates toward the D-branes. In doing so, one finds

$$\tau = \frac{4{\rm Vol}(S^5)L^4}{16\pi G}\,. \tag{2.13}$$

Combining these results, and noting that the volume of an S^5 is π^3, we find

$$\frac{L^4}{\alpha'^2} = 4\pi g_{\rm str}N = g_{\rm YM}^2 N = \lambda_t\,. \tag{2.14}$$

The importance of this standard result can not be understated—we will return to it momentarily.

Of frequent interest is a particular limit of the D3-brane metric, the so-called "near extremal, near horizon" limit, in which $r_0 \ll r \ll L$. In this case, the horizon disappears, *i.e.*, the branes are at zero temperature, and $H(r)$ in (2.10) becomes simply L^4/r^4. The metric (2.9) reduces to

$$ds^2 = \frac{r^2}{L^2}\left[-dt^2 + d\vec{x}^2\right] + \frac{L^2}{r^2}dr^2 + L^2 d\Omega_5^2\,. \tag{2.15}$$

This metric describes a simple cross-product spacetime, namely $AdS_5 \times S^5$, *i.e.*, 5-dimensional anti-de Sitter space (the unique Minkowski-signature space of constant negative curvature) times a 5-dimensional sphere. The physical significance of the parameter L is now clear—it is simply the characteristic radius of both the sphere and AdS factors of this spacetime.

The crucial physics of (2.14) is now easy to understand—it tells us that as the 't Hooft coupling λ_t gets large, the radius of spacetime gets large, and hence the curvature gets small. But small curvature is the regime in which supergravity alone is a good approximation, with negligible corrections from string theory at $\mathcal{O}(\alpha'^3 L^{-6} \sim \lambda_t^{-3/2})$. Hence in the regime of large 't Hooft coupling, where perturbative quantum field theory techniques break down, we can do relatively simple supergravity calculations without having to worry about high-curvature corrections coming from string theory.

2.2.3 The thermodynamics of D3-branes

Let us now consider turning on a temperature for our background, *i.e.*, keeping the horizon radius r_0 finite, but maintaining the "near-horizon" condition $r \ll L$:

$$ds^2 = \frac{r^2}{L^2}\left[-h(r)dt^2 + d\vec{x}^2\right] + \frac{L^2}{r^2 h(r)}dr^2 + L^2 d\Omega_5^2 . \tag{2.16}$$

Then the expression for the temperature (2.11) becomes

$$T = \frac{r_0}{\pi L^2} . \tag{2.17}$$

The presence of a horizon signifies the presence of Hawking radiation, and this is the temperature at which the system of black branes will radiate. Using the standard rule that the entropy of the configuration is given by the area of the horizon divided by $4G_N$, we can compute the entropy as:

$$S = \frac{1}{4G_N}\sqrt{-\det \hat{G}_{\mu\nu}(r = r_0)} = \frac{1}{4G_N} \times \frac{r_0^3 V_3}{L^3} \times L^5 \mathrm{Vol}(S^5) . \tag{2.18}$$

By $\hat{G}$, we mean the metric with the exception of the G_{tt} and G_{rr} components, and V_3 refers to the (formally infinite) longitudinal volume of the three extended directions of the

D3-branes. We can eliminate the horizon radius in favor of the temperature (2.17), and eliminate the Newton constant in favor of the squared string length α' via [24]

$$16\pi G_N = (2\pi)^7 g_{\rm str}^2 \alpha'^4 \,. \tag{2.19}$$

Finally, we use (2.14) to obtain for the entropy density [25]

$$\frac{S}{V_3} = \frac{L^8}{g_{\rm str}^2 \alpha'^4} \frac{T^3}{32} = \frac{\pi^2}{2} N^2 T^3 \,. \tag{2.20}$$

This rather simple result is a significant hint to deep underlying physics, as we will see shortly.

2.2.4 The AdS/CFT correspondence

A particular gauge theory called $\mathcal{N} = 4$ $SU(N)$ Super Yang-Mills (SYM) has a number of interesting properties. It has a very high degree of supersymmetry—the $\mathcal{N} = 4$ refers essentially to the existence of four ladder operators that add or subtract a half unit of spin from a given state. Unlike $\mathcal{N} = 1$ supersymmetry, where a gluon has a single spin-1/2 supersymmetric partner particle, the large number of supersymmetries in $\mathcal{N} = 4$ gives the gauge bosons both spinor and scalar partners, all of them massless and carrying color charge and anti-charge like the gluons.

The theory is also *conformal*, meaning that there is no intrinsic mass scale at either the classical or quantum level. Unlike the coupling constants of the standard model, the coupling constant $g_{\rm YM}$ of the $\mathcal{N} = 4$ theory consequently does not depend on the energy scale—the amount of supersymmetry ensures that any loop diagrams that might correct the coupling constant all cancel amongst each other.

In the free theory where $\lambda_t = g_{\rm YM}^2 N \to 0$, one can easily count the degrees of freedom to find the entropy density of the theory

$$\frac{S}{V_3} = \frac{2\pi^2}{3}(N^2 - 1)T^3 \,. \tag{2.21}$$

The $N^2 - 1$ appears due to the number of color degrees of freedom, and the T^3 factor is required on dimensional grounds and the lack of any other dimensionful parameter in the

theory. But note that in the large N limit, this entropy is identical, up to a pre-factor, to the entropy of the black brane system (2.20)!

The black brane system also shares another common element with $\mathcal{N} = 4$ SYM—the gauge theory has an $SU(4)$ symmetry that rotates the four complex supersymmetry ladder operators. But $SU(4)$ is isomorphic to $SO(6)$, the group of rotations of a five-sphere. Furthermore, the isometry group of AdS_5 is $SO(2,4)$, which is identical to an enhanced Poincaré symmetry of the 4-dimensional gauge theory. Thus these two theories share the exact same global symmetry groups.

The one discrepancy remains the factor of 3/4 difference between (2.20) and (2.21). But note that (2.21) applies to the *free* theory, at zero 't Hooft coupling, whereas in (2.20), we assumed that the AdS radius (and consequently the 't Hooft coupling) was large.

The shared symmetries of these theories, among others similar properties, led Maldacena to his famous conjecture of the AdS/CFT correspondence [4]:

Supergravity on the space $AdS_{D+1} \times S^p$
is *dual* to an $SU(N)$ gauge theory
in D-dimensions in the large N, large λ_t limit.

By "dual", we mean that the theories are in some sense identical, and that calculations performed in one have some analog in the other. This is an incredibly powerful statement: When the 't Hooft coupling is large, and standard perturbative Feynman diagram techniques are not at all useful, one can do relatively simple calculations using general relativity on a higher dimensional space, and translate the results into the gauge theory language via an appropriate dictionary. Somehow, the AdS space magically "knows" about the gauge theory results at large 't Hooft coupling when the graphs with many loops dominate the physics.

Later, as more was learned about the conjecture, it was expanded to include any Einstein space X in place of the p-sphere, and it was understood that the details of the gauge theory, such as the precise gauge group and the number of supersymmetries, were encoded in the details of the space X [26].

The strongly coupled gauge theory is said to "live" on the boundary of AdS, *i.e.*, at distances far from the horizon. This will be important when we look to connect physical objects on the gravity side with their field theory duals.

Furthermore, adding a horizon to the AdS_{D+1} space, a.k.a. AdS-Schwarzschild, corresponds to turning on a finite temperature in the gauge theory. Since the RHIC experiment considers a gauge theory plasma at large, finite temperature, the AdS-Schwarzschild background will be of great importance to us.

2.3 The gravity dual of jet quenching in a hot plasma

As jet quenching is an interesting yet incompletely understood phenomenon of the strongly-coupled RHIC plasma, we might hope to describe it using the AdS/CFT correspondence, and perhaps use it to experimentally probe string theory. Since corrections to the infinite N and λ_t limits are $\mathcal{O}(\lambda_t^{-3/2})$ and $\mathcal{O}(1/N^2)$, each of which are $\mathcal{O}(10\%)$ corrections, physical effects that are uniquely stringy may appear in the plasma dynamics, unlike traditional quantum gravity corrections which are $\mathcal{O}(10^{-15})$ effects in existing particle physics experiments.

The dual description of a quark moving through a finite temperature plasma is given by a string with one endpoint at or near the boundary of AdS. The initial setup was first discussed by Herzog et al [27], and separately and simultaneously by Gubser [28], and we will summarize their essential results here. Similar calculations of RHIC-like physics via AdS/CFT appeared at very nearly the same time [29, 30].

For simplicity, we will consider quarks that move at a constant velocity. The plasma induces a drag force on the quark, and hence the quark deposits energy into the plasma. The constant velocity condition means that we must feed energy into the quark to compensate for this energy loss by dragging it through the plasma with a fictitious external force. Nevertheless, how much energy is lost into the thermal medium, and more to the point, where that energy goes will be our primary concern.

First, we will make a change of coordinates to simplify our calculations—we will take

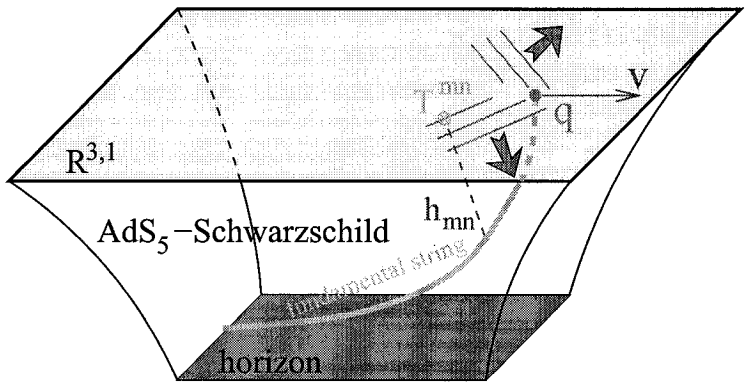

Figure 2.11: A string hangs with one endpoint near the boundary of AdS-Schwarzschild, moving at a constant velocity v.

$y = r_0/r$, so that the boundary is located at $y = 0$, and the horizon is located at $y = 1$. There is nevertheless an infinite proper distance between these surfaces. We will often refer to the horizon location as $z_H = L^2/r_0$, so that the temperature is $T = 1/\pi z_H$. The resulting metric is:

$$ds^2 = \frac{L^2}{z_H^2 y^2}\left(-h dt^2 + d\vec{x}^2 + z_H^2 \frac{dy^2}{h}\right) \qquad h \equiv 1 - y^4 \,. \tag{2.22}$$

For the time being, the S^5 portion of the spacetime will not be needed, so we can simply integrate it out and consider only the AdS_5-Schwarzschild portion.

We need to know the configuration of the string as it moves through the plasma. The conventional approach is to assume a "co-moving" ansatz, in which all parts of the string move together at some fixed velocity v.

$$X^\mu = (t, x^1, x^2, x^3, y) = (\tau, vt + \xi(y), 0, 0, \sigma) \,. \tag{2.23}$$

To derive the equation of motion for $\xi(y)$, we substitute this ansatz into the Nambu-Goto action for the string, which is simply the geometric area:

$$S = \frac{1}{2\pi\alpha'} \int d\tau d\sigma \sqrt{\det G_{\mu\nu} \partial_a X^\mu \partial_b X^\nu} \,. \tag{2.24}$$

We are left with a simple one-dimensional effective Lagrangian for ξ:

$$\mathcal{L} = -\frac{1}{y^2}\sqrt{1 + \frac{h\xi'^2}{z_H^2} - \frac{v^2}{h}} \,. \tag{2.25}$$

The solution to the corresponding Euler-Lagrange equation of motion is simply

$$\xi' = -\frac{v z_H y^2}{1-y^4} \qquad \xi = \frac{v z_H}{2}\left(\arctan y - \operatorname{arctanh} y\right) . \tag{2.26}$$

The solution for ξ looks approximately as shown below.

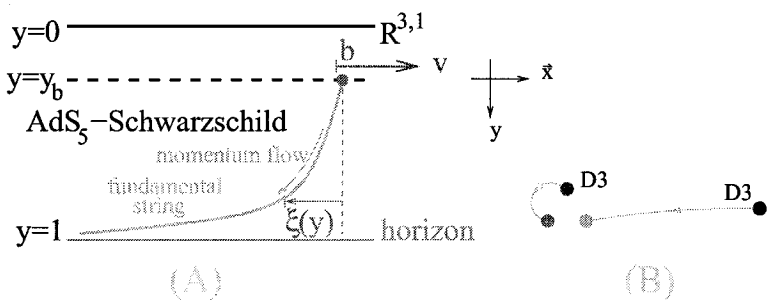

Figure 2.12: (A) The string trails behind the quark with some distance $\xi(y)$. (B) Rather than have the string hang from the boundary, one can imagine splitting off one D3 brane from the large stack, and letting the string hang from that brane.

The solution described above assumes that the quark hangs all the way from the boundary of AdS. The mass of the string and its dual quark are given by the finite string tension times the proper length of the string. Hence the infinite proper length of the string means that the dual quark is infinitely massive. We can consider finite mass quarks by having the string hang from a D-brane placed at a distance slightly below the boundary. Provided that the D-brane is close enough to the boundary, the solution for the string profile does not change—we simply truncate the string at the location of the D-brane.

Before we consider the energy emitted from the quark as it moves through the plasma, we can first ask about the drag force it experiences. The quantity of interest is the flow of spacetime momentum down the y-direction of the string worldsheet. Since this momentum is conserved by the string dynamics, the flow is actually independent of y.

$$\Delta P_1 = -\int_{\mathcal{I}} dt\, \sqrt{-g} P^y{}_{x^1} = \frac{dp_1}{dt}\Delta t \qquad P^a{}_\mu = -\frac{1}{2\pi\alpha'} G_{\mu\nu}\partial^a X^\nu \tag{2.27}$$

dp_1/dt is precisely the drag force:

$$F \equiv \frac{dp}{dt} = -\frac{\pi\sqrt{g_{YM}^2 N T^2}}{2m}\frac{mv}{\sqrt{1-v^2}} . \tag{2.28}$$

Provided that the quark mass is sufficiently large as not to be dominated by thermal effects, so that the usual relativistic dispersion relations hold, the last term in (2.28) is simply the quark's momentum, so we can immediately integrate to obtain the momentum as a function of time:

$$p(t) = p_0 e^{-t/t_0}\,, \qquad t_0 = \frac{2}{\pi\sqrt{g_{YM}^2 N}}\frac{m}{T^2}\,. \tag{2.29}$$

RHIC-relevant values for the temperature and coupling are $T = 318\,\mathrm{MeV}$ and $\lambda = 10$. (We choose this particular value of the temperature for later convenience, since $318\pi \approx 1000$, and since it is reasonably close to observed values.) Consequently we find that $t_0 = 0.6\,\mathrm{fm/c}$ for charm, and $t_0 = 1.9\,\mathrm{fm/c}$ for bottom, both of which are much less than the typical lifetime of the QGP, $t_{\mathrm{QGP}} \approx 6\,\mathrm{fm/c}$. Hence we might say that quarks in our $\mathcal{N} = 4$ SYM plasma are efficiently quenched. That said, the effect is overestimated, since this temperature is more or less the maximum plasma temperature at RHIC. Furthermore, the plasma expands and cools over time, further reducing the quenching effect.

Nevertheless, there is clearly a considerable amount of energy lost in the first moments of the quark's motion through the plasma. With some further insight for the magnitude and direction of this energy loss, we might be able to make some more substantial claims regarding the role of stringy effects in RHIC's Quark-Gluon Plasma.

Chapter 3

The Stress Tensor from a Plasma-Quenched Quark

So far, we have argued that a gravity dual description of a quark moving through a thermal Yang-Mills plasma is an efficient means of computing physical observables, such as the characteristic jet quenching time. A number of other papers [31, 29, 32, 33, 34, 35, 36, 37, 38, 39, 40, 41, 42, 43] have also used AdS/CFT in related ways to describe energy dissipation from a moving quark.

In addition to knowing the amount of energy that gets dissipated, it is also important to understand *where* that energy goes, namely, what the stress-energy tensor is in the boundary gauge theory. It was observed in [27, 28] that $\langle T_{mn} \rangle$ is calculable via AdS/CFT but requires a technically non-trivial analysis of graviton perturbations in AdS_5-Schwarzschild. The aim of this rather technical chapter is to develop the relevant equations and solve them, both in limits that are analytically tractable and through use of numerics for selected values of the velocity. We will closely follow the work described in [44]. Section 3.1 comprises a derivation of the equations. The linearized graviton equations are stated in full at the end of section 3.1. Section 3.2 includes solutions of the equations near the boundary and near the horizon of AdS_5-Schwarzschild, as well as expressions for the stress tensor in the near-field limit. A boundary-value problem in classical five-dimensional gravity is stated at the end

of section 3.2.2 which determines $\langle T_{mn} \rangle$ in the boundary theory. Section 3.3 presents the results of numerical work, and section 3.4 is devoted to discussion of the possible relevance to jet-quenching in relativistic heavy-ion collisions.

The reader wishing to skip all the five-dimensional technicalities and see the "answers" may skip directly to section 3.3 with the following definitions and conventions in mind:

- Wave-numbers $\vec{K} = (K_1, K_2, K_3)$ are rendered dimensionless by including a factor of $z_H = 1/\pi T$.
- Usually we set $K_3 = 0$ and $K_2 = K_\perp > 0$.
- Often we refer to $K = \sqrt{K_1^2 + K_\perp^2}$ and $\theta = \tan^{-1}(K_\perp/K_1)$.
- $\langle T^K_{mn} \rangle$ is the K-th Fourier coefficient of the co-moving part of $\langle T_{mn} \rangle$ in the $3+1$-dimensional boundary gauge theory: see (3.41).
- $Q^{\rm tot}_{mn}$ is a dimensionless quantity proportional to $\langle T^K_{mn} \rangle$: see (3.35).
- Using symmetries and conservation laws, the non-zero components of $Q^{\rm tot}_{mn}$ can be expressed in terms of three complex quantities $Q^{\rm tot}_A$, $Q^{\rm tot}_D$, and $Q^{\rm tot}_E$: see (3.30).
- $Q^{\rm tot}_E$ is the easiest quantity to interpret, as it is directly proportional to $\langle T^K_{00} \rangle$, the K-th Fourier component of the energy density.
- Q^K_X for $X = A$, D, or E is $Q^{\rm tot}_X$ with the Coulombic near-field of the quark subtracted away: see (3.61). Note also that the inhomogeneous term p_{mn} in (3.30) amounts to far-field subtraction in the definition of both $Q^{\rm tot}_X$ and Q^K_X.

3.1 The graviton equations of motion

The relevant part of the action for supergravity plus the string is

$$S = \int d^5x \left[\frac{\sqrt{-G}\,(R + 12/L^2)}{2\kappa_5^2} - \frac{1}{2\pi\alpha'} \int d^2\sigma \sqrt{-g}\, \delta^5(x^\mu - X^\mu(\sigma)) \right], \qquad (3.1)$$

where L is the radius of AdS_5. Typically this action also includes a scalar, massless dilaton field, but we have excluded it from (3.1) because it decouples from the metric at the level of linear perturbations around the AdS_5-Schwarzschild background. To reiterate, the gravitational background of interest is

$$ds^2_{(0)} = G^{(0)}_{\mu\nu}dx^\mu dx^\nu = \frac{L^2}{z_H^2 y^2}\left(-h dt^2 + d\vec{x}^2 + z_H^2 \frac{dy^2}{h}\right) \qquad h \equiv 1 - y^4\,, \tag{3.2}$$

and the position of the string can be described in static gauge as

$$\begin{gathered} X^\mu(t,y) \equiv \begin{pmatrix} t & X^1(t,y) & 0 & 0 & y \end{pmatrix} \\ X^1(t,y) = vt + \xi(y) \qquad \xi(y) = -\frac{z_H v}{4i}\left(\log\frac{1-iy}{1+iy} + i\log\frac{1+y}{1-y}\right). \end{gathered} \tag{3.3}$$

By varying (3.1) with respect to the background metric $G_{\mu\nu}$, we obtain the following five-dimensional Einstein equations

$$R^{\mu\nu} - \frac{1}{2}G^{\mu\nu}R - \frac{6}{L^2}G^{\mu\nu} = \tau^{\mu\nu}\,, \tag{3.4}$$

where

$$\begin{aligned} \tau^{\mu\nu} &= -\frac{\kappa_5^2}{2\pi\alpha'}\int d^2\sigma\,\frac{\sqrt{-g}}{\sqrt{-G}}\,\delta^5(x^\mu - X^\mu)\partial_\alpha X^\mu \partial^\alpha X^\nu \\ &= -\frac{\kappa_5^2}{2\pi\alpha'}\frac{z_H^3}{L^3}y^3\sqrt{1-v^2}\,\delta(x^1 - vt - \xi(y))\delta(x^2)\delta(x^3)\partial_\alpha X^\mu \partial^\alpha X^\nu\,, \end{aligned} \tag{3.5}$$

is the stress-energy tensor due to the string, expressed explicitly in static gauge in the second line. If we perturb

$$G_{\mu\nu} = G^{(0)}_{\mu\nu} + h_{\mu\nu}\,, \tag{3.6}$$

then, schematically, the form of the linearized equations following from (3.4) is

$$\Delta_{AdS} h^{\mu\nu} = \tau^{\mu\nu} \tag{3.7}$$

where $h^{\mu\nu} = G^{\mu\rho}_{(0)}G^{\nu\sigma}_{(0)}h_{\rho\sigma}$ and Δ_{AdS} is a variant of the Lichnerowicz operator.

The stress tensor $\tau^{\mu\nu}$ depends on x^1 and t only through the combination $x^1 - vt$. Thus we can expand

$$\tau^{\mu\nu}(t, x^1, x^2, x^3, y) = \int \frac{d^3K}{(2\pi)^3}\,\tau^{\mu\nu}_K(y)\,e^{i[K_1(x^1 - vt) + K_2 x^2 + K_3 x^3]/z_H}\,. \tag{3.8}$$

(Note that $\vec{K} = z_H \vec{k} = \vec{k}/\pi T$ is dimensionless.) If our interest is the co-moving graviton response, we can make a similar expansion for $h_{\mu\nu}$. Then, again schematically, one obtains from (3.7) a set of coupled ordinary differential equations in y:

$$\mathcal{E}^{\mu\nu} \equiv \Delta^K_{AdS} h^{\mu\nu}_K - \tau^{\mu\nu}_K = 0\,. \tag{3.9}$$

It is these equations which we wish to formulate more precisely and then solve. Note that although the Fourier modes $\tau^{\mu\nu}_K$ and $h^{\mu\nu}_K$ are complex, they satisfy conditions like $\tau^{\mu\nu}_{-K} = (\tau^{\mu\nu}_K)^*$ that ensure the position space quantities are real. From the asymptotic behavior of $h^{\mu\nu}_K$ near the boundary of AdS_5-Schwarzschild one may extract the K-th Fourier mode $\langle T^K_{mn}\rangle$ of the co-moving contribution to the stress tensor. A detailed discussion of the extraction of $\langle T^K_{mn}\rangle$ is deferred to section 3.2.1.

The rotational symmetry around the axis of motion of the quark enables us to choose $\vec{K} = (K_1, K_\perp, 0)$ with $K_\perp \geq 0$. The remaining symmetry is a $\mathbf{Z}_2$ sending $x^3 \to -x^3$. The metric perturbation can be parametrized as

$$h^K_{\mu\nu} = \frac{\kappa_5^2}{2\pi\alpha'} \frac{1}{\sqrt{1-v^2}} \frac{L}{z_H^2 y^2} \begin{pmatrix} H_{00} & H_{01} & H_{02} & H_{03} & 0 \\ H_{10} & H_{11} & H_{12} & H_{13} & 0 \\ H_{20} & H_{21} & H_{22} & H_{23} & 0 \\ H_{30} & H_{31} & H_{32} & H_{33} & 0 \\ 0 & 0 & 0 & 0 & 0 \end{pmatrix}. \tag{3.10}$$

The vanishing entries represent a gauge choice which we will refer to as axial gauge. The K-th Fourier mode of the string's stress tensor is

$$\tau^{\mu\nu}_K = \frac{\kappa_5^2}{2\pi\alpha'} \frac{e^{-iK_1\xi(y)/z_H}}{\sqrt{1-v^2}} \frac{y^5}{L^5} \begin{pmatrix} z_H^2 \dfrac{h+v^2y^4}{h^2} & z_H^2 \dfrac{v}{h} & 0 & 0 & z_H \dfrac{v^2y^2}{h} \\ z_H^2 \dfrac{v}{h} & z_H^2 v^2 & 0 & 0 & z_H v y^2 \\ 0 & 0 & 0 & 0 & 0 \\ 0 & 0 & 0 & 0 & 0 \\ z_H \dfrac{v^2y^2}{h} & z_H v y^2 & 0 & 0 & v^2 - h \end{pmatrix}, \tag{3.11}$$

where $\xi(y)$ is as given in (3.3).

Because (3.9) is an equation for symmetric rank-two tensors, it has 15 algebraically independent component equations. Ten of these, namely $\mathcal{E}^{mn} = 0$ with $0 \leq m \leq n \leq 3$, are second order, and the other five, $\mathcal{E}^{\mu 5} = 0$ with μ unrestricted, are first order constraints.[1] There are 10 dependent variables H_{mn}, so the full system $\mathcal{E}^{\mu\nu} = 0$ seems overdetermined. But it isn't: if the constraints are imposed at one value of y and the second order equations are then solved, the constraints continue to hold automatically for all y.

The $\mathbf{Z}_2$ symmetry that takes $x^3 \to -x^3$ causes the equations (3.9) to partially decouple. The $\mathbf{Z}_2$ "charge" of a component H_{mn} of the metric perturbation is the parity of the number of indices equal to 3. Similar charge assignments can be made to the equations $\mathcal{E}^{\mu\nu} = 0$. Thus for example H_{03} and $\mathcal{E}^{13} = 0$ are odd while H_{33} and $\mathcal{E}^{01} = 0$ are even. The three odd second order equations of motion and the one odd constraint equation involve only the odd variables, whereas the seven even second order equations and the four even constraint equations involve only the even variables. Moreover, only the even equations involve non-zero components of the stress tensor (3.11). So it is consistent to set all the odd variables equal to zero from the outset. In the interests of generality, we will not do this yet, but rather consider how the equations may be further decoupled.

Briefly, we make the following definitions and find the following differential equations:

$$K = \sqrt{K_1^2 + K_\perp^2} \qquad \theta = \tan^{-1}\frac{K_\perp}{K_1} \tag{3.12}$$

$$A = \frac{-H_{11} + 2\cot\theta H_{12} - \cot^2\theta H_{22} + \csc^2\theta H_{33}}{2v^2} \tag{3.13}$$

$$\left[\partial_y^2 + \left(-\frac{3}{y} + \frac{h'}{h}\right)\partial_y + \frac{K^2}{h^2}(v^2\cos^2\theta - h)\right] A = \frac{y}{h} e^{-iK_1\xi/z_H} \tag{3.14}$$

$$B_1 = \frac{H_{03}}{K^2 v} \qquad B_2 = -\frac{H_{13} + \tan\theta H_{23}}{K^2 v^2} \tag{3.15}$$

$$\left[\partial_y^2 + \begin{pmatrix} -\frac{3}{y} & 0 \\ 0 & -\frac{3}{y} + \frac{h'}{h} \end{pmatrix}\partial_y + \frac{K^2}{h^2}\begin{pmatrix} -h & v^2\cos^2\theta h \\ -1 & v^2\cos^2\theta \end{pmatrix}\right]\begin{pmatrix} B_1 \\ B_2 \end{pmatrix} = \begin{pmatrix} 0 \\ 0 \end{pmatrix} \tag{3.16}$$

[1] We associate y with $\mu = 5$. There is no coordinate associated with $\mu = 4$. This convention serves as a reminder that y is the fifth dimension.

$$B_1' - hB_2' = 0 \tag{3.17}$$

$$C = \frac{-\sin\theta H_{13} + \cos\theta H_{23}}{K} \tag{3.18}$$

$$\left[\partial_y^2 + \left(-\frac{3}{y} + \frac{h'}{h}\right) + \frac{K^2}{h^2}(v^2\cos^2\theta - h)\right] C = 0 \tag{3.19}$$

$$D_1 = \frac{H_{01} - \cot\theta H_{02}}{2v} \qquad D_2 = \frac{-H_{11} + 2\cot 2\theta H_{12} + H_{22}}{2v^2} \tag{3.20}$$

$$\left[\partial_y^2 + \begin{pmatrix} -\frac{3}{y} & 0 \\ 0 & -\frac{3}{y} + \frac{h'}{h} \end{pmatrix} \partial_y + \frac{K^2}{h^2}\begin{pmatrix} -h & v^2\cos^2\theta h \\ -1 & v^2\cos^2\theta \end{pmatrix}\right] \begin{pmatrix} D_1 \\ D_2 \end{pmatrix} = \frac{y}{h} e^{-iK_1\xi/z_H} \begin{pmatrix} 1 \\ 1 \end{pmatrix} \tag{3.21}$$

$$D_1' - hD_2' = \frac{y^3}{ivK_1} e^{-iK_1\xi/z_H} \tag{3.22}$$

$$E_1 = \frac{1}{2}\left(-\frac{3}{h}H_{00} + H_{11} + H_{22} + H_{33}\right) \qquad E_2 = \frac{H_{01} + \tan\theta H_{02}}{2v}$$

$$E_3 = \frac{H_{11} + H_{22} + H_{33}}{2} \qquad E_4 = \frac{-H_{11} - H_{22} + 3\cos 2\theta(-H_{11} + H_{22}) + 2H_{33} - 6\sin 2\theta H_{12}}{4} \tag{3.23}$$

$$\left[\partial_y^2 + \begin{pmatrix} -\frac{3}{y} + \frac{3h'}{2h} & 0 & 0 & 0 \\ 0 & -\frac{3}{y} & 0 & 0 \\ 0 & 0 & -\frac{3}{y} + \frac{h'}{2h} & 0 \\ 0 & 0 & 0 & -\frac{3}{y} + \frac{h'}{h} \end{pmatrix} \partial_y \right.$$
$$\left. + \frac{K^2}{3h^2}\begin{pmatrix} -2h & 12v^2\cos^2\theta & 6v^2\cos^2\theta + 2h & 0 \\ 0 & 0 & 2h & h \\ 0 & 0 & -2h & -h \\ 2h & -12v^2\cos^2\theta & 0 & 3v^2\cos^2\theta + h \end{pmatrix}\right] \begin{pmatrix} E_1 \\ E_2 \\ E_3 \\ E_4 \end{pmatrix} \tag{3.24}$$
$$= \frac{y}{h} e^{-iK_1\xi/z_H} \begin{pmatrix} 1 + \frac{v^2}{h} \\ 1 \\ -1 + v^2 - \frac{v^2}{h} \\ v^2\frac{1+3\cos 2\theta}{2} \end{pmatrix}$$

$$\left[\begin{pmatrix} 0 & 1 & 1 & 0 \\ -h & 0 & -3v^2\cos^2\theta - h & -h \\ h & 0 & 2 & 0 \end{pmatrix}\partial_y \right.$$
$$\left. + \frac{1}{6h}\begin{pmatrix} 0 & -6h' & -3h' & 0 \\ -3hh' & 18v^2\cos^2\theta h' & 3(3v^2\cos^2\theta + h)h' & 0 \\ 2K^2yh & -12K^2v^2y\cos^2\theta & -2K^2y(3v^2\cos^2\theta - h) & 2K^2yh \end{pmatrix}\right]\begin{pmatrix} E_1 \\ E_2 \\ E_3 \\ E_4 \end{pmatrix}$$
$$= \frac{h'}{4Kyh}e^{-iK_1\xi/z_H}\begin{pmatrix} -ivy\sec\theta \\ 3ivy\cos\theta(v^2+h) \\ K(v^2-h) \end{pmatrix}. \tag{3.25}$$

Let us summarize the salient features of these equations:

- The 15 equations $\mathcal{E}^{\mu\nu} = 0$ split up into five sets, decoupled from one another.
- The B and C sets (3.15)-(3.19) involve only the $\mathbf{Z}_2$-odd components of the metric, and so it is inevitable that they are homogeneous. We may set $B_1 = B_2 = C = 0$ and focus on the A, D, and E equations.
- The A equation (3.14) happens to be identical to the dilaton equation of motion up to a factor multiplying the source term, so we may borrow directly from [35] to find its solution. The C equation (3.19) is also the same as the dilaton equation except that it is homogeneous.
- The B and D equations, (3.16)-(3.17) and (3.21)-(3.22), are identical except that the former are homogeneous and the latter are not. Each set involves one constraint and two second order equations of motion.
- The E set (3.23)-(3.25) involves four second order equations of motion and three constraints.
- The total momentum K enters the equations of motion only as a multiplicative factor

on the non-derivative coefficient matrices and through the source terms. Elaborations of the WKB method may therefore be suitable for approximately solving the equations at large K, and series solutions in K may be used at small K. Section 3.2.5 includes further discussion of small K approximations.

3.2 Analytic approximations

Although the discussion at the end of the previous section allows us to set the three odd H_{mn} to 0, and correspondingly $B_1 = B_2 = C = 0$, we sometimes refrain from doing so in the following discussion of limiting forms of the equations.

Our general procedure will be as follows: First we will find exact solutions to the 10 second-order ODE's near both the boundary of AdS ($y = 0$) and the horizon ($y = 1$). We will find that within each set of equations, there is precisely one non-vanishing oscillatory solution, and by symmetry, there must be both a positive and negative frequency solution. One of these corresponds to a wave falling into the black hole, and one corresponds to a wave coming out of it. The outfalling wave is non-physical: Coherent, semi-classical information can not come out of a black hole. We must therefore choose our integration constants to eliminate this solution.

Each set has n second-order equations for n gravitational perturbative modes, and $n-1$ first-order constraint equations. Thus, within each set, there are $2n$ integration constants coming from the second-order equations. We fix those integration constants as follows: We require each mode to vanish asymptotically at the boundary, fixing n constants. The $n-1$ first-order constraints, which are redundant to the equations of motion, amount to requiring $n-1$ various relationships between the integration constants, which we impose at the boundary as well. This leaves us with a single integration constant in each set. We then vary this constant at the boundary until we find the particular value that eliminates the outfalling mode at the horizon. For some given v and $\vec{K}$, this uniquely determines the solution.

To do this, we first need to know how the solutions behave as we approach both the

boundary and horizon asymptotically, so we can match our full numerical solutions onto exact analytical solutions in each region.

3.2.1 Near the boundary

By solving the equations of motion in a series expansion in y one obtains the leading forms

$$X = -\frac{P_X}{3}y^3 + Q_X^{\rm tot}y^4 + R_X \qquad X = A, B_1, B_2, C, D_1, D_2, E_1, E_2, E_3, E_4\,, \tag{3.26}$$

where

$$\begin{gathered} P_A = P_{D_1} = P_{D_2} = P_{E_2} = -P_{E_3} = 1 \qquad P_{E_1} = 1+v^2 \qquad P_{E_4} = v^2(3\cos^2\theta - 1) \\ P_{B_1} = P_{B_2} = P_C = 0\,. \end{gathered} \tag{3.27}$$

The $Q_X^{\rm tot}$ are integration constants related to the VEV's of the stress tensor. The R_X are integration constants which can be set to zero because non-zero values would correspond to deformations of the gauge theory lagrangian. As noted above, the constraint equations imply relations among the $Q_X^{\rm tot}$:

$$\begin{gathered} Q_{D_1}^{\rm tot} - Q_{D_2}^{\rm tot} = \frac{\sec\theta}{4ivK} \qquad Q_{B_1}^{\rm tot} - Q_{B_2}^{\rm tot} = 0 \\ Q_{E_1}^{\rm tot} - 2Q_{E_2}^{\rm tot} = \frac{v\sec\theta}{2iK} \qquad Q_{E_1}^{\rm tot} + 2Q_{E_3}^{\rm tot} = 0 \\ (1-3v^2\cos^2\theta)Q_{E_1}^{\rm tot} + 2Q_{E_4}^{\rm tot} = \frac{3iv(1+v^2)\cos\theta}{2K}\,. \end{gathered} \tag{3.28}$$

The meaning of the equations (3.28) becomes clearer in terms of the original variables H_{mn}, whose series expansion near the boundary of AdS_5-Schwarzschild includes the leading terms

$$H_{mn} = -\frac{P_{mn}}{3}y^3 + Q_{mn}^{\rm tot}y^4 + R_{mn}\,. \tag{3.29}$$

P_{mn}, $Q_{mn}^{\rm tot}$, and R_{mn} are linear combinations, respectively, of P_X, $Q_X^{\rm tot}$, and R_X, as can be deduced by inverting the relations (3.13), (3.15), (3.18), (3.20), and (3.23). In particular, after setting $\mathbf{Z}_2$-odd quantities to zero and using (3.28) to eliminate $Q_{D_2}^{\rm tot}$, $Q_{E_2}^{\rm tot}$, $Q_{E_3}^{\rm tot}$, and $Q_{E_4}^{\rm tot}$ in favor of $Q_A^{\rm tot}$, $Q_{D_1}^{\rm tot} \equiv Q_D^{\rm tot}$, and $Q_{E_1}^{\rm tot} \equiv Q_E^{\rm tot}$, one obtains

$$Q_{mn}^{\rm tot} = a_{mn}Q_A^{\rm tot} + d_{mn}Q_D^{\rm tot} + e_{mn}Q_E^{\rm tot} + p_{mn} \tag{3.30}$$

where

$$\left(a_{mn}\right) = \frac{v^2 \sin^2\theta}{2}\begin{pmatrix} 0 & 0 & 0 & \\ 0 & -2\sin^2\theta & \sin 2\theta & 0 \\ 0 & \sin 2\theta & -2\cos^2\theta & 0 \\ 0 & 0 & 0 & 2 \end{pmatrix} \tag{3.31}$$

$$\left(d_{mn}\right) = \frac{v}{2}\begin{pmatrix} 0 & 4\sin^2\theta & -2\sin 2\theta & 0 \\ 4\sin^2\theta & -2v\sin^2 2\theta & v\sin 4\theta & 0 \\ -2\sin 2\theta & v\sin 4\theta & 2v\sin^2 2\theta & 0 \\ 0 & 0 & 0 & 0 \end{pmatrix} \tag{3.32}$$

$$\left(e_{mn}\right) = \frac{1}{4}\begin{pmatrix} -4 & 4v\cos^2\theta & 2v\sin 2\theta & 0 \\ 4v\cos^2\theta & 4e_{11} & (1-3v^2\cos^2\theta)\sin 2\theta & 0 \\ 2v\sin 2\theta & (1-3v^2\cos^2\theta)\sin 2\theta & 4e_{22} & 0 \\ 0 & 0 & 0 & -2+2v^2\cos^2\theta \end{pmatrix} \tag{3.33}$$

$$e_{11} = \frac{1}{2}\left[-1+(1+v^2)\cos^2\theta - 3v^2\cos^4\theta\right]$$

$$e_{22} = \frac{1}{2}\cos^2\theta(-1-2v^2+3v^2\cos^2\theta)$$

$$\left(p_{mn}\right) = \frac{iv\cos\theta}{4K}\begin{pmatrix} 0 & 2v & 2v\tan\theta & 0 \\ 2v & -3+v^2+(1-3v^2)\cos^2\theta & \left[-2+(1-3v^2)\cos^2\theta\right]\tan\theta & 0 \\ 2v\tan\theta & \left[-2+(1-3v^2)\cos^2\theta\right]\tan\theta & 2-2v^2-(1-3v^2)\cos^2\theta & 0 \\ 0 & 0 & 0 & 1+v^2 \end{pmatrix} \tag{3.34}$$

The $Q^{\rm tot}_{mn}$ are integration constants which are proportional to entries of $\langle T^K_{mn}\rangle$:

$$\langle T^K_{mn}\rangle = \frac{\pi^3 T^4\sqrt{g^2_{YM}N}}{\sqrt{1-v^2}}Q^{\rm tot}_{mn}\,. \tag{3.35}$$

What we mean by $\langle T^K_{mn}\rangle$ is a co-moving Fourier coefficient of the quark's contribution to $\langle T_{mn}\rangle$. The overall factor in (3.35) can be determined through first principles along the lines of [45], but we find it more instructive to obtain it heuristically by considering what may seem at first to be a digression: AdS_5-Schwarzschild in axial gauge.

Defining a new radial variable q through

$$y^2 = \frac{q^2}{1+q^4/4}\,, \tag{3.36}$$

one finds that the line element (3.2) becomes

$$\begin{aligned} ds^2 &= \frac{L^2}{z_H^2 q^2}(-dt^2 + d\vec{x}^2 + z_H^2 dq^2) + h_{\mu\nu}dx^\mu dx^\nu \\ h_{\mu\nu} &= \frac{L^2 q^2}{4z_H^2}\,\mathrm{diag}\left\{\frac{3-q^4/4}{1+q^4/4}, 1, 1, 1, 0\right\}. \end{aligned} \tag{3.37}$$

This is indeed an axial gauge description of AdS_5-Schwarzschild because $h_{\mu 0} = 0$; note however that (3.37) is an exact rewriting of (3.2).

On general grounds, the stress tensor of the boundary theory must be proportional to the coefficient of q^4 in h_{mn}. But in the case of AdS_5-Schwarzschild, there is a pre-existing determination of the energy density and pressure based on [25]:

$$\frac{\epsilon}{3} = p = \frac{\pi^2}{8}N^2T^4\,. \tag{3.38}$$

Therefore we conclude that

$$\langle T_{mn}\rangle = \frac{\pi^2}{8}N^2T^4 \lim_{q\to 0}\frac{z_H^2}{q^3L^2}\partial_q(q^2 h_{mn})\,. \tag{3.39}$$

Returning to the setup with a string dangling into AdS_5-Schwarzschild means that on top of the "perturbation" $h_{\mu\nu}$ that deforms AdS_5 into AdS_5-Schwarzschild we must add an additional perturbation, namely the $h_{\mu\nu}$ whose Fourier coefficients are given in (3.10). The result (3.39) applies unchanged, except that the limit exists only after certain divergent delta-function contributions have been subtracted. After using (3.29) and the standard relations

$$N^2\kappa_5^2 = 4\pi^2 L^3 \qquad \frac{L^2}{\alpha'} = \sqrt{g_{YM}^2 N} \tag{3.40}$$

one obtains

$$\langle T_{mn}\rangle = \frac{\pi^2}{8}N^2T^4\,\mathrm{diag}\{3,1,1,1\} + \int \frac{d^3K}{(2\pi)^3}\langle T^K_{mn}\rangle e^{i[K_1(x^1-vt)+K_2x^2+K_3x^3]/z_H} \tag{3.41}$$

where $\langle T^K_{mn}\rangle$ is indeed given by (3.35).

Because T_{mn} is conserved and traceless (the latter due to conformal invariance), one expects that $K^m Q^{\rm tot}_{mn} = 0$ where

$$K^m = \begin{pmatrix} vK_1 & K_1 & K_\perp & 0 \end{pmatrix}, \tag{3.42}$$

and also

$$\operatorname{tr} Q^{\text{tot}} \equiv -Q^{\text{tot}} + Q_{11}^{\text{tot}} + Q_{22}^{\text{tot}} + Q_{33}^{\text{tot}} = 0\,. \tag{3.43}$$

The tracelessness condition (3.43) is indeed satisfied, but conservation fails: instead,

$$\left(K^m Q_{mn}^{\text{tot}}\right) = \frac{iv}{2}\begin{pmatrix} v & -1 & 0 & 0 \end{pmatrix}. \tag{3.44}$$

The result (3.44) is independent of Q_A, Q_D, and Q_E: that is, only the last term in the decomposition (3.30) fails to be conserved.

The non-conservation (3.44) could have been anticipated. It is the manifestation of the energy-momentum imparted by the quark to the thermal medium. The quark is prescribed to travel with constant velocity, so it does not slow down as it loses energy-momentum. The non-conservation (3.44) should precisely reflect the external force required to keep the quark's momentum from changing, which is minus the drag force (2.28). This argument is formal because the quark's mass is infinite, hence so is its momentum. But changes in the momentum, and therefore forces, can be finite. To verify that (2.28) can be recovered from (3.44), consider some finite region V of $\mathbf{R}^3$. The external force on this region is

$$F^j = \frac{d}{dt}\int_V d^3x\,\langle T^{0j}\rangle + \oint_{\partial V} d^2a\,n_i\langle T^{ij}\rangle = \int_V d^3x\,\partial_m\langle T^{mj}\rangle\,. \tag{3.45}$$

Here and in the following, i and j are three-dimensional spatial indices, while m and n are $3+1$-dimensional Lorentz indices. The first term in the middle expression of (3.45) is the rate of change of momentum in this region, and the second term is the rate of escape of momentum through its boundaries. Using (3.41), one obtains

$$\begin{aligned} F^j &= \int_V d^3x \int \frac{d^3K}{(2\pi)^3}\frac{i}{z_H} K_m \langle T_K^{mj}\rangle e^{i\left[K_1(x^1-vt)+K_2x^2+K_3x^3\right]/z_H} \\ K_m &= \begin{pmatrix} -vK_1 & K_1 & K_2 & K_3 \end{pmatrix}. \end{aligned} \tag{3.46}$$

The expression for K^m in (3.46) is equivalent to (3.42) except that we have not specialized to $K_2 = K_\perp > 0$ and $K_3 = 0$. Now take the limit where V covers all of $\mathbf{R}^3$ so as to obtain the force on the whole system. Performing the x integral first, one obtains

$$F^j = iz_H^2 \int d^3K\, K_m \langle T_K^{mj}\rangle e^{-ivK_1t}\delta(K_1)\delta(K_2)\delta(K_3) = iz_H^2 \lim_{\vec{K}\to 0} K_m\langle T_K^{mj}\rangle \tag{3.47}$$

where we have anticipated that $K_m\langle T_K^{mj}\rangle$ has a smooth limit as $\vec{K} \to 0$. Indeed, using (3.35) and then (3.44) we arrive at

$$F^1 = i\frac{\pi T^2\sqrt{g_{YM}^2 N}}{\sqrt{1-v^2}} \lim_{\vec{K}\to 0} K_m Q^{m1} = \frac{\pi\sqrt{g_{YM}^2 N}}{2} T^2 \frac{v}{\sqrt{1-v^2}} \tag{3.48}$$

As promised, this is minus the drag force (2.28).

To restore conservation of T_{mn}, one may add to it a "counterterm:"

$$T_{mn} \to T_{mn} + \mathcal{T}_{mn} \tag{3.49}$$

where, after passing to a co-moving Fourier description,

$$K^m \mathcal{T}^K_{mn} = -K^m\langle T^K_{mn}\rangle = -\frac{iv}{2}\frac{\pi^3 T^4\sqrt{g_{YM}^2 N}}{\sqrt{1-v^2}}\begin{pmatrix} v & -1 & 0 & 0\end{pmatrix}. \tag{3.50}$$

A solution to (3.50) which is also traceless is

$$\begin{pmatrix} \mathcal{T}^K_{00} & \mathcal{T}^K_{01} \\ \mathcal{T}^K_{10} & \mathcal{T}^K_{11}\end{pmatrix} = \frac{iv}{2}\frac{\pi^3 T^4\sqrt{g_{YM}^2 N}}{(1-v^2)^{3/2}}\begin{pmatrix} 1+v^2 & -2v \\ -2v & 1+v^2\end{pmatrix} \tag{3.51}$$

with other components of $\mathcal{T}^K_{mn}$ vanishing. Using

$$\int \frac{d^3K}{(2\pi)^3}\frac{1}{K_1} e^{i[K_1(x^1-vt)+K_2x^2+K_3x^3]/z_H} = iz_H^2\theta(x^1-vt)\delta(x^2)\delta(x^3), \tag{3.52}$$

one finds

$$\begin{pmatrix} \mathcal{T}_{00} & \mathcal{T}_{01} \\ \mathcal{T}_{10} & \mathcal{T}_{11}\end{pmatrix} = -\frac{v}{2}\frac{\pi T^2\sqrt{g_{YM}^2 N}}{(1-v^2)^{3/2}}\theta(x^1-vt)\delta(x^2)\delta(x^3)\begin{pmatrix} 1+v^2 & -2v \\ -2v & 1+v^2\end{pmatrix}. \tag{3.53}$$

It would be cleaner if $\mathcal{T}_{mn}$ had delta function support at the location of the quark, but this does not appear to be possible: $\mathcal{T}^K_{mn}$ would then be analytic in K_1 and $K_\perp$, and there are no analytic solutions to (3.50). The form (3.53) of the counterterm indicates an unphysical "string," wholly in the boundary theory, that pulls forward on the quark to counteract the drag force.

The upshot of this somewhat extended discussion is that the original non-conserved form (3.30) captures the dynamics of dissipation and is non-conserved because it leaves out the external motive force that keeps the momentum of the quark from decreasing.

3.2.2 Near the horizon

Near the horizon of AdS_5-Schwarzschild, and for $vK_1 \neq 0$, the leading approximations to solutions to the equations of motion (3.14) and (3.21) are

$$A = \frac{e^{-\frac{ivK_1}{8}(\pi - \log 4)}}{4\left(1 - \frac{ivK_1}{2}\right)}(1-y)^{1-ivK_1/4} + U_A(1-y)^{-ivK_1/4} + V_A(1-y)^{ivK_1/4} \tag{3.54}$$

$$\begin{aligned}\begin{pmatrix} D_1 \\ D_2 \end{pmatrix} &= v^2\cos^2\theta \frac{e^{-\frac{ivK_1}{8}(\pi-\log 4)}}{4\left(1-\frac{ivK_1}{4}\right)^2}\begin{pmatrix} 1-y \\ s_{D_2} \end{pmatrix}(1-y)^{-ivK_1/4} + T_D^{(1)}\begin{pmatrix} v^2\cos^2\theta \\ 1 \end{pmatrix} \\ &+ T_D^{(2)}\begin{pmatrix} 1 \\ t_{D_2} \end{pmatrix}(1-y) + U_D\begin{pmatrix} u_{D_1}(1-y) \\ 1 \end{pmatrix}(1-y)^{-ivK_1/4} \\ &+ V_D\begin{pmatrix} v_{D_1}(1-y) \\ 1 \end{pmatrix}(1-y)^{ivK_1/4}\end{aligned} \tag{3.55}$$

$$\begin{aligned} s_{D_2} &= \frac{i}{vK_1}\left(1 - \frac{ivK_1}{4}\right) + \frac{4K^2}{(vK_1)^4}\left(1 - \frac{ivK_1}{4}\right)^2 \\ t_{D_2} &= \frac{K^2}{16 + (vK_1)^2} \qquad u_{D_1} = -\frac{ivK_1}{1 - \frac{ivK_1}{4}} \qquad v_{D_1} = \frac{ivK_1}{1 + \frac{ivK_1}{4}} \end{aligned} \tag{3.56}$$

$$\begin{aligned}\begin{pmatrix} E_1 \\ E_2 \\ E_3 \\ E_4 \end{pmatrix} &= \frac{ive^{-\frac{ivK_1}{8}(\pi-\log 4)}}{2K_1\left(1+\frac{ivK_1}{2}\right)}\begin{pmatrix} 1 \\ 0 \\ 1 \\ 0 \end{pmatrix} + T_E^{(1)}\begin{pmatrix} 1 \\ -\frac{1}{2} \\ 1 \\ -2 \end{pmatrix} + T_E^{(2)}\begin{pmatrix} \frac{3}{2}K_1^2v^2 \\ \frac{1}{4}K^2(1-y^4) \\ 0 \\ 0 \end{pmatrix} + \frac{T_E^{(3)}}{\sqrt{1-y}}\begin{pmatrix} 3(4+K_1^2v^2) \\ 0 \\ 4K^2(1-y) \\ -8K^2(1-y) \end{pmatrix} \\ &+ T_E^{(4)}\begin{pmatrix} K_1^2v^2\log(1-y) \\ 2 \\ 0 \\ 8 \end{pmatrix} + T_E^{(5)}\begin{pmatrix} 1 \\ 0 \\ 0 \\ \frac{8}{3}K^2(1-y) \end{pmatrix} + \frac{T_E^{(6)}}{\sqrt{1-y}}\begin{pmatrix} 3(4+K_1^2v^2) \\ 0 \\ 4(6+K^2)(1-y) \\ -8K^2(1-y) \end{pmatrix} \\ &+ U_E(1-y)^{-ivK_1/4}\begin{pmatrix} 0 \\ 0 \\ 0 \\ 1 \end{pmatrix} + V_E(1-y)^{ivK_1/4}\begin{pmatrix} 0 \\ 0 \\ 0 \\ 1 \end{pmatrix}.\end{aligned} \tag{3.57}$$

In these solutions, U_X, V_X, and $T_X^{(i)}$ are integration constants. Near-horizon solutions to the B and C equations are identical, respectively, to the D and A solutions (3.55) and (3.54), except that the particular solutions are zero.

For each set of equations, the solution multiplied by U_X is infalling (meaning that gravitons are falling into the black hole), while the solution multiplied by V_X is outfalling. The solutions multiplied by $T_X^{(i)}$ are neither infalling nor outfalling but can be categorized by their regularity properties at the horizon. The standard boundary condition imposed at a black hole horizon is that outfalling modes must vanish: $V_X = 0$ for $X = A$, B, C, D, and E.

The constraint equations (3.22) and (3.25) imply

$$T_D^{(2)} = T_E^{(3)} = T_E^{(4)} = T_E^{(5)} = 0\,. \tag{3.58}$$

The solutions in (3.55) and (3.57) multiplied by $T_D^{(1)}$, $T_E^{(1)}$, and $T_E^{(2)}$ are in fact exact solutions to the equations of motion for all y. Note that the exact solutions do not overlap with the ones removed by (3.58). This suggests that in the coupled systems of equations of motion and constraints for D_i and E_i, it may be possible to make further reductions of order. We have not pursued this avenue, but it might facilitate future numerical studies.

To further understand the boundary value problem that determines $\langle T_{mn}^K \rangle$, it is useful to again review the counting of integration constants, constraints, and boundary conditions:

- The ten second order equations of motion have 20 constants of integration which must be fixed in order to specify a unique solution.
- Ten constants of integration are fixed by requiring $R_X = 0$ at the boundary (no deformations of the gauge theory). The other ten are the $Q_X^{\rm tot}$, which are linear combinations of entries of $\langle T_{mn}^K \rangle$.
- Five relations among the $Q_X^{\rm tot}$ follow from imposing the constraints at the boundary.
- Five more boundary conditions must be imposed at the horizon to suppress the outfalling solutions.

Evidently, the number of constraints plus boundary conditions equals the number of integration constants in the equations of motion. So the boundary value problem is well posed. All the integration constants are complex, and the constraints and boundary conditions are too.

Similar counting of integration constants can be done after dividing the equations into the decoupled sets, A through E. Let us include this counting in a summary of the numerical algorithm we used. In the A set, one must impose $R_A = 0$. If we supply in addition an *ad hoc* value q for $Q_A^{\rm tot}$, then Cauchy data has been specified at the boundary. More precisely, approximate Cauchy data can be specified at a finite but small value $y = y_0$ by setting $R_A = 0$ and $Q_A^{\rm tot} = q$ equal to its *ad hoc* value and using (3.26) to determine $A(y_0)$ and $A'(y_0)$. The second order equation of motion (3.14) can then be integrated numerically to $y = y_1$, where y_1 is close to 1. The numerical solution can then be fit to the asymptotic form (3.54), and values of U_A and V_A can be extracted. Because all the equations are affine (meaning linear with inhomogeneous terms), V_A (as well as U_A) is an affine function $V_A(q)$ of the *ad hoc* value we supplied for $Q_A^{\rm tot}$. The equation $V_A(q) = 0$ may easily be solved for the physically meaningful value of $Q_A^{\rm tot}$.

For the D and E sets, the situation is only slightly more complicated. After setting $R_X = 0$ (see (3.26)) and imposing the constraint (for D) or constraints (for E), there is only one degree of freedom left at the boundary, which we can fix by supplying an ad hoc value for the quantity $Q_D^{\rm tot}$ or $Q_E^{\rm tot}$ that enters (3.30). Cauchy data for the equations of motion can be generated at $y = y_0$, and after numerically solving the equations of motion, the integration constants $T_X^{(i)}$, V_X, and $Q_X^{\rm tot}$ can be extracted by matching numerics to horizon asymptotics at $y = y_1$. To determine $Q_D^{\rm tot}$ or $Q_E^{\rm tot}$, one solves an affine equation $V_X(q) = 0$. It would have been numerically more efficient to eschew one of the equations of motion in the D set and all but one in the E set in favor of the first order constraint equations. But we found it a useful check of numerical accuracy to evaluate at $y = y_1$ the $T_X^{(i)}$ which are required by (3.58) to vanish.

The method of obtaining an affine function at the horizon by first specifying Cauchy

data at the boundary was described in [46] for graviton perturbations in AdS_5-Schwarzschild in the absence of the trailing string.

3.2.3 Large K behavior

The large K behavior of $Q^{\rm tot}_{mn}$ is dominated by the near-field of the quark. For $v = 0$, this field is entirely color-electric, and it is perfectly Coulombic because of the conformal symmetry of $\mathcal{N} = 4$ super-Yang-Mills theory. These observations alone, together with the radial symmetry and the conservation and tracelessness conditions, fix the $v = 0$ form of $Q^{\rm tot}_{mn}$ up to an overall prefactor:

$$Q^{\rm near}_{mn} = -\frac{\pi}{24|\vec{K}|}\begin{pmatrix} 2\vec{K}^2 & 0 & 0 & 0 \\ 0 & K_2^2+K_3^2 & -K_1K_2 & -K_1K_3 \\ 0 & -K_1K_2 & K_1^2+K_3^2 & -K_2K_3 \\ 0 & -K_1K_3 & -K_2K_3 & K_1^2+K_2^2 \end{pmatrix}. \tag{3.59}$$

In section 3.2.4 we explain how to fix the overall prefactor in (3.59).

$Q^{\rm near}_{mn}$ for $v \neq 0$ can be obtained by applying a Lorentz boost to (3.59). After this is done, one may define

$$Q^{K}_{mn} = Q^{\rm tot}_{mn} - Q^{\rm near}_{mn}\,. \tag{3.60}$$

Then $Q^K_{mn} \to 0$ as $K \to \infty$.[2] More useful in section 3.3 will be the equivalent forms

$$Q^K_X = Q^{\rm tot}_X - Q^{\rm near}_X \qquad X = A, D, E \tag{3.61}$$

where

$$Q^{\rm near}_A = Q^{\rm near}_D = \frac{\pi K}{16}\sqrt{1-v^2\cos^2\theta} \qquad Q^{\rm near}_E = \frac{\pi K}{24}\frac{2+v^2(1-3\cos^2\theta)}{\sqrt{1-v^2\cos^2\theta}}\,. \tag{3.62}$$

Recall that $Q_D = Q_{D_1}$ and $Q_E = Q_{E_1}$. To derive (3.62) one must compare the conserved terms in (3.30) with the Lorentz-boosted version of (3.59), with $K_3 = 0$ and $K_2 = K_\perp$ in the rest frame of the thermal plasma.

[2] Actually, Q^K_{mn} can be arranged to have an arbitrary $\vec{K}$-independent limit for large K by adjusting the choice of particular solution. This corresponds to adjusting a subtraction scheme for the infinite self-energy of the external quark. The form of solutions specified in (3.29), where the particular solution is assumed not to have a quartic term, is a sort of holographic minimal subtraction scheme.

3.2.4 Normalizing the near field

The prefactor can be fixed by observing that the equations (3.9) for $v = 0$, $h = 1$, and $\xi = 0$, as appropriate for a static string in AdS_5, can be solved for $K_\perp = 0$ by setting all the $H_{mn} = 0$ except for H_{00}, $H_{11} = 2y^3/9$, and $H_{22} = H_{33} = H_{00}/2 = -2f/3$, where $f(y)$ satisfies

$$\left[\partial_y^2 - \frac{3}{y}\partial_y - K_1^2\right] f = y\,. \tag{3.63}$$

This is precisely the equation satisfied by the $K_\perp = 0$ Fourier modes $\tilde{\phi}_K$ of the dilaton sourced by the same static string configuration: see (17) of [35]. Although (3.63) is non-trivial to solve directly, position space methods are available to extract the dilaton profile [47]. From them one can Fourier transform back to find $B_K = \pi|K_1|/16$, where B_K is defined through the asymptotic behavior

$$\tilde{\phi}_K = -\frac{y^3}{3} + B_K y^4\,. \tag{3.64}$$

From $H_{00} = -4f/3$ it follows that $Q_{00}^{\rm near} = -4B_K/3$; hence the prefactor in (3.59). Comparing (23) of [35] to (3.35) above, one may conclude that

$$\langle T_{00}\rangle = \frac{4}{3}\langle \mathcal{O}_{F^2}\rangle\,. \tag{3.65}$$

This is a positive quantity because $\mathcal{O}_{F^2} \sim \mathrm{tr}\,\vec{E}^2$ for the static quark. We do not know how to account for the factor of 4/3 in (3.65).

It is instructive to examine the same static quark solution using the equations (3.13)-(3.25). Taking $h = 1$ and $\xi = 0$ in these equations poses no difficulties. $K_\perp = 0$ means $\theta = 0$, which appears to lead to difficulties in (3.13) and (3.20) (the definitions of A, D_1, and D_2 in terms of H_{mn}). But the inverse relations expressing H_{mn} in terms of the $ABCDE$ variables are entirely non-singular in the limit $K_\perp \to 0$: they read

$$\begin{aligned}
H_{00} &= -\frac{2}{3}E_1 + \frac{2}{3}E_3 & H_{01} &= 2vE_2 \\
H_{02} &= 0 & H_{11} &= \frac{2}{3}E_3 - \frac{2}{3}E_4 \\
H_{12} &= 0 & H_{22} &= \frac{2}{3}E_3 + \frac{1}{3}E_4 \\
H_{33} &= \frac{2}{3}E_3 + \frac{1}{3}E_4\,.
\end{aligned} \tag{3.66}$$

We have omitted expressions for the $\mathbf{Z}_2$-odd components of the metric in terms of B_i and C because all these quantities vanish in the solution we're interested in. The equations of motion and constraints for A, D_i, and E_i are also non-singular in the limit $K_\perp \to 0$. The equations of motion and constraints for A and E_i are non-singular if one additionally takes $v \to 0$, but the constraint for D_i is not. Therefore in (3.67)-(3.71) we partially quote and partially solve the equations of motion and constraints for A and E_i after having set $v = 0$, but for D_i we keep v finite.

$$\left[\partial_y^2 - \frac{3}{y}\partial_y - K_1^2\right] A = y \tag{3.67}$$

takes precisely the same form as (3.63).

$$D_1 = d_1 + \frac{iy^4}{4K_1}\frac{v}{1-v^2} \qquad D_2 = d_1 + \frac{iy^4}{4K_1}\frac{1}{v(1-v^2)} \tag{3.68}$$

is the general solution of the D constraint consistent with the requirement that $D_i \to 0$ as $y \to 0$. The function d_1 satisfies

$$\left[\partial_y^2 - \frac{3}{y}\partial_y + K_1^2(1-v^2)\right] d_1 = y\,, \tag{3.69}$$

which takes the same form as (3.63) except for the replacement $K_1 \to K_1\sqrt{1-v^2}$.

$$E_1 = \frac{4}{3}e_1 + \frac{y^3}{9} \qquad E_2 = -E_3 = \frac{2}{3}e_1 - \frac{y^3}{9} \qquad E_4 = -\frac{2}{3}e_1 - \frac{2y^3}{9} \tag{3.70}$$

is the general solution of the E constraint consistent with the requirement that $E_i \to 0$ as $y \to 0$. The function e_1 satisfies

$$\left[\partial_y^2 - \frac{3}{y}\partial_y - K_1^2\right] e_1 = y\,, \tag{3.71}$$

which again is precisely the same form as (3.63),

Because (3.66) involves only the E_i, it was superfluous to explicitly solve the A and D_i equations in (3.67). But it is a worthwhile check to ensure that the quantities D_i, though singular in the limit $v \to 0$ (as well as in the limit $K_1 \to 0$), cause no problems for H_{mn}. Indeed one recovers the results for H_{mn} stated briefly around (3.63).

3.2.5 Small K behavior

A series expansion in small K allows some progress to be made on solving the equations of motion. We will first focus on the simplest case, namely the A equation. Plugging

$$A = \alpha_0 + K\alpha_1 + K^2\alpha_2 + \dots \tag{3.72}$$

into (3.14), one can find the differential equations satisfied by each α_j. The first three are:

$$\begin{aligned}
&\frac{y^3}{h}\partial_y\frac{h}{y^3}\partial_y\alpha_0 = \frac{y}{h}\\
&\frac{y^3}{h}\partial_y\frac{h}{y^3}\partial_y\alpha_1 = -i\frac{y}{h}\frac{\cos\theta\xi}{z_H}\\
&\frac{y^3}{h}\partial_y\frac{h}{y^3}\partial_y\alpha_2 = -\frac{y}{h}\left(\frac{\cos\theta}{z_H}\right)^2 - \frac{v^2\cos^2\theta - h}{h^2}\alpha_0\,.
\end{aligned} \tag{3.73}$$

Evidently, these equations are solvable through repeated integration. Integrating α_0 is easy, and after matching to the boundary asymptotics with $R_A = 0$ and the horizon asymptotics with $V_A = 0$, (both suitably expanded in K) one obtains

$$\alpha_0 = -\frac{1}{2}\log(1+y) - \frac{1}{4}\log(1+y^2) + \frac{i}{4}\log\frac{1-iy}{1+iy} = -\frac{y^3}{3} + \frac{y^4}{4} + O(y^7)\,, \tag{3.74}$$

which implies $Q_A^{\rm tot} = 1/4 + O(K)$. Higher order corrections to $Q_A^{\rm tot}$ can be found by solving the corresponding differential equations for each of the α_j's, and matching the solutions to the horizon and boundary asymptotics. To order $O(K^2)$ we have obtained

$$\begin{aligned}
Q_A^{\rm tot} = \frac{1}{4} - \frac{i\log 2}{8}vK_1 + \frac{K^2}{192}(6\pi - 12\log 2)\Big[&\sin^2\theta\\
&+ \left(1 - v^2 + v^2\frac{\pi^2 - 12(\log 2)^2}{6\pi - 12\log 2}\right)\cos^2\theta\Big] + O(K^3)\,.
\end{aligned} \tag{3.75}$$

A similar analysis can be carried out for the D and E sets. For the D set, for example, one first writes down series expansions in K for the second order differential equations (3.21), and solves for the corrections to D_1 and D_2 iteratively. By imposing the constraint (3.22) and by matching, at each order, the small K solution to the boundary asymptotics with $R_{D_1} = R_{D_2} = 0$ and to the horizon asymptotics with $V_D = 0$, one can then solve for the four integration constants and the corresponding corrections to $Q_{D_1}^{\rm tot}$, $Q_{D_2}^{\rm tot}$, U_D, $T_D^{(1)}$, and

$T_D^{(2)}$. To linear order in K, we find

$$Q_D^{\rm tot} = -\frac{i\sec\theta}{4vK} - \frac{\sec^2\theta - 4v^2}{16v^2} + \frac{iK\sec^3\theta}{64v^3}\big[1 + (2\log 2)v^2\cos^2\theta - (8\log 2)v^4\cos^4\theta\big] + O(K^2)\,. \tag{3.76}$$

Similarly, for the E set, we find

$$\begin{aligned} Q_E^{\rm tot} &= \frac{3iv(1+v^2)\cos\theta}{2K\left(1-3v^2\cos^2\theta\right)} - \frac{3v^2\cos^2\theta\left[2+v^2\left(1-3\cos^2\theta\right)\right]}{2\left(1-3v^2\cos^2\theta\right)^2} + O(K) \\ &= \frac{3iv(1+v^2)\cos\theta}{2K}\,\frac{1}{\left(1-3v^2\cos^2\theta\right)\left(1-\frac{ivK\cos\theta}{1+v^2}\right) - ivK\cos\theta} + O(K)\,. \end{aligned} \tag{3.77}$$

The striking feature of the expression is the singular behavior at $\theta = \cos^{-1}(1/v\sqrt{3})$, which is the Mach angle. From this we may conclude that there is a sonic boom in the thermal medium involving large amplitude but small momentum fields. In the second expression, we have shown how the $O(1)$ term may be "resummed" into the leading $O(1/K)$ expression so as to blunt the singularity into a form resembling a Lorentzian lineshape.

3.3 Results of numerics

Let us briefly recap the five-dimensional gravitational calculation that has been our main focus so far. The trailing string of [27, 28] sources the graviton, which propagates classically in AdS_5-Schwarzschild with purely infalling boundary conditions at the black hole horizon. The graviton's behavior near the boundary of AdS_5-Schwarzschild determines $\langle T_{mn}\rangle$ in the boundary gauge theory. Thus $\langle T_{mn}\rangle$ is a shadow (other authors might prefer the term "hologram") of the trailing string. See figure 3.1.

Our aim is to describe $\langle T_{mn}\rangle$ in the boundary theory. We will focus on Fourier coefficients Q_X^K for $X = A$, D, and E. As reviewed at the end of section 4.1, these quantities are Fourier coefficients of linear combinations of entries of $\langle T_{mn}\rangle$ with a near-field subtraction. Our numerical algorithm is outlined at the end of section 3.2.2. It was implemented primarily using Mathematica's `NDSolve`. To achieve good accuracy, it was necessary to develop asymptotic power series solutions to a considerably higher order than shown in sections 3.2.1

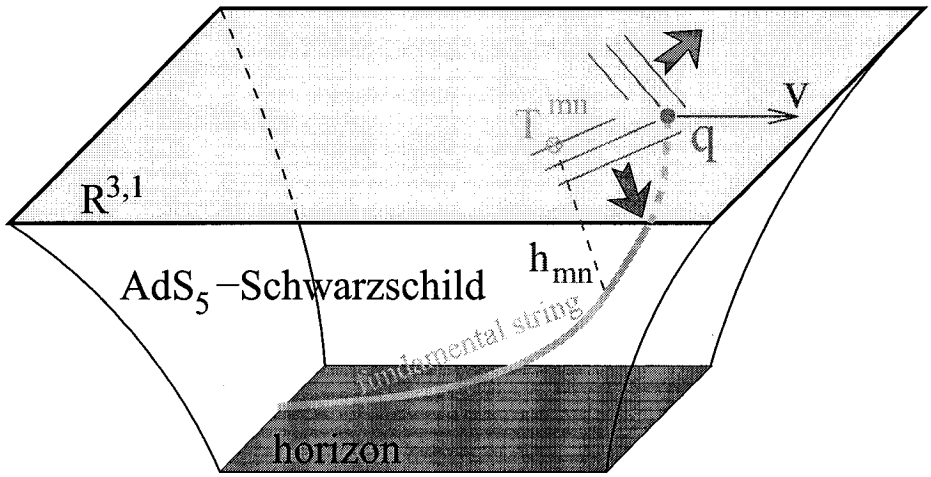

Figure 3.1: The AdS_5-Schwarzschild background is part of the near-extremal D3-brane, which encodes a thermal state of $\mathcal{N} = 4$ supersymmetric gauge theory [25]. The external quark trails a string into the five-dimensional bulk, representing color fields sourced by the quark's fundamental charge and interacting with the thermal medium.

and 3.2.2. Experience as well as common sense suggest that large K regions become more numerically challenging. We believe we have adequately met this challenge, partly by allowing arbitrarily many steps in `NDSolve` and calculating with a working precision of 30 digits (i.e. roughly twice the standard double precision of modern PC's). Another challenging region is small K_1, where the outfalling and infalling solutions are nearly constant until y is very close to 1. Experience suggests that at most a narrow region with $K_1 \ll K_\perp$ is problematic.

We found excellent agreement between the numerically computed $Q_X^{\rm tot}$ and the analytical approximations $Q_X^{\rm near}$ for large K and for $X = A$, D, and E. Only the subtracted quantities $Q_X^K = Q_X^{\rm tot} - Q_X^{\rm near}$ appear in the plots in figures 3.2-3.3. For Q_A^K and Q_D^K, we also found excellent agreement with the small K asymptotics (3.75) and (3.76) in the expected ranges. For Q_E^K, the nearly singular behavior near the origin is difficult for numerics to capture. This difficulty shows up in the ragged contours in figure 3.4c,d. The problem is not numerical error in evaluations of Q_E^K at individual points; rather, the ragged contours in figure 3.4c,d are due mostly to imperfect interpolations over a grid of limited resolution. Indeed, individual evaluations of Q_E^K for $K = \sqrt{K_1^2 + K_\perp^2} = 0.08$ agree with the small K

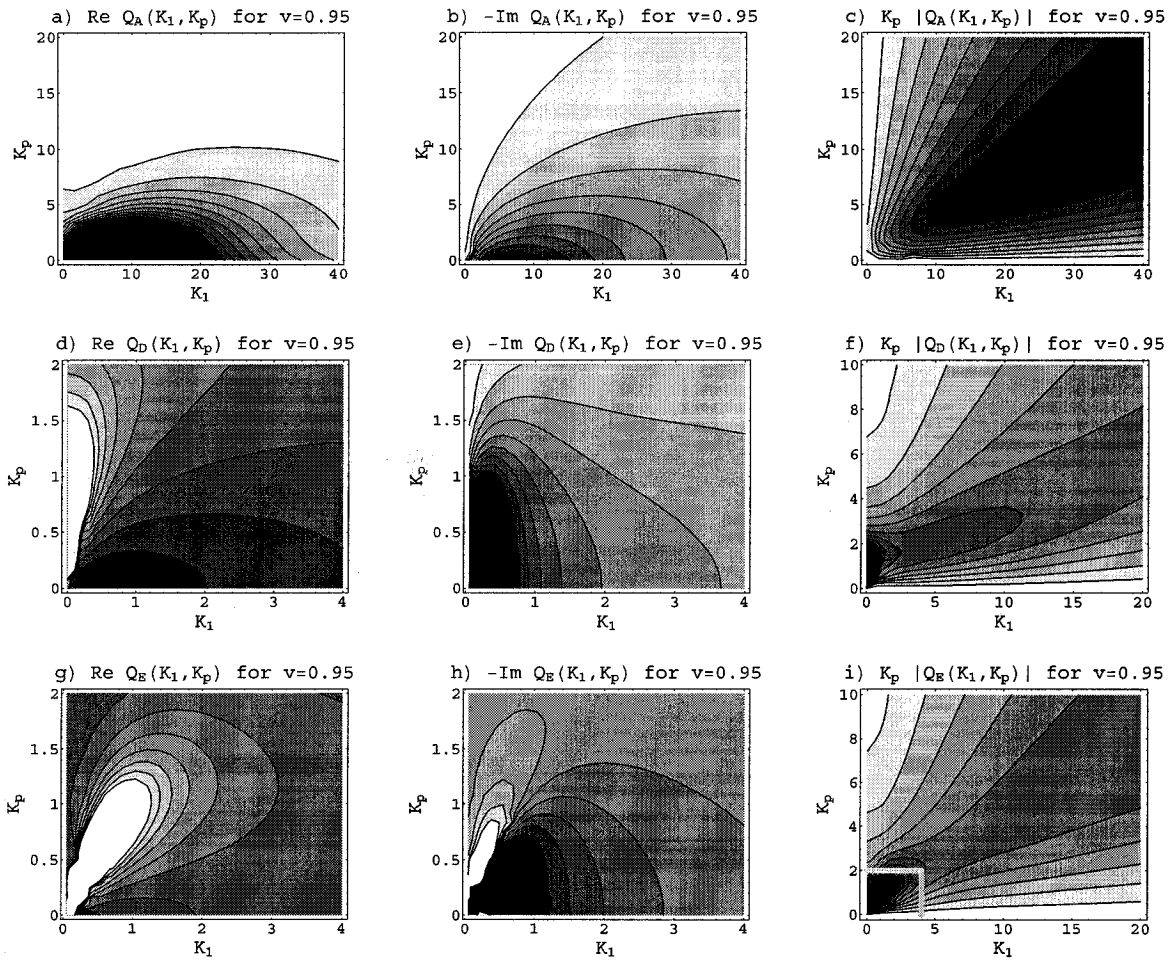

Figure 3.2: Contour plots of Q_A^K, Q_D^K, and Q_E^K for $v = 0.95$. The darker regions are more positive. All components of $\langle T_{mn}^K \rangle$ can be deduced from Q_A^K, Q_D^K, and Q_E^K using (3.30), (3.35), and (3.61). All three Q_X^K go to zero at large K. The momentum vector $\vec{K} = \vec{k}/\pi T$ can be read in GeV/c if one chooses $T = 318\,\mathrm{MeV}$: see (3.78). The range of momenta in each plot was chosen to show the most distinctive structures. The boxed region in (i) is plotted in more detail in figure 3.3c.

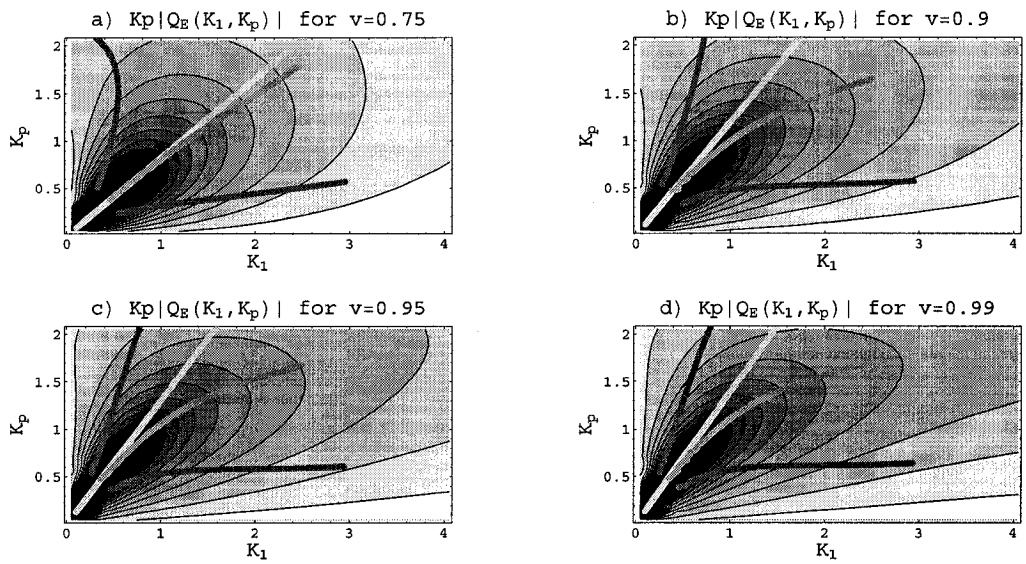

Figure 3.3: Contour plots of $K_\perp |Q_E^K|$ for various values of v. Q_E^K is proportional to the K-th Fourier component of the energy density after a near-field subtraction: see (3.30), (3.35), and (3.61). The phase space factor $K_\perp$ arises in Fourier transforming back to position space. The green line shows the Mach angle. The red curve shows where $K_\perp |Q_E^K|$ is maximized for fixed $K = \sqrt{K_1^2 + K_\perp^2}$. The blue curves show where $K_\perp |Q_E^K|$ takes on half its maximum value for fixed K.

asymptotics (3.77) at the level of about a percent. A high-resolution plot of $K_\perp |Q_E^K|$ at $K = 0.08$ is shown in figure 3.5a. In this plot, the results of numerics are visually indistinguishable from the analytic form (3.77). Even in the coarser-grained numerical evaluations of Q_E^K shown in figure 3.4, agreement with (3.77) was good a distance $\delta K \sim 0.015$ away from the central ridge.

Two qualitative features visible in figures 3.2-3.3 are worthy of note. The first is the high momentum ridges, which are most distinctive in figure 3.2c. This is the same feature that was noted in [35]; indeed, Q_A^K above is identical to B_K of [35]. High momentum ridges are also present in Q_D^K and Q_E^K. For $v = 0.95$ and $v = 0.99$, we find empirically that $Q_A^K \approx 4Q_D^K$ on the high momentum ridges. A more approximate relation for a similar region of momenta is $Q_E^K = 3Q_D^K$.

The second feature worthy of note is the sharp structures at low momentum in figures 3.2g,h,i. A more detailed view of these structures is shown in figure 3.3. As we will

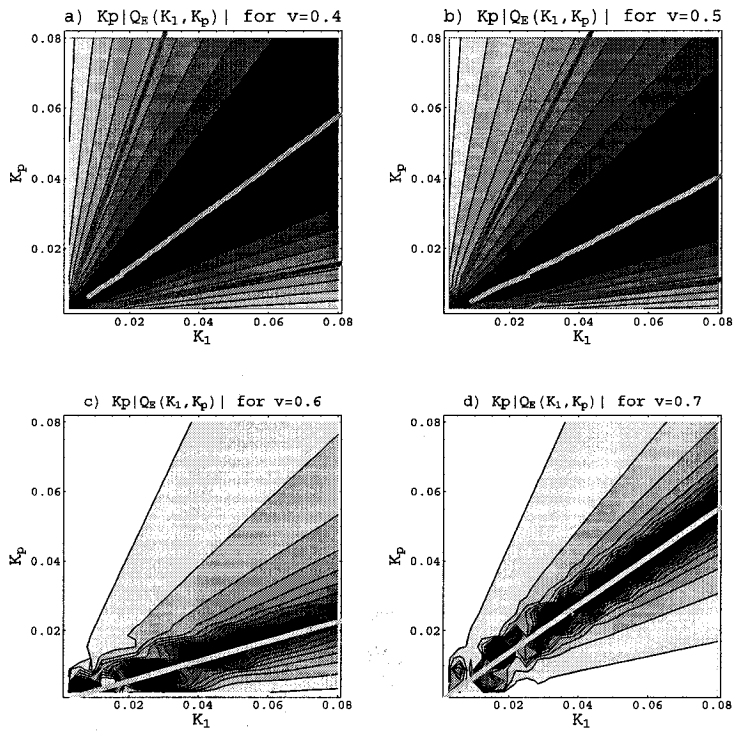

Figure 3.4: Contour plots of $K_\perp |Q_E^K|$ for various values of v at low momenta. The green line shows the Mach angle. The red curve shows where $K_\perp |Q_E^K|$ is maximized for fixed $K = \sqrt{K_1^2 + K_\perp^2}$. The blue curves show where $K_\perp |Q_E^K|$ takes on half its maximum value for fixed K.

discuss in section 4.5, the lobes in figure 3.3 are suggestive of high angle emission of particles in energy ranges accessible to experiments at RHIC. The lobes become narrower as one passes to small $\vec{K}$, corresponding to momenta much less than the temperature: see figure 3.4c,d. Low momentum is the hydrodynamic limit, so it is gratifying to see a highly directional feature corresponding to a sonic boom. Figures 3.4c,d thus serve as visual confirmation of the appearance of a sonic boom that we anticipated based on (3.77). Figures 3.4a,b show what happens when the velocity of the quark falls below the speed of sound $1/\sqrt{3} \approx 0.577$ in the thermal medium. Evidently, there is still directional emission, but it becomes abruptly less focused. The peak amplitude also decreases abruptly. Intriguingly, the drag force (2.28) behaves completely smoothly as one passes through $v = 1/\sqrt{3}$.

Readers wishing to examine our results more quantitatively are referred to [48].

3.4 Application to RHIC physics

Because all the calculations in this chapter were carried out in the framework of five-dimensional supergravity coupled to a classical string, the gauge theory results are accurate only to leading order in large N and large $g_{YM}^2 N$. Large 't Hooft coupling is largely inaccessible to standard techniques of finite-temperature quantum field theory, with the important exception of lattice gauge theory. But finite-temperature lattice methods are not well-adapted to real-time dissipative phenomena, in contrast to AdS/CFT, which provides ready access to both static and dissipative properties. Moreover, the AdS/CFT prescription for computing gauge theory observables is conceptually the same at all energy scales, giving some advantage over hydrodynamical approximations that are best justified in the infrared limit. So AdS/CFT occupies a unique niche in the range of tools available for understanding strongly coupled gauge theories at finite temperature. Its principal drawback is that the dual gauge theory is $\mathcal{N} = 4$ $SU(N)$ super-Yang-Mills, which in some ways is quite distant from real-world QCD. Within the limitations that we have described, the calculation of $\langle T_{mn} \rangle$ provides a fairly comprehensive description of dissipation from the heavy quark. All possible gauge interactions are included, in particular secondary interactions with the thermal medium of energetic particles radiated from the quark.

For the sake of definiteness, let us set

$$T = \frac{1}{\pi}\,\mathrm{GeV} = 318\,\mathrm{MeV}\,. \tag{3.78}$$

We understand this number to be in the upper range of temperatures for the quark-gluon plasma (QGP) produced at RHIC. It is a convenient choice for us because the K_1 and $K_\perp$ axes in figures 3.2, 3.3, and 3.4 can then be read in units of GeV/c.

In [35] we suggested that the high momentum ridges might be evidence that the strongly coupled thermal medium enhances fragmentation near the kinematic limit. But one of our warnings was that one should compute $\langle T_{mn} \rangle$ before making definitive statements. In light of the pronounced directional peak in $K_\perp |Q_E^K|$ at low K, we are inclined to regard the high momentum ridges as less immediately important to attempts to compare string theory

calculations to recent experimental results on jet-quenching. It is plausible that these ridges are the expression in Fourier space of a sharp "prow" of color fields supported near the quark. Moreover, we must bear in mind that at the typical energy scale $E \gtrsim 10\,\mathrm{GeV}$ where the high momentum ridges are pronounced, QCD is no longer particularly strongly coupled, so there is less justification for a connection with the supergravity approximation in AdS/CFT.[3]

Our most striking results are the directional lobes in $K_\perp |Q_E^K|$, as seen in figure 3.3. Recall that the factor of $K_\perp$ is appropriate because it is the measure factor arising in a Fourier transform back to position space after the azimuthal integral is performed. Recall also that Q_E^K is directly proportional to the K-th Fourier coefficient $\langle T_{00}^K \rangle$ of the energy density with the Coulombic near field subtracted away, whereas Q_A^K and Q_D^K are combinations of components of $\langle T_{mn}^K \rangle$ and non-conserved terms: see (3.30), (3.35), and (3.61). From figure 3.3 we conclude that in strongly coupled $\mathcal{N} = 4$ gauge theory at finite temperature, directional emission from a hard probe is present, but not sharply focused, at momenta several times the temperature. This seems to us an intuitively appealing conclusion: Rescattering effects broaden the directionality of the "wake" in Fourier space.

In figure 3.5 we show a small sampling of our numerical results in a format more suggestive of a comparison with experimental results [50, 51] on the splitting of the away side peak in di-jet hadron pair correlations. What we find attractive is that at momenta comparable to the window $1\,\mathrm{GeV}/c < p_T < 2.5\,\mathrm{GeV}/c$ of transverse momenta for the partner hadrons, there are broad peaks in the Fourier components $\langle T_{00}^K \rangle$ of the energy density: see figure 3.5c,d. These peaks are not unlike the ones seen at $\Delta\phi \approx 2$ in gold-on-gold collisions more central than 60%: see figure 2 of [51]. They are quite different from the narrow peak that we find at $80\,\mathrm{MeV}/c$ (figure 3.5a). At $80\,\mathrm{MeV}/c$, which is about a quarter the temperature, a hydrodynamic description is probably justified, and we should interpret the narrow

[3] When hadron pair correlators are plotted with higher momenta windows for the hadrons, we understand from an experimental colleague that the away side peak reappears [49]. The high momentum ridges might be relevant to such correlators: forward emission is indeed what they imply. But it is perhaps more plausible to attribute the reappearance of the away-side peak to away-side partons that have enough energy to punch through the QGP with only modest deflection.

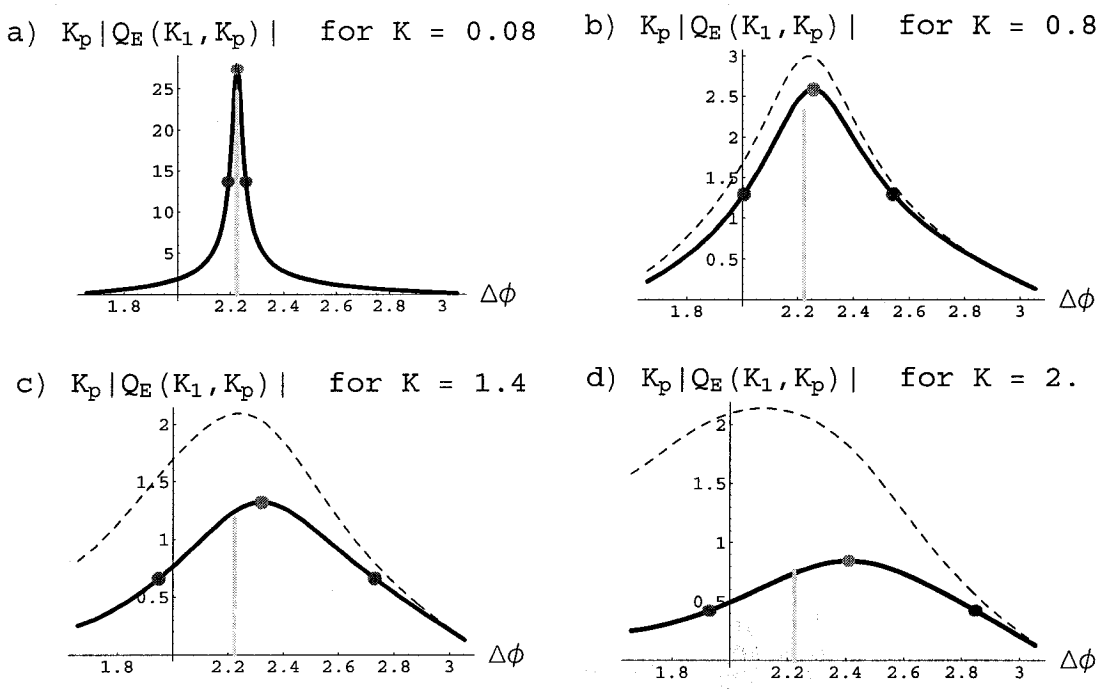

Figure 3.5: $K_\perp |Q_E^K|$ at fixed $K = \sqrt{K_1^2 + K_\perp^2}$ as a function of angle, for $v = 0.95$ and for various values of K. To facilitate comparison with di-jet hadron pair correlations, we have parameterized the angle as $\Delta\phi = \pi - \theta$, where $\theta = \tan^{-1} K_\perp / K_1$. With the usual assignment $T = 318\,\mathrm{MeV}$ (see (3.78)), K can be read in units of GeV/c. In each plot, the solid curve is from numerics; the dashed curve is the analytical approximation (3.77); the green line indicates the Mach angle; the red dot is at the maximum of $K_\perp |Q_E^K|$; and the blue dots indicate the points where $K_\perp |Q_E^K|$ is half of its peak value.

peak as a sonic boom. The analytic form

$$\langle T_{00}^K \rangle = \frac{\pi^3 T^4 \sqrt{g_{YM}^2 N}}{\sqrt{1-v^2}} \frac{3v(1+v^2)\cos\theta}{2iK} \frac{1}{(1-3v^2\cos^2\theta)\left(1 - \frac{ivK\cos\theta}{1+v^2}\right) - ivK\cos\theta} + O(K)\,, \tag{3.79}$$

which follows from (3.30), (3.35), and (3.77), is highly accurate in the infrared limit. One can see from figure 3.5 that for $v = 0.95$, (3.79) loses validity around $K \approx 1$, corresponding to $1\,\mathrm{GeV}/c$. In the interesting region of 1 to a few GeV/c, $\langle T_{00}^K \rangle$ decreases significantly more quickly with increasing K than the approximation (3.79) would indicate. This falloff may be a positive feature in comparing to data.

Let us enumerate the reasons to treat with caution the connection we allege between

our AdS/CFT calculations and the RHIC results on away side jet splitting.

1. Q_E^K is the hardest quantity to compute of the three that we investigated: the system of equations is more formidable, and the nearly singular behavior of Q_E^K near the origin makes numerical evaluations less stable. Moreover, our analytic approximation (3.77) is not as precise as for Q_A^K and Q_D^K, meaning that we have less extensive checks on numerics.

2. The $\Delta\phi$ in figure 2 of [51] is the separation in azimuthal angle, whereas in our figure 3.5 it is π minus the angle between the emission direction and the motion of the heavy quark.

3. The broad peaks at $\Delta\phi \approx 2$ in [51] are distinctive only after a subtraction related to elliptic flow.

4. The peaks of di-jet hadron pair correlations are closer to $\Delta\phi \approx 2$ than to the peak angle $\Delta\phi \approx 2.4$ in figure 3.5.

5. The experimental studies [50, 51] do not include heavy quark tagging, so most of the away side partons are presumably light quarks or gluons. But perhaps, for high-angle emission, what matters most is not the quark mass but simply the color current associated with a hard parton.

6. After a parton leaves the QGP, it fragments, and then its fragmentation products must be detected. We do not have the expertise to add these important aspects of the physics to our calculations.

7. The QGP cools, expands, and hadronizes, and its equation of state changes with time as a result. The conformal result $c_s = 1/\sqrt{3}$ is likely to be a reasonable approximation only in the QGP regime, at temperatures significantly above the deconfinement transition. As remarked in [52], a steeper emission angle results from a time-averaged speed of sound that could be as low as $c_s \approx 0.33$. It might be possible to partially mimic the changing equation of state by some deformation of AdS_5-Schwarzschild, but it's

not clear that the result would have the same status as a first-principles calculation that can be claimed for our analysis.

8. One of our many idealizations of the true experimental setup is that we replaced the QGP by a thermal medium of infinite extent. This could mean that we are exaggerating the effects of secondary rescatterings. It would be desirable to have some position space representations of components of the stress tensor to address this issue.

9. It remains a deep mystery when and why strongly coupled $\mathcal{N} = 4$ gauge theory should be directly compared with real-world QCD. Doing so somewhat above the deconfinement and chiral symmetry breaking transitions is clearly the best hope. But we return to the basic conundrum: are near-extremal D3-branes merely an analogous system to the QGP, or can they capture the dynamics sufficient precisely to be a useful guide to RHIC physics?

It is clear from figure 3.3 that as one passes to higher momenta, the peak emission direction becomes more forward, although at the same time the peak keeps broadening. It would be interesting to compare the dependence of $\langle T^K_{00} \rangle$ on both the magnitude and angle of $\vec{K}$ with two-dimensional histograms of p_T and $\Delta\phi$ for partner hadrons.

As K increases beyond the range shown in figure 3.3, one eventually passes into the region of high momentum ridges, which become more and more forward as $v \to 1$.[4] As we understand the experimental situation, the away side peak reappears as one increases the momentum window for the hadrons. An optimistic read of this situation is that AdS/CFT calculations may have some relevance up to an unexpectedly high range of momenta; but perhaps it is more reasonable simply to suppose that sufficiently high-momentum partons can punch through the QGP without much deflection.

There have been other notable theoretical efforts to understand the splitting of the away side jet. An account of the sonic boom picture can be found in [52]. Investigations of the

[4]We thank J. Casalderrey-Solana for pointing out that the peak angle of the high momentum ridges decreases roughly as $1/\gamma$, and for the interesting remark that this behavior may signal some connection with the Landau-Pomeranchuck-Migdal effect (see for example [53]).

Cerenkov radiation have been pursued in [54, 55]. The conical flow picture has been seen in [56] using the hydrodynamical evolution of QGP, and in [57] using linear response theory. In [57] the Mach cone picture appears only in the strongly coupled QGP. In comparing with these more phenomenological works, it must be admitted that we have made dramatic and risky idealizations of the experimental setup. Yet, despite the potential stumbling blocks, it is exciting to see a simple type IIB string theory construction approaching quantitative comparisons with a data-rich experimental field.

Chapter 4

Higher-Order Corrections to Einstein Gravity

In the previous chapter, we used $AdS_5 \times S^5$ at finite temperature, the gravity dual in the AdS/CFT sense of an $\mathcal{N} = 4$ Super Yang-Mills plasma, to try to calculate the string theory prediction for jet quenching at RHIC. However, there were some obvious problems—the field content of $\mathcal{N} = 4$ SYM is not the same as QCD, and strictly speaking, the calculation is valid only at $1/\lambda_t = 0$, whereas the value of the inverse 't Hooft coupling at RHIC is in the 0.05 to 0.1 range.

The D3-brane construction takes place in the context of Type IIB string theory, and it is known that the leading curvature correction to Einstein gravity from Type IIB is proportional to $\alpha'^3 R^3$ (relative to the leading term of order R) where R is a curvature tensor. Roughly, this means that corrections to SYM computations should be $\mathcal{O}(\alpha'^3 L^{-6}) = \mathcal{O}(\lambda_t^{-3/2})$. At RHIC, this is on the order of a few percent, which is the reason why there is some hope to detect uniquely stringy effects, should some admittedly significant theoretical and experimental hurdles be crossed.

In this chapter, we detail a methodology for computing all higher order corrections to Einstein gravity coming from the Type II string. Our method is precise only for highly symmetric spacetimes, but fortunately for AdS/CFT, this is precisely the regime of interest.

Furthermore, we will still need to use some perturbative techniques. Rather than expand in the traditional parameter of $\alpha' R$, we will instead expand in $1/D$, the spacetime dimension of the dual conformal field theory. Doing so allows us to extract information on all higher order corrections like $\alpha'^k R^k$.

Along the way, we will find other candidate string theory backgrounds, including pure AdS_5 in the absence of D-branes, which at least has the correct symmetries to be dual to non-supersymmetric Yang-Mills theory. The existence of this background was originally proposed in [58]. It will also have finite curvature and hence finite 't Hooft coupling, making it a curious candidate for further study.

4.1 A basic review of string worldsheet theory

The string "worldsheet" is the two-dimensional surface swept out by the string as it propagates [24, 59]. The usual story in string theory is that the coordinates of spacetime $X^\mu(\tau, \sigma)$ are functions of the coordinates of the worldsheet, and that the action of the string is simply its geometric area:

$$S = \frac{1}{2\pi\alpha'} \int d^2\sigma \sqrt{-\det G_{\mu\nu} \partial_a X^\mu \partial_b X^\nu} \,. \tag{4.1}$$

The metric for these coordinates $G_{\mu\nu}$ is interpreted as the metric of spacetime, often referred to as the "target space". Through a particular transformation, this action can be reduced to the so-called "Polyakov action":

$$S = \frac{1}{2\pi\alpha'} \int d^2\sigma \sqrt{-\det \gamma_{ab}} \gamma^{ab} G_{\mu\nu}(X) \partial_a X^\mu \partial_b X^\nu \,. \tag{4.2}$$

Instead of an action representing the geometric area of the string, this now looks like a two-dimensional quantum field theory, where the spacetime coordinates X^μ are a set of quantum fields and γ_{ab} is the two-dimensional metric. Classically, this theory is "conformally invariant" as a worldsheet theory. This means that if one makes a conformal transformation such as $\gamma_{ab} \to e^{\varphi(\tau,\sigma)} \gamma_{ab}$, the action remains invariant, since $\sqrt{-\det \gamma_{ab}} \to e^{\varphi} \sqrt{-\det \gamma_{ab}}$, and the metric with two upper indices picks up a factor of $e^{-\varphi}$.

On a quantum level, the story is different. The spacetime metric $G_{\mu\nu}(X)$ appears from a two-dimensional perspective as a set of couplings multiplying the kinetic terms of the fields X^μ. Thus, like most couplings in a quantum field theory, they will depend on the energy scale—this is, for instance, the basis behind the idea that the standard model interactions unify at some energy scale where their couplings all take on nearly the same value. This energy-scale dependence is in complete contradiction to the notion of a "conformal field theory", since a CFT requires that all physical observables be independent of any length or energy scale. However, in order for the string theory to depend only on the spacetime coordinates X^μ, and not on any choice of worldsheet coordinates or conformal factors e^φ, we must require that the theory remain conformal at a quantum level.

To do so, the couplings $G(X)$ must take on very special values, called "fixed points" of their energy-dependent flow. Recall that the beta function for a coupling L tells us how that coupling depends on the energy scale M of the problem:

$$\beta(L) \equiv \frac{\partial L}{\partial M} \,. \tag{4.3}$$

Generically the beta function will depend on L, and if it happens to vanish at some particular value of L, then *at that value*, the coupling will not change as we change the energy scale. Hence this particular value of L is called a fixed point.

Since the spacetime metric $G_{\mu\nu}$ appears as a set of couplings in the theory, we have a set of beta functions. In fact, the beta function is [60]:

$$\beta_{\mu\nu}(G) = R_{\mu\nu} + \mathcal{O}(\alpha' R^2) \,. \tag{4.4}$$

where the first term on the right-hand side is simply the Ricci tensor for the metric G. This is quite an amazing result: It tells us that in order for the theory to be conformal at the quantum level, the spacetime must satisfy $R_{\mu\nu} = 0$. But this also means that the spacetime must satisfy Einstein's equations in vacuum! It is in this way that string theory reproduces classical general relativity when the curvature is small.

Note though that the omitted terms in (4.4) are those terms that string theory predicts for corrections to Einstein gravity when the curvature reaches the order of the string scale

α'. As noted above, it is precisely those terms that we aim to compute in this chapter.

We will restrict ourselves from the start to symmetric spacetimes with negative curvature, *i.e.*, AdS spaces and their Euclidean versions, also called hyperbolic spaces. We will allow the overall radius of the space L to vary, and the high symmetry of the target space means that this characteristic radius is the only coupling in the theory. We will see that, to the best of our ability to calculate, there does exist a fixed point when $L^2 \sim \alpha'$.

Since the same theory on a sphere instead of a hyperboloid is referred to as the $O(N)$ vector model, or the non-linear sigma model, and we will often adopt language from that set of literature. In particular, we will often refer to the spacetime fields X^μ as $\vec{n}$ instead.

We also estimate the central charge of the non-trivial fixed point [59]. Recall that the central charge is in some sense a measure of the number of degrees of freedom of the worldsheet theory, and contains information about the required dimension of spacetime. In order for the spacetime interpretation of the theory to be well-defined, there is a requirement that the total central charge of the theory must vanish. In the bosonic theory, one gets a negative contribution of -26 coming from the freedom to change coordinates on the worldsheet. When the target space is flat, $G_{\mu\nu} = \eta_{\mu\nu}$, the worldsheet bosons $\vec{n}$ supply one unit of central charge each, hence there is net zero central charge when $\vec{n}$ has 26 members, *i.e.*, when spacetime is 26 dimensional. In the supersymmetric case, the ability to reparameterize gives a central charge of -15. The worldsheet bosons still contribute one unit each, but each fermionic superpartner contributes $1/2$, giving a critical dimension of 10. When the target space is curved, we will see that the story changes, and the critical dimension is not so simple.

4.2 Our worldsheet theory of interest

Consider the bosonic non-linear sigma model (NLσM) in d dimensions, whose target space is Euclidean anti-de Sitter space (AdS_{D+1}) with $D+1$ dimensions. Explicitly, the classical

action is

$$S = \frac{1}{4\pi\alpha'} \int d^d x \, (\partial n_\mu)^2 \tag{4.5}$$

where n_μ is constrained to satisfy

$$n_\mu^2 = n_0^2 - n_1^2 - \ldots - n_{D+1}^2 = -L^2 < 0 \,. \tag{4.6}$$

We will present some evidence that the NLσM (4.5), as well as supersymmetric generalizations of it, has a fixed point in $d = 2$ when $\alpha' D/L^2$ is close to 1, at least for sufficiently large D, in addition to the usual trivial zero at flat space $L \to \infty$. Briefly, the evidence is this: the most accurate calculations that we know, both as an expansion to fixed order in α'/L^2, and as an expansion in $1/D$ with finite $\alpha' D/L^2$, lead to beta functions which have non-trivial zeroes. It is worth noting that these fixed points do not rely on the presence of stress-energy from extended objects like D-branes, *i.e.*, so-called Ramond-Ramond fields on the worldsheet. Instead, these zeroes arise because of competition between the one-loop term and higher loop terms. In the language of an effective action on target space, the zeroes arise because of competition between the Einstein-Hilbert term and higher powers of the curvature.

It is possible that this evidence is misleading. Higher order contributions to the beta function, both in an α'/L^2 expansion and in a $1/D$ expansion, could be as large or larger than the ones that we are able to compute.

The bulk of this chapter is devoted to an exposition of two methods of computing the beta function for the theory (4.5) and its supersymmetrizations. In section 4.3 we review results at fixed order in α', *i.e.* fixed loop order. The state of the art is four loops. In section 4.4 we explain how the leading D dependence (and, in the bosonic case, the first sub-leading D dependence) of all higher loop terms can be extracted from a $1/D$ expansion with finite $\alpha' D/L^2$. There the state of the art is terms of order $1/D^2$ relative to the one loop term. We note a peculiar feature of the beta function: its slope is large and negative at its non-trivial zero, so corrections to scaling are controlled by an operator of *negative* dimension, *i.e.*, its two-point function *increases* with distance. We offer a heuristic explanation of what this could mean, hinging on the supposition that infrared fluctuations are large.

In section 4.5, we discuss possible consequences of a zero of the beta function: in particular, based on the results for the central charge, we speculate that the supersymmetric AdS_5 NLσM may provide a string-scale holographic dual of Yang-Mills theory, and that finite volume quotients of AdS_3 may be used in compactifications to four dimensions. In section 4.6, we review the results and conjectures made in this chapter.

4.3 Anti-de Sitter target spaces at fixed order in α'

The partition function of the NLσM (4.5) depends on α' and L^2 only in the combination

$$g = -\frac{\alpha'}{L^2}\,, \tag{4.7}$$

which we define to be negative in order to anticipate a connection with the literature on $O(N)$ vector models. In the scheme of dimensional regularization with minimal subtraction, one obtains the following beta function, up to four loops [61, 62, 63]:

$$\begin{aligned}\beta(g) = &-Dg^2 - Dg^3 - \frac{1}{4}D(D+4)g^4 \\ &+ \left(\frac{D^3}{12} - \frac{3}{2}(1+\zeta(3))D^2 + \frac{1}{2}(3\zeta(3)-1)D\right)g^5 + O(g^6)\,.\end{aligned} \tag{4.8}$$

As is evident from figure 4.1, the non-trivial fixed point is present or absent depending on how many terms one retains. This is discouraging. At first glance, it seems not merely plausible but likely that a computation of the $O(g^6)$ term would make the non-trivial zero disappear. However, as we shall describe in section 4.4, merging the fixed order information (4.8) with the best results we could obtain from a large D expansion, one winds up with a beta function that does have a non-trivial fixed point. The large D results contain partial information about terms in $\beta(g)$ with arbitrarily high powers of g.

Before presenting results from a large D expansion, we will describe the relation of the AdS_{D+1} NLσM to the $O(N)$ vector model with $N = D + 2$, present the supersymmetrizations of the AdS_{D+1} NLσM, and briefly survey results on the beta functions of each model.

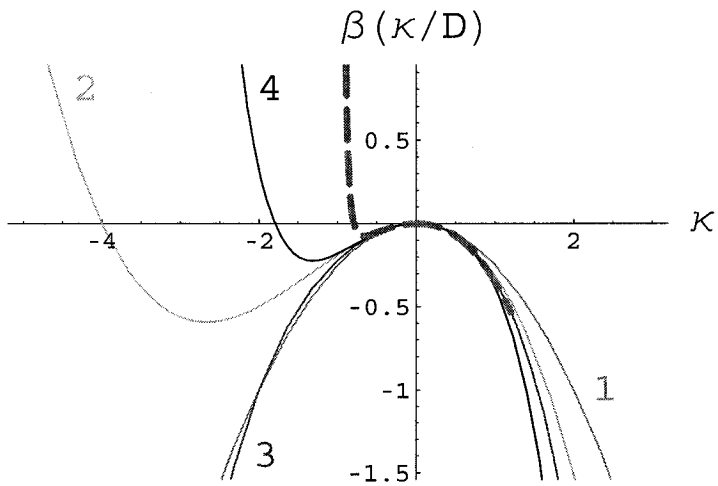

Figure 4.1: The solid lines show successive fixed-order approximations to $\beta(g)$ for $D = 4$. For comparison with large D results, it is convenient to use $\kappa = gD$ to parametrize the horizontal axis. Each approximation is marked with its loop order. The dashed line is the large D result through order D^{-2}, also for $D = 4$.

4.3.1 The $O(N)$ vector model continued to negative coupling

The partition function for the bosonic AdS_{D+1} NLσM can be written in a variety of ways:

$$\begin{aligned} Z &= \int \mathcal{D}n_\mu \, \delta(n_\mu^2 + L^2)\theta(n_0) \exp\left\{-\frac{1}{4\pi\alpha'}\int d^dx \, (\partial n_\mu)^2\right\} \\ &= \int \frac{\mathcal{D}\vec{n}}{\sqrt{L^2+\vec{n}^2}} \exp\left\{-\frac{1}{4\pi\alpha'}\int d^dx \left[(\partial\vec{n})^2 - (\partial\sqrt{L^2+\vec{n}^2})^2\right]\right\} \\ &= \int \frac{\mathcal{D}\vec{\Pi}}{\sqrt{1-g\vec{\Pi}^2}} \exp\left\{-\frac{1}{4\pi}\int d^dx \left[(\partial\vec{\Pi})^2 + \frac{1}{g}\left(\partial\sqrt{1-g\vec{\Pi}^2}\right)^2\right]\right\} \end{aligned} \tag{4.9}$$

where we have split $n_\mu = (n_0, \vec{n})$ into the time-like component and the spatial $(D+1)$-component vector $\vec{n}$, defined $\vec{\Pi} = \vec{n}/\sqrt{\alpha'}$, dropped some inessential prefactors,[1] and defined g as in (4.7). Recall that $g < 0$.

Now recall the classic perturbative treatment of the low-temperature phase [65], in which one starts with an N-component Euclidean vector field n_μ subject to the constraint

[1] Dropping infinite prefactors is a formal manipulation, particularly since one of them is the reciprocal of the infinite volume of AdS_{D+1}. To see why this factor should be there, consider defining the NLσM on a finite lattice rather than in a continuum limit. Then to get a finite partition function, one must fix one spin to a particular location in AdS_{D+1}. See [64] for a more thorough discussion. This subtlety shouldn't affect the beta function.

$n_\mu^2 = \delta^{\mu\nu} n_\mu n_\nu = L^2 > 0$ and writes the partition function as

$$\begin{aligned} Z &= \int \mathcal{D}n_\mu \, \delta(n_\mu^2 - L^2) \exp\left\{ -\frac{1}{4\pi\alpha'} \int d^d x \, (\partial n_\mu)^2 \right\} \\ &= \int \frac{\mathcal{D}\vec{n}}{\sqrt{L^2 - \vec{n}^2}} \exp\left\{ -\frac{1}{4\pi\alpha'} \int d^d x \left[(\partial \vec{n})^2 + (\partial \sqrt{L^2 - \vec{n}^2})^2 \right] \right\} \\ &= \int \frac{\mathcal{D}\vec{\Pi}}{\sqrt{1 - g\vec{\Pi}^2}} \exp\left\{ -\frac{1}{4\pi} \int d^d x \left[(\partial \vec{\Pi})^2 + \frac{1}{g} \left(\partial \sqrt{1 - g\vec{\Pi}^2} \right)^2 \right] \right\} \end{aligned} \tag{4.10}$$

where we have again split $n_\mu = (n_0, \vec{n})$ into a single (Euclidean) component n_0 and a $(N-1)$-component vector $\vec{n}$. $\vec{\Pi}$ is defined identically as in (4.9), but now $g = \alpha'/L^2$. Note that $g > 0$.

The key observation is that the last lines of (4.9) and (4.10) are identical. The sign of g determines whether one is treating the S^{N-1} model or the AdS_{D+1} model.[2] So, at the perturbative level, one may simply continue a quantity like $\beta(g)$ from the $O(N)$ model to negative g, set $N = D + 2$, and apply the result to the AdS_{D+1} NLσM. At a non-perturbative level, it is less clear that there is a definite relation between the $O(N)$ model and the AdS_{D+1} model: the obvious difficulty in comparing the last lines of (4.9) and (4.10), for example, is that in the latter case one must explicitly bound $|\vec{\Pi}|^2 < 1/g$. (More precisely, one must attach the lower hemisphere of S^{N-1} to complete the partition function.)

4.3.2 Supersymmetrizations of the $O(N)$ model

Having understood that results from the $O(N)$ model can be applied directly to the AdS_{D+1} via the continuation discussed in the previous section, let us now re-express the $O(N)$ model and its supersymmetrizations in the form that is most convenient for perturbative calculations:

$$\begin{aligned} Z &= \int \mathcal{D}S \, \delta(S^2 - 1) \exp\left\{ -\frac{1}{4\pi g} \int d^d x (\partial S)^2 \right\} \\ &= \int \mathcal{D}S \mathcal{D}\sigma \exp\left\{ -\frac{1}{4\pi g} \int d^d x \Big[(\partial S)^2 + \sigma(S^2 - 1) \Big] \right\}, \end{aligned} \tag{4.11}$$

[2] We will persist in using both D and $N = D+2$ in order to ease the notational transition from well-known results on the $O(N)$ vector model to the $\mathrm{AdS}_{D+1}/\mathrm{CFT}_D$ correspondence.

where σ runs over imaginary values and we omit the target space index on S. The $(1,1)$ supersymmetric extension of the $O(N)$ model involves N superfields $\mathbf{S}_\mu = (S_\mu, \psi_\mu, F_\mu)$ and one additional superfield $\mathbf{\Phi} = (\phi, u, \sigma)$ to enforce the constraint $\mathbf{S}^2 = 1$ [66, 67]:

$$S = \frac{1}{4\pi g}\int d^2x \left[(\partial S)^2 + \bar{\psi} i \not{\partial} \psi + F^2 + \sigma(S^2-1) + \phi\bar{\psi}\psi + 2\bar{u}\psi S + 2SF\phi\right]. \qquad (4.12)$$

The $(1,0)$ supersymmetric extension involves N superfields $\mathbf{S}_\mu = (S_\mu, \psi_\mu)$ and an additional spinorial superfield $\mathbf{U} = (u, \sigma)$ to enforce the constraint:

$$S = \frac{1}{4\pi g}\int d^2x \left[(\partial S)^2 + \bar{\psi} i \not{\partial} \psi + \sigma(S^2-1) + 2\bar{u}\psi S\right]. \qquad (4.13)$$

ψ_μ and u are both chiral, but with opposite handedness. In all cases, $g = \alpha'/L^2$ where L is the radius of S^{N-1}. Appropriate continuations of (4.12) and (4.13) to negative g lead to supersymmetric AdS_{D+1} NLσM's, analogously to the treatment in section 4.3.1 of the bosonic case.

One can regard (4.11), (4.12), and (4.13) as the starting points for describing bosonic, type II, and heterotic strings propagating on a sphere S^{N-1} with radius $L = \sqrt{\alpha'/g}$. These are not consistent string backgrounds, but one may nevertheless borrow from the literature [68, 69, 70, 71, 72, 73] on general NLσM's on the string worldsheet to extract fully covariant forms of the beta function. In a minimal subtraction scheme, we have

$$\begin{aligned}
&\text{bosonic:} && \beta_{ij} = \alpha' R_{ij} + \frac{\alpha'^2}{2} R_{iklm} R_j{}^{klm} + O(\alpha'^3) \\
&\text{heterotic:} && \beta_{ij} = \alpha' R_{ij} + \frac{\alpha'^2}{4} R_{iklm} R_j{}^{klm} + O(\alpha'^3) \\
&\text{type II:} && \beta_{ij} = \alpha' R_{ij} + \frac{\zeta(3)\alpha'^4}{2} R_{mhki} R_{jrt}{}^{m} (R^k{}_{qs}{}^r R^{tqsh} + R^k{}_{qs}{}^t R^{hrsq}) + O(\alpha'^5).
\end{aligned} \qquad (4.14)$$

To obtain (4.14), we have set to zero all deformations corresponding to matter fields (for example, B_{ij}), and assumed $R_{ijkl;m} = 0$, as is appropriate for any symmetric space. The beta function for g may be expressed as

$$\beta(g) \equiv M\frac{\partial g}{\partial M} = -\frac{g}{N-1} G^{ij}\beta_{ij}. \qquad (4.15)$$

Plugging

$$R_{ijkl} = \frac{1}{L^2}(g_{ik}g_{jl} - g_{jk}g_{il}) \tag{4.16}$$

into (4.14), and using (4.15), one obtains

$$\begin{aligned}
&\text{bosonic:} && \beta(g) = -Dg^2 - Dg^3 + O(g^4) \\
&\text{heterotic:} && \beta(g) = -Dg^2 - \frac{1}{2}Dg^3 + O(g^4) \\
&\text{type II:} && \beta(g) = -Dg^2 - \frac{3}{2}\zeta(3)D(D-1)g^5 + O(g^6)\,,
\end{aligned} \tag{4.17}$$

where we have expressed the final results in terms of $D = N - 2$ to facilitate comparison with (4.8). Evidently, the bosonic result agrees with (4.8),[3] and all three beta functions to the order specified have non-trivial zeroes for negative g.

Let us now briefly anticipate the gist of section 4.4. The fixed-order results so far sketched for the bosonic NLσM and its $(1,1)$ supersymmetrization can be supplemented by the leading-order D dependence of the coefficients of all higher powers in g from a large D expansion, obtained for the most part from [74, 75] in the bosonic case and [66, 67] in the $(1,1)$ supersymmetric case. The results will be beta functions with zeroes for gD slightly larger than -1. The analogous calculation in the heterotic case was carried out in [76].

4.3.3 Scheme dependence

It is well known (see for example [77]) that field redefinitions can alter terms in the beta function at two loops and higher so that they involve only the Weyl tensor. Such redefinitions do not affect the S-matrix elements that were used [70] to anticipate the existence of an α'^3 term in the beta function for the general $(1,1)$ supersymmetric NLσM.

AdS_{D+1} has no Weyl curvature, so we can conclude for the AdS_{D+1} NLσM (and its supersymmetrizations) that there is a scheme—call it a "Weyl tensor" scheme—where higher loop terms make no contribution to the beta function at all. If a Weyl tensor scheme is

[3]Note that we do not even need to appeal to the continuation argument of section 4.3.1 to relate the bosonic result in (4.14) to (4.8): we could plug the negative curvature metric of AdS_{D+1} into the covariant expressions directly and wind up with the same two-loop result.

employed, then clearly there can be no non-trivial zero of the beta function.[4]

Existence or non-existence of a fixed point is supposed not to depend on scheme. But what could happen is that a Weyl scheme pushes the zero to $g \to -\infty$. In the absence of a systematic treatment of the stability of various schemes, it seems best to us to choose a standard one (like dimensional regularization with minimal subtraction) that does not presuppose an answer to the question we're interested in—as a Weyl scheme effectively does for the existence or non-existence of a non-trivial AdS_{D+1} fixed point.

4.4 Anti-de Sitter target spaces in a $1/D$ expansion

It is apparent from (4.8) that the effective expansion parameter is gD rather than g. More precisely: except for the one-loop term, the coefficient of the $O(g^n)$ term in $\beta(g)$ is a polynomial in D of order $n-2$. In the $(1,1)$ supersymmetric case displayed in (4.17), the coefficient of the $O(g^5)$ term is only quadratic in D—one power less than the corresponding coefficient in (4.8).

These observations can be systematized through sophisticated large D techniques pioneered by Vasiliev et al [74, 75] for the bosonic $O(N)$ NLσM and extended by Gracey [66, 67] to the $(1,1)$ supersymmetric case. For our purposes, the first significant claim (see [66, 67]) is that in

$$d = 2\mu = 2 + \epsilon \tag{4.18}$$

worldsheet dimensions, one may express

$$\frac{\beta(g)}{g} = \epsilon - \kappa + \frac{1}{D} b_1(\kappa) + \frac{1}{D^2} b_2(\kappa) + O(D^{-3}), \tag{4.19}$$

where $\kappa = gD$ and $O(D^{-3})$ means $1/D^3$ times a function of κ only. The functions $b_n(\kappa)$ have a power series expansion around $\kappa = 0$ whose first term is at least order κ^{n+1}.

[4] A preference for the scheme that leads to dependence of higher loop terms only on the Weyl tensor stems from the fact that there is an on-shell superspace formulation of type IIB supergravity [78] in which the Weyl tensor rather than the Riemann tensor enters into the superfield for linearized perturbations (in other words, the on-shell graviton superfield). Unless one can show that an off-shell formulation in which supersymmetry requires using the Weyl tensor in place of the Riemann tensor, we do not see any compelling reason to choose a Weyl scheme even in the $(1,1)$ supersymmetric case.

The second significant claim is that, in a minimal subtraction scheme, there is no ϵ dependence except as shown explicitly in (4.19). To see this, recall that in such a scheme, the bare coupling g_B and the renormalized coupling g_R are related by

$$g_B = M^{-\epsilon} \sum_{k=0}^{\infty} \frac{a_k(g_R)}{\epsilon^k}, \tag{4.20}$$

where $a_0(g_R) = g_R$ and the remaining $a_k(g_R)$ are power series in g_R whose coefficients do not depend on M or ϵ. The left side of (4.20) is obviously independent of M. In order for the right hand side to be independent of M, one must have

$$M\frac{\partial g_R}{\partial M} \equiv \beta(g_R) = \epsilon g_R + \left(1 - g_R \frac{\partial}{\partial g_R}\right) a_1(g_R). \tag{4.21}$$

Evidently, $\beta(g)/g$ depends on ϵ only additively, as indicated in (4.19).[5]

For ϵ greater than 0 but less than some finite upper bound, there is a non-trivial fixed point at a positive κ_c satisfying

$$\epsilon = \kappa_c - \frac{1}{D} b_1(\kappa_c) - \frac{1}{D^2} b_2(\kappa_c) + O(D^{-3}) \tag{4.23}$$

The leading corrections to power law scaling near the fixed point are determined by the slope of the beta function, i.e. in terms of the quantity

$$\lambda = -\frac{1}{2}\beta'(g_c) \tag{4.24}$$

where of course $g_c = \kappa_c/D$, and the derivative of $\beta(g)$ is taken with ϵ held fixed. The third main claim of [74, 75] is that position space diagrammatic techniques allow an independent determination of λ as a power series in $1/D$:

$$\lambda = \lambda_0(\epsilon) + \frac{\lambda_1(\epsilon)}{D} + \frac{\lambda_2(\epsilon)}{D^2} + O(D^{-3}), \tag{4.25}$$

where the functions $\lambda_i(\epsilon)$ in (4.25) have been computed explicitly.

[5] Renormalizability requires that the higher a_k satisfy so-called pole equations, which accounts for the fact that $\beta(g_R)$ depends only on a_1:

$$\left(1 - g_R \frac{\partial}{\partial g_R}\right) a_{k+1}(g_R) = \left(1 - g_R \frac{\partial}{\partial g_R}\right) a_1(g_R) \frac{\partial}{\partial g_R} a_k(g_R). \tag{4.22}$$

Given (4.19)-(4.25), one can determine the b_i in terms of the λ_i. Here is the algebra: first one uses (4.23) to rewrite (4.25) as

$$\begin{aligned}\lambda = \lambda_0(\kappa_c) &+ \frac{1}{D}\Big[\lambda_1(\kappa_c) - b_1(\kappa_c)\lambda_0'(\kappa_c)\Big] \\ &+ \frac{1}{D^2}\left[\lambda_2(\kappa_c) - b_2(\kappa_c)\lambda_0'(\kappa_c) - b_1(\kappa_c)\lambda_1'(\kappa_c) + \frac{1}{2}b_1(\kappa_c)^2\lambda_0''(\kappa_c)\right] + O(D^{-3})\,.\end{aligned} \tag{4.26}$$

Next one computes $\beta'(g_c)$ in terms of the series expansion (4.19):

$$\begin{aligned}-\frac{1}{2}\beta'(g_c) &= -\frac{\epsilon}{2} + \kappa_c - \frac{1}{2D}\Big[b_1(\kappa_c) + \kappa_c b_1'(\kappa_c)\Big] - \frac{1}{2D^2}\Big[b_2(\kappa_c) + \kappa_c b_2'(\kappa_c)\Big] + O(D^{-3}) \\ &= \frac{\kappa_c}{2} - \frac{\kappa_c b_1'(\kappa_c)}{2D} - \frac{\kappa_c b_2'(\kappa_c)}{2D^2} + O(D^{-3})\,,\end{aligned} \tag{4.27}$$

where in the second line we have again used (4.23) to eliminate ϵ. Finally, one compares terms in the second lines of (4.26) and (4.27) to obtain

$$\begin{aligned}\lambda_0(\kappa_c) &= \frac{\kappa_c}{2} \\ \lambda_1(\kappa_c) - b_1(\kappa_c)\lambda_0'(\kappa_c) &= -\frac{1}{2}\kappa_c b_1'(\kappa_c) \\ \lambda_2(\kappa_c) - b_2(\kappa_c)\lambda_0'(\kappa_c) - b_1(\kappa_c)\lambda_1'(\kappa_c) + \frac{1}{2}b_1(\kappa_c)^2\lambda_0''(\kappa_c) &= -\frac{1}{2}\kappa_c b_2'(\kappa_c)\,.\end{aligned} \tag{4.28}$$

The equations (4.28) hold for any κ_c greater than 0 and less than some finite upper bound: thus the second and third can be regarded as differential equations for b_1 and b_2. They may be integrated to obtain

$$b_1(\kappa) = -2\kappa\int_0^\kappa d\xi\,\frac{\lambda_1(\xi)}{\xi^2} \qquad b_2(\kappa) = -2\kappa\int_0^\kappa d\xi\,\frac{\lambda_2(\xi) - b_1(\xi)\lambda_1'(\xi)}{\xi^2}\,. \tag{4.29}$$

It is not obvious from what we have summarized so far that the lower limits of the integrals in (4.29) should be 0. This will become clear once the explicit expressions for the λ_i are in hand.

It is to be emphasized that $b_1(\kappa)$ and $b_2(\kappa)$ are defined through (4.29) for finite κ. More precisely: the treatment (4.24)-(4.29) defines $b_1(\kappa)$ and $b_2(\kappa)$ directly on some interval starting at 0 and extending to finite positive values of κ. Through analytic continuation, as in section 4.3.1, we extract the beta function of the AdS_{D+1} NLσM through order $1/D^2$, again for finite $\kappa = -\alpha' D/L^2$. As we shall describe in section 4.4.5, no singularities are encountered in this analytic continuation until $\kappa = -3$ for $b_1(\kappa)$ and $\kappa = -1$ for $b_2(\kappa)$.

The critical exponent λ is (in principle) a measurable quantity pertaining to the non-trivial fixed point in $d = 2 + \epsilon$ dimensions of the $O(N)$ NLσM, with $D = N - 2$. As such, it doesn't suffer from any scheme ambiguities. There is clearly a certain attractiveness in the strategy of folding all the difficult diagrammatic calculations into a determination of λ (as well as other critical exponents) and then extracting the beta function in a minimal subtraction scheme in the very last step.

Having summarized all but the difficult calculations, we will turn in section 4.4.1 to the promised determinations of $\lambda_1(\epsilon)$ and $\lambda_2(\epsilon)$ in the bosonic NLσM. The final results can be previewed in figure 4.1. As promised, there is once again a non-trivial fixed point for negative κ, corresponding, apparently, to a CFT with target space AdS_{D+1}. The reader who wishes to skip the technical details can find the main results in equations (4.40) and (4.53), supplemented by the definitions (4.32), (4.35),and (4.47).

4.4.1 Explicit results for the bosonic case

In this section, we will give a fairly complete summary of the bosonic calculation through $O(D^{-2})$ [74, 75] for three reasons: first, the position space techniques employed are less well known than fixed order perturbative techniques; second, we find a minor discrepancy in the final result of [75], at least as it appears in translation as cited; and third, we will identify one particular three loop diagram which is almost entirely responsible for the effects we are interested in.

To fix notation, consider the following generating functionals:

$$\begin{aligned} Z[J_S, J_\sigma] &= \int \mathcal{D}S\mathcal{D}\sigma \, \exp\left\{-\frac{1}{4\pi g_B}\int d^dx \, \left[(\partial S)^2 + \sigma(S^2-1)\right] + \int d^dx \, [J_S S + J_\sigma \sigma]\right\} \\ &= e^{W[J_S,J_\sigma]} = \operatorname*{extremum}_{\sigma} \exp\left\{-\Gamma[S,\sigma] + \int d^dx \, [J_S S + J_\sigma \sigma]\right\} \end{aligned} \tag{4.30}$$

The connected Green's functions $G^{(n_S,n_\sigma)}$ are derivatives of W, i.e. the connected (n_S+n_σ)-point function $\langle S(x_1)\cdots S(x_{n_S})\sigma(y_1)\cdots\sigma(y_{n_\sigma})\rangle_c$. The 1PI Green's functions $\Gamma^{(n_S,n_\sigma)}$ are analogous derivatives of Γ. For two-point functions we will adopt notations like G^{SS} instead of $G^{(2,0)}$. Near an ultraviolet-stable fixed point, the scaling parts of G^{SS} and $G^{\sigma\sigma}$ and the

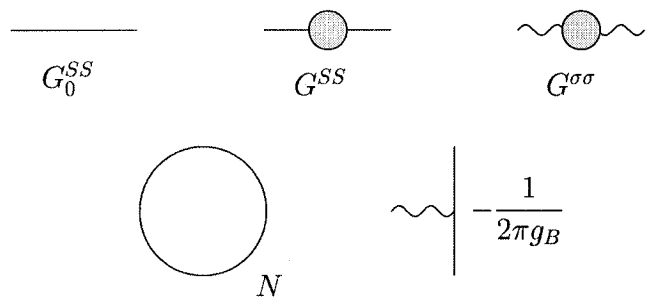

Figure 4.2: Feynman rules for the $O(N)$ model (4.30). Shaded circles indicate a dressed propagator. There is no undressed propagator for σ. There is a tadpole for σ which we omit because it does not contribute to the calculations of interest. A loop of S_μ picks up a factor of N whether the propagators in it are dressed or undressed, and regardless of how many $SS\sigma$ vertices it may include.

leading correction to them may be expressed for small but non-zero x as

$$G^{SS}(x) = \frac{C^{SS}}{x^{2\Delta_S}}\left[1 + \tilde{C}^{SS}x^{2\lambda} + \ldots\right] \qquad G^{\sigma\sigma}(x) = \frac{C^{\sigma\sigma}}{x^{2\Delta_\sigma}}\left[1 + \tilde{C}^{\sigma\sigma}x^{2\lambda} + \ldots\right], \tag{4.31}$$

where as noted above, $2\lambda = -\beta'(g_c)$ at the UV critical point. We have omitted to write the tensor structure of G^{SS}: it is proportional to $\delta_{\mu\nu}$. Indeed, because both the bare propagator for S_μ and the bare $SS\sigma$ vertex are $\delta_{\mu\nu}$ times a scalar function, all Green's functions $G^{(n_S,n_\sigma)}$ or $\Gamma^{(n_S,n_\sigma)}$ may be expressed as scalar functions times symmetrized products of $\delta_{\mu_i\mu_j}$ where $i,j = 1,2,\ldots,n_S$: in particular, no factors like $(x_1 - x_2)^{\mu_i}$ can ever appear. Tensor structure may be completely ignored for the calculations of interest to us; the only rule to remember is that every loop of S_μ picks up a factor of N. See figure 4.2 for the Feynman rules that we will use.

The renormalized dimensions of the operators in this theory can be expanded in $1/D$:

$$\begin{aligned}
\Delta_S &= \Delta_{S0} + \frac{\Delta_{S1}}{D} + \frac{\Delta_{S2}}{D^2} + \ldots \\
\Delta_\sigma &= \Delta_{\sigma 0} + \frac{\Delta_{\sigma 1}}{D} + \frac{\Delta_{\sigma 2}}{D^2} + \ldots \\
\lambda &= \lambda_0 + \frac{\lambda_1}{D} + \frac{\lambda_2}{D^2} + \ldots .
\end{aligned} \tag{4.32}$$

The method of [74, 75] is to self-consistently determine the Δ_S, Δ_σ, and λ to some order in $1/D$ by plugging (4.31) and (4.32) into Dyson equations which are represented graphically in figure 4.3. The graphs contributing to the Dyson equations are precisely the 1PI graphs,

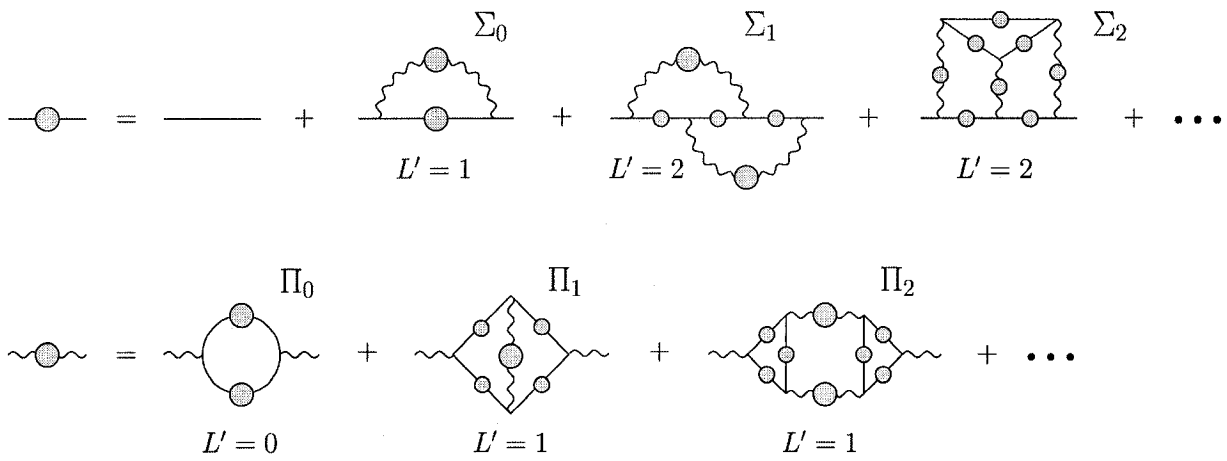

Figure 4.3: Graphical representation of the Dyson equations for G^{SS} and $G^{\sigma\sigma}$. All graphs have external legs amputated, so (for instance) the left hand sides are Γ^{SS} and $\Gamma^{\sigma\sigma}$. The effective loop order L', defined as the number of loops minus the number of loops of S_μ, is indicated for each graph. See the beginning of section 4.4.3 for a more complete discussion of effective loop order. The graph labeled Π_2 makes the crucial contribution leading to a non-trivial zero of the beta function; see section 4.4.5.

with the exception of graphs containing subgraphs that already appear at a lower efffective loop order. So, for example, the two-loop rainbow graph correction to Γ^{SS} is omitted from the Dyson equations because it would be generated by iterating the Dyson equation for G^{SS} truncated after the term labeled Σ_0. The undressed amputated SS propagator is a distribution supported at $x = 0$, so it makes no contribution to the scaling form (4.31). Thus the first term in the Dyson equation for G^{SS} could have been omitted. Graphs with σ tadpoles also do not contribute to the scaling forms (4.31), so we have entirely suppressed them.

4.4.2 Lowest order results

The lowest order treatment is to include only the graphs Σ_0 and Π_0 in the Dyson equations:

$$\begin{aligned} \Gamma^{SS}(x) = \Sigma_0 &= -\left(\frac{1}{2\pi g_B}\right)^2 G^{SS}(x) G^{\sigma\sigma}(x) \\ \Gamma^{\sigma\sigma}(x) = \Pi_0 &= -\frac{N}{2}\left(\frac{1}{2\pi g_B}\right)^2 G^{SS}(x)^2 . \end{aligned} \tag{4.33}$$

(The overall minus signs on the right hand sides are due to the sign on $\Gamma[S,\sigma]$ in (4.30).) Explicitly,

$$\begin{aligned}
\frac{p(\Delta_S)}{C^{SS}}\frac{1}{x^{2(2\mu-\Delta_S)}}\left[1-\tilde{C}^{SS}q(\Delta_S,\lambda)x^{2\lambda}\right] &= -\left(\frac{1}{2\pi g_B}\right)^2\frac{C^{SS}C^{\sigma\sigma}}{x^{2(\Delta_S+\Delta_\sigma)}}\left[1+(\tilde{C}^{SS}+\tilde{C}^{\sigma\sigma})x^{2\lambda}\right] \\
\frac{p(\Delta_\sigma)}{C^{\sigma\sigma}}\frac{1}{x^{2(2\mu-\Delta_\sigma)}}\left[1-\tilde{C}^{\sigma\sigma}q(\Delta_\sigma,\lambda)x^{2\lambda}\right] &= -\frac{N}{2}\left(\frac{1}{2\pi g_B}\right)^2\frac{(C^{SS})^2}{x^{4\Delta_S}}\left[1+2\tilde{C}^{SS}x^{2\lambda}\right]
\end{aligned} \tag{4.34}$$

where $\mu = d/2 = 1+\epsilon/2$, as in (4.18), and

$$a(\Delta)\equiv\frac{\Gamma(\mu-\Delta)}{\Gamma(\Delta)} \qquad p(\Delta)\equiv\frac{a(\Delta-\mu)}{\pi^{2\mu}a(\Delta)} \qquad q(\Delta,\lambda)=\frac{a(\Delta-\lambda)a(\Delta+\lambda-\mu)}{a(\Delta)a(\Delta-\mu)}\,. \tag{4.35}$$

The factors of p and q in (4.34) come from the inverse propagators Γ, which one finds by passing to momentum space using a standard Fourier integral:

$$\int d^dx\frac{e^{-ik\cdot x}}{x^{2\Delta}}=\frac{\pi^\mu a(\Delta)2^{2(\mu-\Delta)}}{k^{2(\mu-\Delta)}}\,, \tag{4.36}$$

and noting that in Fourier space, the inverse propagator is simply the algebraic inverse.

The equations (4.34) imply

$$2\Delta_S+\Delta_\sigma=2\mu \qquad p(\Delta_S)=-z=\frac{2}{N}p(\Delta_\sigma) \qquad z\equiv\frac{(C^{SS})^2C^{\sigma\sigma}}{(2\pi g_B)^2} \tag{4.37}$$

from matching the leading powers of x, and

$$\begin{pmatrix}1+q(\Delta_S,\lambda) & 1\\ 2 & q(\Delta_\sigma,\lambda)\end{pmatrix}\begin{pmatrix}\tilde{C}^{SS}\\ \tilde{C}^{\sigma\sigma}\end{pmatrix}=0 \tag{4.38}$$

from matching the subleading powers. In order for (4.38) to admit a solution with non-zero $\tilde{C}^{SS}$ and $\tilde{C}^{\sigma\sigma}$, the determinant of the matrix must vanish, which is to say

$$\left[q(\Delta_S,\lambda)+1\right]q(\Delta_\sigma,\lambda)=2\,. \tag{4.39}$$

Once μ and $N=D+2$ are specified, (4.37) and (4.39) can be solved straightforwardly for Δ_S, Δ_σ, and λ in the $1/D$ expansions (4.32):

$$\begin{aligned}
&\Delta_{S0}=\mu-1 \qquad \Delta_{S1}=-2\frac{a(2-\mu)a(\mu-1)}{a(2)\Gamma(\mu+1)} \\
&\Delta_{\sigma 0}=2 \\
&\lambda_0=\mu-1 \qquad \lambda_1=-2\Delta_{S1}\frac{(2\mu-1)(\mu-1)}{\mu-2}
\end{aligned} \tag{4.40}$$

and also

$$z = z_0 + \frac{z_1}{D} + \frac{z_2}{D^2} + O(D^{-3}) \tag{4.41}$$

where

$$z_0 = 0 \qquad z_1 = \Delta_{S1} \frac{\Gamma(\mu+1)\Gamma(\mu-1)}{\pi^{2\mu}} . \tag{4.42}$$

Although it is possible to obtain expressions for Δ_{S2}, $\Delta_{\sigma 1}$, λ_2, and z_2 from (4.37) and (4.39), these coefficients also receive contributions from the graphs Σ_1, Σ_2, Π_1, and Π_2, as we shall summarize in the next section.

4.4.3 Effects at order D^{-2}

To determine the order in $1/D$ at which a given graph begins to contribute, replace each propagator G^{SS} by the overall coefficient C^{SS}, and likewise replace $G^{\sigma\sigma}$ by $C^{\sigma\sigma}$. The "scaling amplitude" of the graph is then some monomial in C^{SS}, $C^{\sigma\sigma}$, $1/g_B$, and N. It is straightforward to show that the scaling amplitudes of all the graphs contributing to a given Dyson equation are some fixed monomial times powers of z and D, and that if one replaces N by D and z with $1/D$—consistent with the scaling (4.42)—then the resulting power of D is $D^{1-L'}$, where the "effective loop order" L' is the number of loops minus the number of loops of S_μ. For example, Π_0 has scaling amplitude $\frac{(C^{SS})^2 N}{g_B^2}$, whereas Π_2 has scaling amplitude

$$\frac{(C^{SS})^6 (C^{\sigma\sigma})^2}{g_B^6} N^2 \sim \frac{(C^{SS})^2 N}{g_B^2} z^2 N \sim \frac{(C^{SS})^2 N}{g_B^2} \frac{1}{D} . \tag{4.43}$$

In the first step of (4.43) we have used the definition of z and discarded factors of 2 and π; in the second step we have used (4.41) and discarded further $O(1)$ factors. Evidently, Π_2 is suppressed relative to Π_0 by a single power of D, as the effective loop order leads us to expect. In short, each graph starts to contribute at order $D^{1-L'}$. See figure 4.3 for the effective loop order of each graph. The number of graphs increases quickly as one proceeds to higher effective loop orders.

To evaluate Π_1, Π_2, Σ_1, and Σ_2 in position space, one must integrate over internal vertices. Certain identities to facilitate these computations were developed in [74, 75]; see

also [79] for a systematic exposition. Infinities arise in these position space integrals if one uses $2\Delta_S + \Delta_\sigma = 2\mu$, as obtained in (4.37). These infinities are naturally regulated: each of the four amplitudes of interest can be expanded as singular term, proportional to $1/(2\mu - 2\Delta_S - \Delta_\sigma)$, plus terms that remains finite as we take $2\Delta_S + \Delta_\sigma \to 2\mu$. The singular terms vanish provided we set[6]

$$\Delta_{\sigma 1} = 4\Delta_{S1}\frac{(2\mu-1)(\mu-1)}{\mu-2}\,, \tag{4.44}$$

and from the finite terms one eventually finds corrections to (4.37), (4.38), and (4.39) [74, 75]. The corrections to (4.37) are

$$p(\Delta_S) + z + z^2\Sigma_1' + z^3 N\Sigma_2' = 0 \qquad \frac{2}{N}p(\Delta_\sigma) + z + z^2\Pi_1' + z^3 N\Pi_2' = 0 \tag{4.45}$$

where

$$\begin{aligned}
\Sigma_1' &= \frac{1}{2}\Pi_1' = \frac{\pi^{2\mu}a(\Delta_S)^2 a(\Delta_\sigma)}{\Gamma(\mu)}\left(B(\Delta_\sigma) - B(\Delta_S)\right) \\
\Sigma_2' &= \frac{2\pi^{4\mu}a(\Delta_S)^3 a(\Delta_\sigma)^3 a(\mu+\Delta_S-\Delta_\sigma)}{\Gamma(\mu)}\left(B(\Delta_\sigma) - B(\Delta_S)\right) \\
\Pi_2' &= \frac{\pi^{4\mu}a(\Delta_S)^3 a(\Delta_\sigma)^3 a(\mu+\Delta_S-\Delta_\sigma)}{\Gamma(\mu)}\left(4B(\Delta_\sigma) - 3B(\Delta_S) - B(\mu+\Delta_S-\Delta_\sigma)\right)
\end{aligned} \tag{4.46}$$

and

$$B(x) = \psi(x) + \psi(\mu - x)\,. \tag{4.47}$$

The quantities Σ_1', Σ_2', Π_1', and Π_2', each a function only of μ, are the coefficients of the leading power of x in the finite parts of the corresponding graphs, with powers of C^{SS}, $C^{\sigma\sigma}$, g_B, and N removed, as the dependence on these parameters has already been extracted into (4.45). We still define $z = \frac{(C^{SS})^2 C^{\sigma\sigma}}{(2\pi g_B)^2}$, as in (4.37).

[6] It is actually no coincidence that $\Delta_{\sigma 1} = -2\lambda_1$—it is a consequence of the fact that $\Delta_\sigma = d - 2\lambda$.

The corrections to (4.38) are

$$\begin{pmatrix} T^{SS} & T^{S\sigma} \\ T^{\sigma S} & T^{\sigma\sigma} \end{pmatrix} \begin{pmatrix} \tilde{C}^{SS} \\ \tilde{C}^{\sigma\sigma} \end{pmatrix} = 0$$

$$\begin{aligned} T^{SS} &= -p(\Delta_S)q(\Delta_S,\lambda) + z + z^2\Sigma'_{1S} + z^3 N\Sigma'_{2S} \\ T^{S\sigma} &= z + z^2\Sigma'_{1\sigma} + z^3 N\Sigma'_{2\sigma} \\ T^{\sigma S} &= 2z + z^2\Pi'_{1S} + z^3 N\Pi'_{2S} \\ T^{\sigma\sigma} &= -\frac{2}{N}p(\Delta_\sigma)q(\Delta_\sigma,\lambda) + z^2\Pi'_{1\sigma} + z^3 N\Pi'_{2\sigma}\,, \end{aligned} \tag{4.48}$$

where

$$\begin{aligned} \Sigma'_{1S} &= 2D_1 + D_2 & \Sigma_{1\sigma} &= 2D_3 \\ \Sigma'_{2S} &= 2D_6 + 2D_7 + D_8 & \Sigma'_{2\sigma} &= 2D_9 + D_{10} \\ \Pi'_{1S} &= 4D_4 & \Pi'_{2\sigma} &= D_5 \\ \Pi'_{2S} &= 4D_{11} + 2D_{12} & \Pi'_{2\sigma} &= 2D_{13} \end{aligned} \tag{4.49}$$

and, following the notation of [74, 75],

$$\begin{aligned} D_1 &= -\frac{\pi^{2\mu}}{(2-\mu)\Gamma(\mu)^2} \\ D_2 &= \frac{\pi^{2\mu}}{(2-\mu)^2\Gamma(\mu-1)^2} \\ D_3 = D_4 &= \frac{\pi^{2\mu}(\mu^2-3\mu+1)}{(2-\mu)^2\Gamma(\mu)^2} \\ D_5 &= \frac{3\pi^{2\mu}}{(2-\mu)(2\mu-3)\Gamma(\mu-1)^2}R_1 \\ D_6 &= -\frac{\pi^{4\mu}(\mu^2-3\mu+1)\Gamma(1-\mu)}{(2-\mu)^3\Gamma(\mu)\Gamma(2\mu-3)} \\ D_7 &= \frac{\pi^{4\mu}\Gamma(2-\mu)}{(2-\mu)\Gamma(\mu-1)\Gamma(2\mu-2)}\left[\frac{2\mu-3}{(2-\mu)^2}+3R_1\right] \\ D_8 &= -\frac{\pi^{4\mu}\Gamma(4-\mu)}{(2-\mu)^5\Gamma(\mu-1)\Gamma(2\mu-4)} \\ D_9 = D_{11} &= \frac{\pi^{4\mu}\Gamma(1-\mu)(-2\mu^2+7\mu-4)}{(2-\mu)^3\Gamma(\mu)\Gamma(2\mu-3)} \\ D_{10} = D_{12} &= \frac{3\pi^{4\mu}\Gamma(3-\mu)}{(2-\mu)^3\Gamma(\mu-1)\Gamma(2\mu-2)}R_1 \\ D_{13} &= \frac{\pi^{4\mu}\Gamma(2-\mu)}{2(2-\mu)^3\Gamma(\mu-1)\Gamma(2\mu-2)}\left[6R_1 - R_2 - R_3^2\right]\,, \end{aligned} \tag{4.50}$$

with[7]

$$\begin{aligned} R_1 &= \psi'(\mu-1) - \psi'(1) \\ R_2 &= \psi'(2\mu-3) - \psi'(2-\mu) - \psi'(\mu-1) + \psi'(1) \\ R_3 &= \psi(2\mu-3) + \psi(2-\mu) - \psi(\mu-1) - \psi(1)\,. \end{aligned} \tag{4.51}$$

The equations (4.48) arise from comparing a subleading term in Γ^{SS} or $\Gamma^{\sigma\sigma}$ to its form obtained from the right hand side of a Dyson equation. To match powers of x, each graph on the right hand side needs to have all but one of its propagators set equal to their leading power law behaviors—that is, $C^{SS}/x^{2\Delta_S}$ or $C^{\sigma\sigma}/x^{2\Delta_\sigma}$—while the last propagator is set equal to $C^{SS}\tilde{C}^{SS}/x^{2(\Delta_S-\lambda)}$ or $C^{\sigma\sigma}\tilde{C}^{\sigma\sigma}/x^{2(\Delta_\sigma-\lambda)}$. Σ'_{1S}, a function only of μ, denotes the coefficient of the finite part of Σ_1, with one S propagator replaced by its subleading behavior, and with factors of C^{SS}, $C^{\sigma\sigma}$, g_B, N, and $\tilde{C}^{SS}$ removed. The other expressions in (4.49) have analogous meanings. Each contribution D_i arises from a particular choice of which propagator to assign subleading behavior to.

The corrections to (4.39), of course, are

$$T^{SS}T^{\sigma\sigma} - T^{S\sigma}T^{\sigma S} = 0\,. \tag{4.52}$$

It is now straightforward though tedious to plug the expansions (4.32) and (4.41) into (4.45) and (4.52) and obtain coefficients of arbitrarily high orders in $1/D$. The ones which

[7]Note that [74] includes two inconsistent definitions for R_3—the one in the main text of the paper is correct, whereas the definition in the appendix contains an error.

do not suffer further corrections from higher order graphs are

$$
\begin{aligned}
z_2 &= -2z_1 + \frac{z_1\eta_1}{\mu-2}\Bigg(4 + \frac{8}{\mu-2} + 14\mu - 6\mu^2 \\
&\qquad + 2\big[B(\mu-2) - B(2-\mu)\big] + \mu(2\mu-3)\big[B(3-\mu) + B(\mu-2) - 2B(2-\mu)\big]\Bigg) \\
\Delta_{S2} &= -2\Delta_{S1} + 2\Delta_{S1}^2\left(\frac{8\mu^5 - 42\mu^4 + 65\mu^3 - 34\mu^2 + 8\mu - 4}{2\mu(\mu-1)(\mu-2)^2} + \frac{z_2}{2\Delta_{S1}z_1}\right) \\
\lambda_2 &= -2\lambda_1 + 2\Delta_{S1}^2\frac{\mu(\mu-1)}{(2-\mu)^2}\Bigg(\frac{2(-4\mu^4 + 12\mu^3 - 5\mu^2 - 6\mu + 2)}{\mu(\mu-1)}\big[B(2-\mu) - B(\mu-1)\big] \\
&\qquad + \frac{2\mu(2\mu-3)^2}{2-\mu}\big[6R_1 - R_2 - R_3^2\big] + 3\mu(8\mu-11)R_1 \\
&\qquad + 12\mu^2 - 18\mu + 20 + \frac{6}{\mu} - \frac{2}{\mu^2} - \frac{10}{2-\mu} + \frac{10}{\mu-1} - \frac{3}{(\mu-1)^2}\Bigg).
\end{aligned}
\tag{4.53}
$$

In comparing with [75], one needs to know that $\eta = 2(\Delta_S - \Delta_{S0})$, and that the series expansions employed there are in $1/N$ rather than $1/D$: for instance, $z = z_0 + z_1/N + \tilde{z}_2/N^2$, where $\tilde{z}_2 = z_2 + 2z_1$. Thus, to obtain the coefficient $\tilde{z}_2$ of $1/N^2$, one simply removes the first term from the right hand side of the first equation in (4.53).

4.4.4 Consistency checks

The discrepancies we find with [75] are some minor differences in Δ_{S2} and λ_2 and the analogous quantities quoted there. A highly non-trivial check made in [75] is to compare $\nu = 1/2\lambda$ with results obtained in $d = 3$ (that is, $\mu = 3/2$) by studying the high-temperature phase of the $O(N)$ vector model [80]:

$$
\nu = \sum_{n=0}^{\infty}\frac{\tilde{\nu}_n}{N^n} \qquad \tilde{\nu}_0 = 1\,, \quad \tilde{\nu}_1 = -\frac{32}{3\pi^2}\,, \quad \tilde{\nu}_2 = \frac{32}{\pi^4}\left(\frac{112}{27} - \pi^2\right). \tag{4.54}
$$

These expressions agree with the results one gets using (4.40) and (4.53). In particular,

$$
\tilde{\nu}_2 = \frac{\lambda_1^2 - \lambda_0(\lambda_2 + 2\lambda_1)}{2\lambda_0^3}\,. \tag{4.55}
$$

The final expression in [75] for ν_2 leads to a result that differs from the one quoted in (4.54) by a factor $(176 + 27\pi^2)/(-112 + 27\pi^2)$. Thus we believe that our expressions are correct,

and that the inaccuracies appearing in [75] are typographical.[8]

With λ_1 and λ_2 in hand, we may return to (4.29) to extract the beta function. Series expansions

$$\begin{aligned}\lambda_0 &= \frac{\epsilon}{2} \\ \lambda_1 &= \frac{\epsilon^2}{2} + \frac{\epsilon^3}{4} - \frac{\epsilon^4}{8} + O(\epsilon^5) \\ \lambda_2 &= \frac{5 + 9\zeta(3)}{4}\epsilon^4 + O(\epsilon^5)\end{aligned} \tag{4.56}$$

lead immediately to

$$\begin{aligned}\beta(g) = \epsilon g - Dg^2 - Dg^3 - \frac{1}{4}D(D+4)g^4 \\ + \left(\frac{D^3}{12} - \frac{3}{2}(1+\zeta(3))D^2\right)g^5 + O(g^6)\,,\end{aligned} \tag{4.57}$$

which agrees with (4.8) except for a term scaling as Dg^5. This term corresponds to an $O(D^{-3})$ contribution to λ, so it is evidently excluded from the calculations in this section.

There appeared to be some arbitrariness in choosing the lower limits of integration in (4.29) to be 0. This arbitrariness is removed by requiring agreement with the one- and two-loop terms in (4.8).[9] Thus the non-trivial check in comparing (4.57) to (4.8) is the three- and four-loop terms.

4.4.5 A singularity at $\epsilon = -1$

Because $\Gamma(z)$ has all its singularities on the real axis, the same is true of $\lambda_1(\epsilon)$. The singularity of $\lambda_1(\epsilon)$ closest to $\epsilon = 0$ is at $\epsilon = -3$, whereas the singularity of $\lambda_1(\epsilon)$ closest to $\epsilon = 0$ is at $\epsilon = -1$. It's clear from (4.29) that $b_1(\kappa)$ and $b_2(\kappa)$ have the same radii of convergence around $\epsilon = 0$ as $\lambda_1(\epsilon)$ and $\lambda_2(\epsilon)$, respectively. Near their respective singularities, one can

[8] We have tried without success to contact the authors of [74, 75] in order to discover whether the errors might be in translation.

[9] There is a small caveat: there are two other choices for the lower limit of integration on the integral that determines $b_1(\kappa)$. Both are irrational, and choosing one of them instead of 0 does not alter the higher loop terms. For the $b_2(\kappa)$ integral, there appears to be one choice other than 0, but it is less than -1, hence on the other side of the singularity of primary interest to us.

show that

$$\begin{aligned} \lambda_1(\epsilon) &= -\frac{3/2\pi^2}{\epsilon+3} + O(1) & b_1(\kappa) &= -\frac{\log(3+\kappa)}{\pi^2} + O(1) \\ \lambda_2(\epsilon) &= \frac{32/3\pi^4}{(\epsilon+1)^4} + O\big[(\epsilon+1)^{-3}\big] & b_2(\kappa) &= -\frac{64/9\pi^4}{(\kappa+1)^3} + O\big[(\kappa+1)^{-2}\big]\,. \end{aligned} \tag{4.58}$$

All terms in λ_2 are regular at $\epsilon = -1$ (*i.e.*, $\mu = 1/2$), except for R_3, which originates only from the diagram Π_2 of figure 4.3, upon replacing a σ propagator with its leading correction to scaling (see the quantity D_{13} in (4.50)). Evidently, this diagram is somehow responsible for the existence of the fixed point at this order.

The singular behavior of $b_2(\kappa)$ is crucial to the question of whether there is a zero of $\beta(g)$ for negative g in $d = 2$. In the expansion

$$\frac{\beta(g)}{g} = \sum_{n=0}^{\infty} \frac{b_n(\kappa)}{D^n}\,, \tag{4.59}$$

if one stops after the term $b_1(\kappa)/D$, then as one decreases g from 0 to negative values, $\beta(g)$ becomes singular (at $\kappa = -3$, as explained above) before it has a zero. But if one includes also the term $b_2(\kappa)/D^2$, then the competition between positive $b_0(\kappa)$ and negative $b_2(\kappa)$ leads to a zero before the singularity at $\kappa = -1$. In short, the behavior in figures 4.1 and 4.4 is typical.

If one further expands

$$b_n(\kappa) = \sum_{k=n+1}^{\infty} b_{n,k}\kappa^k \tag{4.60}$$

then the singular behaviors (4.58) translate into the statements

$$b_{1,k} = P_1(k)(-1/3)^k \qquad b_{2,k} = P_2(k)(-1)^{k+1}\,, \tag{4.61}$$

where $P_1(k)$ and $P_2(k)$ are positive for all but finitely many k and have at most polynomial growth. Physically, the zero of the beta function computed through order D^{-2} arises not so much from competition of one-loop and two-loop terms as in [81], but more so from competition of the one-loop result from the asymptotics of high loop orders—or, in spacetime language, from competition between the Einstein-Hilbert term and high powers of the curvature tensor.

The outstanding question, of course, is what happens at higher orders in $1/D$. We have no real answers in the bosonic case, and only partial information in the supersymmetric case, but let us contemplate the two main alternatives.

1. Most optimistic is the supposition that higher orders in $1/D$ are no more singular than $b_2(\kappa)$, so that the beta function is well-approximated by the $1/D^2$ result that we have developed in this section. This would seem more plausible if it could be shown that general amplitudes contributing to $\lambda_i(\epsilon)$ have their singularities at integer ϵ, or, equivalently, integer d.

2. Alternatively, one could imagine that the $b_n(\kappa)$ become singular at progressively small values of κ—for example, at $\kappa = -3/(2n+1)$. Then for finite D, $\beta(g)$ does not have a convergent power series expansion. This would not be atypical of perturbive expansions.

Even in case (2), it could still be that correct qualitative information can be gleaned from a partial summation of the beta function, such as the $1/D^2$ results that we have in hand. After all, fairly good agreement is obtained for the $O(N)$ model between these results in $d = 3$ and other treatments [74, 75].

Because $\beta(g)$ computed through $1/D^2$ slopes steeply down at its non-trivial zero, $g_c < 0$, the critical exponent $\lambda = -\frac{1}{2}\beta'(g_c)$ is large and positive. The corresponding operator then must have a dimension which is large and negative (see figure 4.4 and table 4.1), *i.e.*, its two-point function increases with distance, rather than decreases. This appears to violate unitarity, and we might wonder anew whether the fixed point really exists. Let us reflect, however, on another CFT with non-compact target space, namely the free massless boson X in $d = 2$. The correlator $\langle X(x)X(0)\rangle \sim \log|x|$ grows at large $|x|$, signalling large infrared fluctuations. AdS_{D+1} is in some sense much "bigger" than $\mathbf{R}^{D+1}$, because the volume enclosed within a radius ℓ of a given point grows exponentially with ℓ rather than as a power. So we should not be too surprised to find even wilder infrared fluctuations, mediated perhaps by operators whose two-point correlators do grow as positive powers. Two-point functions

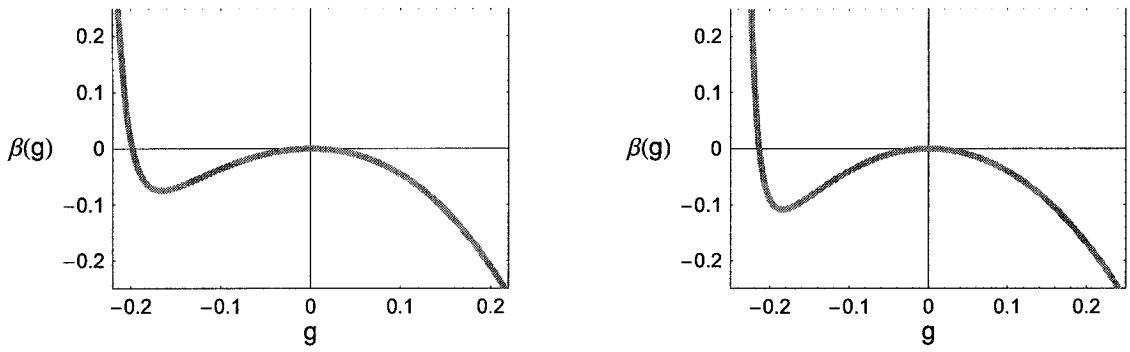

(A) (B)

Figure 4.4: (A) $\beta(g)$ versus g for the bosonic AdS_5 NLσM ($D = 4$). The non-trivial zero is at $g \approx -0.198$. (B) The analogous results for the type II AdS_5 NLσM. The zero is at $g \approx -0.217$.

that increase weakly with distance were found in [64], and their observation that the AdS_{D+1} NLσM has non-normalizable ground states appears to dovetail with the expectation of large infrared fluctuations.

We are also struck by the observation that the integral form (4.29) for the beta function coefficients must draw a large contribution from regions where ϵ is close to κ_c, which is finite and negative—in fact, κ_c is close to -1 when D is very large. Perhaps this means that configurations in target space with a Hausdorff dimension closer to 1 than 2 make a large contribution to the path integral. Such configurations would be somewhere between smooth surfaces (dimension 2) and branched polymer configurations (dimension 1). It is natural to expect positive power laws in correlators for field theories in $d < 2$ dimensions. Perhaps strong infrared fluctuations in the AdS_{D+1} target space result in an effective lowering of the dimension in which the field theory is defined.

4.4.6 Central charge of the non-trivial fixed point

Besides dimensions of operators at the fixed point, another scheme-independent quantity is central charge. The non-trivial fixed point is UV stable, and if it is perturbed slightly toward smaller g, there is an RG flow to flat space. Because the beta function is roughly speaking the gradient of the central charge, the non-trivial fixed point has a higher central

charge than flat space of the same dimension. More precisely,

$$\frac{\partial c}{\partial g} = \frac{3(D+1)}{2g^2}\beta(g)\,. \tag{4.62}$$

We defer a derivation of (4.62) until after (4.64). The prefactor comes from the metric on the space of couplings, and it may be corrected by loop effects. As we will now see, leading order expressions are sufficient to make a reasonable estimate of c at the non-trivial fixed point, at least for D large. Indeed, integrating across the RG flow from the non-trivial fixed point to flat space leads to

$$\begin{aligned} c &= D+1+\frac{3(D+1)}{2}\int_0^{\kappa_c}\frac{d\kappa}{\kappa}\frac{\beta(g)}{g} \\ &= D+1+\frac{3(D+1)}{2}\int_0^{\kappa_c}\frac{d\kappa}{\kappa}\left[-\kappa+\frac{1}{D}b_1(\kappa)+\frac{1}{D^2}b_2(\kappa)\right] \\ &\approx (D+1)\left[1-\frac{3\kappa_c}{2}\right] \end{aligned} \tag{4.63}$$

where in the second equality we have used (4.19). In the approximate equality we simply note that the integrand is nearly constant over nearly the entire range of integration: it is dominated by the one-loop term in $\beta(g)$. The main way in which the higher loop terms participate is in fixing κ_c. In table 4.1, we have obtained more precise results by numerically integrating the second line of (4.63). Evidently,

$$c \le \frac{5}{2}(D+1)\,, \tag{4.64}$$

and this bound saturates in the limit of large D. It seems to us likely that c does not exceed the the bound (4.64) even when higher $1/D$ corrections and a more precise treatment of $\mathcal{G}^{ij,kl}$ are included, for two reasons: first, such corrections cannot move κ_c to a value less than -1; and second, they have little chance of making the integrand in (4.63) significantly larger over an appreciable range.

Let us now return to the derivation of (4.62). A general metric perturbation of flat space is accomplished through

$$\delta S = \int d^2z\,\delta G_{ij}\,\mathcal{O}^{ij} \qquad \mathcal{O}^{ij} = \frac{1}{2\pi\alpha'}\partial X^i\bar{\partial}X^j\,, \tag{4.65}$$

where we employ the normalizations of [59]. As explained, for example, in section 15.8 of [24],

$$\begin{aligned} \frac{\partial c}{\partial G_{ij}} &= 24\pi^2 \mathcal{G}^{ij,kl}\beta_{kl} = \frac{3}{2}\beta^{ij} \\ \mathcal{G}^{ij,kl} &= |z|^4\langle \mathcal{O}^{ij}(z,\bar{z})\mathcal{O}^{kl}(0,0)\rangle = \frac{\delta^{ik}\delta^{jl}}{16\pi^2}\,, \end{aligned} \tag{4.66}$$

where in the second step of the first line we have used the final expression in the second line for the metric on the space of couplings, $\mathcal{G}^{ij,kl}$. Note that $\mathcal{G}^{ij,kl}$ is computed in free field theory: this is why we remarked below (4.62) that it may suffer loop corrections.

Let us now apply the result $\frac{\partial c}{\partial G_{ij}} = \frac{3}{2}\beta^{ij}$ to the AdS_{D+1} NLσM. We express the metric as $G_{ij} = -\frac{1}{g}G^{(0)}_{ij}$, where $G^{(0)}_{ij}$ is the metric on AdS_{D+1} with radius of curvature $\sqrt{\alpha'}$ rather than L. Thus $G_{ij}\partial/\partial G_{ij} = -g\partial/\partial g$, and we find

$$g\frac{\partial c}{\partial g} = -\frac{3}{2}G_{ij}\beta^{ij} = \frac{3}{2}\frac{D+1}{g}\beta(g)\,, \tag{4.67}$$

where in the last step we used (4.15), which is an exact expression. A non-trivial check on the calculation is to compare a series expansion of c in small g,

$$c = (D+1) - \frac{3}{2}D(D+1)g - \frac{3}{4}D(D+1)g^2 + \ldots \tag{4.68}$$

with the tree-level spacetime effective action (see for example [59])

$$S = \frac{1}{2\kappa^2}\int d^{D+1}x\,\sqrt{G}e^{-2\Phi}\left[-\frac{2(D-25)}{3\alpha'} + R + 4(\partial\Phi)^2 + \frac{\alpha'}{4}R_{ijkl}R^{ijkl} + \ldots\right]. \tag{4.69}$$

It is understood [62, 63, 82] that, to the order shown, in the scheme of minimal subtraction, and up to an overall multiplicative factor, the quantity in square brackets in (4.69) must coincide with the central charge (4.68), plus -26 to account for reparametrization ghosts. Our central charge expression (4.68) indeed satisfies this constraint. Furthermore, any corrections to $\mathcal{G}^{ij,kl}$ in (4.66) must be at least $O(\alpha'^2)$ for this matching to be satisfied. Note that this is an off-shell test: the comparison between (4.68) and (4.69) is being made for a very weakly curved AdS_{D+1} space.

4.4.7 Explicit results for the $(1,1)$ supersymmetric case

Calculations analogous to those in sections 4.4.2 and 4.4.3 were carried out in a series of papers by Gracey [66, 67, 83, 84]. The computations were done for the $(1,1)$ supersymmetric

	Bosonic			Supersymmetric		
$D+1$	g_cD	c	λ_c	g_cD	c	λ
3	-0.6603	5.228	1.698	-0.8105	7.732	4.583
4	-0.7435	7.538	2.687	-0.8447	10.58	6.026
5	-0.7926	9.899	3.734	-0.8696	**13.49**	7.614
6	-0.8247	12.29	4.801	-0.8872	**16.42**	9.209
7	-0.8473	14.69	5.866	-0.9001	19.36	10.78
8	-0.8642	17.11	6.921	-0.9101	22.3	12.32
9	-0.8773	19.54	7.96	-0.918	25.26	13.82
10	-0.8877	21.97	8.982	-0.9244	28.21	15.28
11	-0.8962	**24.41**	9.986	-0.9298	31.17	16.71
12	-0.9034	**26.85**	10.97	-0.9343	34.13	18.11
13	-0.9094	29.3	11.94	-0.9381	37.1	19.48

Table 4.1: Values of the central charge and critical exponent λ in the bosonic and supersymmetric case for various choices of D. Included in the central charge in the supersymmetric case is the fermionic contribution of $(D+1)/2$, as well as some known $1/D^3$ contributions—see (4.78). We compute λ as $-\beta'(g_c)/2$. In bold we show the cross-over points between sub-critical and super-critical values of the central charge for both the bosonic and supersymmetric cases.

$O(N)$ NLσM in component formalism, starting with the action (4.12). The final results for λ are:

$$\begin{aligned}
\lambda_0 &= \mu - 1 \\
\lambda_1 &= 0 \\
\lambda_2 &= \frac{8(\mu-1)\Gamma(2\mu-2)^2}{\Gamma(2-\mu)^2\Gamma(\mu-1)^4\Gamma(\mu)^2}\Bigg[-\frac{4\left(\psi(2-\mu)-\psi(\mu)+\psi(2\mu-1)-\psi(1)\right)}{\mu-1} \\
&\quad -2\left(\psi(2-\mu)-\psi(\mu)+\psi(2\mu-1)-\psi(1)\right)^2 \\
&\quad +2\psi'(2-\mu)+5\psi'(\mu)-2\psi'(2\mu-1)-5\psi'(1)\Bigg].
\end{aligned} \tag{4.70}$$

The relative simplicity of (4.70) over (4.40) and (4.53) results from non-trivial cancellations among several dozen Feynman graphs. Because $\lambda_1 = 0$, we have

$$\begin{aligned}
\frac{\beta(g)}{g} &= \epsilon - \kappa + \frac{1}{D^2}b_2(\kappa) + O(D^{-3}) \\
b_2(\kappa) &= -2\kappa\int_0^\kappa d\xi \frac{\lambda_2(\xi)}{\xi^2}.
\end{aligned} \tag{4.71}$$

It is interesting to examine the structure of the series expansion of $\beta(g)$ computed through order $1/D^2$: from (4.70) and (4.71),

$$\beta(g) = -Dg^2 - \frac{3}{2}\zeta(3)D^2g^5 + \frac{27}{32}\zeta(4)D^3g^6 - \frac{29}{20}\zeta(5)D^4g^7 + \frac{1}{192}\left[245\zeta(6) + 104\zeta(3)^2\right]D^5g^8 - \frac{1}{224}\left[311\zeta(7) + 156\zeta(3)\zeta(4)\right]D^6g^9 + \dots . \tag{4.72}$$

Just as in section 4.4.4, one can make a non-trivial check of (4.70) and (4.71) by comparing (4.72) with the third line of (4.17). The four-loop term—related to the famous $\alpha'^3\zeta(3)R^4$ term in the type II string theory action—agrees up to a term of order Dg^5, which corresponds to an $O(D^{-3})$ contribution to λ.[10] It is evident from (4.72)—and it can be proven starting from (4.70)—that the coefficient of the term $D^{k-2}g^{k+1}$ in (4.72) is a polynomial in the transcendental numbers $\zeta(q)$ for integers $q > 2$, such that each term is a rational multiple of $\zeta(q_1)\zeta(q_2)\cdots\zeta(q_s)$ with $\sum_r q_r = k - 1$.[11] The significance of this will emerge in section 4.5.4.

It is also evident from (4.72) that after the Einstein term $-Dg^2$, the sign of each term alternates, in such a way that for $g < 0$,

$$\beta(g) = -c_1|g|^2 + c_4|g|^5 + c_5|g|^6 + c_6|g|^7 + \dots , \tag{4.75}$$

where $c_k > 0$ for all k. Thus there must be a zero of the beta function (to the order we have computed it) before there is a singularity: the first term balances against all the rest.

[10] Recall that in the dimensional regularization scheme being used, it is the Riemann tensor, rather than the Weyl tensor, that appears in this R^4 term.

[11] To see this, note that from (4.71) that the g^{m+2} term of the beta function comes from the ϵ^m term in the series expansion of λ_2 around $\mu = 1 + \epsilon/2 = 1$. To prove the claim regarding the ζ dependence, start by noting that the series expansion of the term in square brackets in (4.70) can be written as

$$[\dots] = \sum_{k=1}^{\infty} a_k\epsilon^k\zeta(k+2) + \sum_{k=4}^{\infty}\sum_{k'=3}^{k-1} b_{kk'}\epsilon^k\zeta(k')\zeta(k-k'+2)\,, \tag{4.73}$$

where the a_k and $b_{kk'}$ are rational. Next, rewrite the remaining factors as

$$\frac{\epsilon^3}{4}\frac{\Gamma(1+\epsilon)^2}{\Gamma(1-\epsilon/2)^2\Gamma(1+\epsilon/2)^6} \equiv \frac{\epsilon^3}{4}F(\epsilon)\,. \tag{4.74}$$

Note that $F(0) = 1$. Furthermore, $F'(\epsilon) = F(\epsilon)\left[2\psi(1+\epsilon) + \psi(1-\epsilon/2) - 3\psi(1+\epsilon/2)\right] \equiv F(\epsilon)G(\epsilon)$. Next, note that $G(0) = 0$, $G'(0) = 0$, and $G^{(n)}(0) \propto \zeta(n+1)$ with non-zero, rational proportionality, since $\psi^{(n)}(1) = (-1)^{n+1}n!\zeta(n+1)$. Finally, $F^{(n)}(0)$ is equal to $F(0) = 1$ times a polynomial of derivatives of G at $\epsilon = 0$, such that the number of derivatives plus factors of G in a given term sums to n. These factors can then be easily recompiled to prove the claim.

This pattern of signs is related to the fact that $b_2(\kappa)$ is positive and singular at $\kappa = -1$:

$$\lambda_2(\epsilon) = \frac{4/\pi^4}{(\epsilon+1)^4} + O\big[(\epsilon+1)^{-3}\big] \qquad b_2(\kappa) = -\frac{8/3\pi^4}{(\kappa+1)^3} + O\big[(\kappa+1)^{-2}\big]\,. \tag{4.76}$$

As in the bosonic case, $b_2(\kappa)$ has all its singularities on the real axis, and $\kappa = -1$ is the one closest to the origin.

The distinctive singular behavior at $\kappa = -1$ is the same as in the bosonic case: see figure 4.4 and table 4.1. And, just as in the bosonic case, we must be careful to qualify the claim that there is a zero of the beta function with the caution that higher order terms in the $1/D$ expansion could change the story. The particular danger emphasized in section 4.4.5 was that $b_3(\kappa)$ and/or higher $b_n(\kappa)$'s could become singular for less negative values of κ than -1. In the all-orders beta function, expressed as a power series as in (4.75), each coefficient c_k is a polynomial in D. The large D calculations performed to date (i.e. through $O(D^{-2})$) tell us only the leading behavior of each c_k for large D. Terms in these polynomials which are subleading in D could nevertheless eventually dominate the contribution of high loop terms and control the existence of a fixed point. The two main alternatives contemplated in section 4.4.5 are alternatives still for the supersymmetric case.

In an attempt to obtain partial information available about $b_3(\kappa)$ and other high order terms, Gracey [66] has noted that consistency with the results of [85] demands that the tensor structure $R^{(n)}_{ab}$ entering into $\beta(g)$ for a general homogenous space at $k = n+3$ loops ($n > 0$) should vanish on Kähler manifolds. He noted that a satisfactory form of the $R^{(n)}_{ab}$ is

$$R^{(n)}_{ab} = R_{acde}R_{bpq}{}^{e}\left[R^{c}{}_{l_1m_1}{}^{p}R^{ql_nm_nd} + R^{c}{}_{l_1m_1}{}^{q}R^{dpm_nl_n}\right]\prod_{i=1}^{n-1} R_{l_{i+1}}{}^{l_im_i}{}_{m_{i+1}}\,. \tag{4.77}$$

If the $R^{(n)}_{ab}$ were the only tensor structures contributing to the beta function at loop order $k = n+3$, then the coefficients c_k would not change sign as compared to their behavior at leading order in D: indeed,

$$\begin{aligned} n \text{ odd:} \quad R^{(n)}_{ab} &= (g^{n+3}G_{ab})\left[2(D-1)D^3\sum_{k=0}^{(n-3)/2} D^{2k} + 3D(D-1)\right] \\ n \text{ even:} \quad R^{(n)}_{ab} &= -(g^{n+3}G_{ab})\left[2(D-1)D^2\sum_{k=0}^{(n-2)/2} D^{2k}\right]\,. \end{aligned}$$

In terms of the large D expansion, we may summarize the discussion as follows:

$$\frac{\beta(g)}{g} \approx \epsilon - \kappa + \frac{D-1}{D^3} b_2(\kappa)\,. \tag{4.78}$$

It is not claimed that the form (4.78) entirely accounts for $O(D^{-3})$ effects, but it does capture the four-loop term in (4.17) exactly, and it also correctly captures the one-loop exactness of the $O(3)$ model [86]. And, of course, it retains the zero for negative κ which has been our main interest.

There is another constraint on tensor structures that contribute to the beta function at higher loops in a minimal subtraction scheme: they cannot involve factors of the Ricci scalar or Ricci tensor. We learn this from the background field method [62, 69]. In this scheme, the beta function depends only on the simple poles of the dimensional regularization parameter ϵ in Feynman diagrams that have only "external vertices". Each external vertex comes with one or two powers of the Riemann tensor. Factors of the Ricci scalar or tensor would come from lines that loop back to the same vertex—propagators of internal lines proportional to δ_{ij} result in self-contractions of the Riemann tensor. Such a loop contributes a simple pole in ϵ. The remainder of the diagram must contribute at least a simple pole in ϵ, hence the entire diagram has a pole of at least ϵ^{-2}, and therefore does not contribute to the beta function.

As in the bosonic case (see section 4.4.5) the operator controlling the leading corrections to short-distance scaling is predicted to have negative dimension. We offer again the suggested interpretation that large infrared fluctuations, possibly leading to an embedding in target space with Hausdorff dimension less than 2, lead to the power-law growth in certain two-point functions that negative operator dimensions imply.

The central charge computation also goes through almost as in section 4.4.6. The main difference is that the $\kappa \to 0$ limit of the central charge is $\frac{3}{2}(D+1)$ rather than $D+1$ due to the contribution of fermions. A free-field treatment of the metric on the space of couplings leads to

$$\frac{\partial c}{\partial g} = \frac{3(D+1)}{2g^2}\beta(g)\,, \tag{4.79}$$

identically to the bosonic case (4.62). We defer a justification of (4.79) until after (4.81). Integrating (4.79),

$$\begin{aligned} c &= \frac{3}{2}(D+1) + \frac{3(D+1)}{2}\int_0^{\kappa_c}\frac{d\kappa}{\kappa}\frac{\beta(g)}{g} \\ &= \frac{3}{2}(D+1) + \frac{3(D+1)}{2}\int_0^{\kappa_c}\frac{d\kappa}{\kappa}\left[-\kappa + \frac{D-1}{D^3}b_2(\kappa)\right] \\ &\approx \frac{3}{2}(D+1)\left[1-\kappa_c\right], \end{aligned} \tag{4.80}$$

and we conclude that

$$c \leq 3(D+1), \tag{4.81}$$

with the bound saturating as $D \to \infty$. In table 4.1, we have obtained more precise results by numerically integrating the second line of (4.80).

Let us now return to the derivation of (4.79). The considerations of (4.65) and (4.66) generalize straightforwardly: the metric perturbation operator is

$$\mathcal{O}^{ij} = \frac{1}{4\pi}\left(\frac{2}{\alpha'}\partial X^i \bar{\partial} X^j + \psi^i \bar{\partial}\psi^j + \tilde{\psi}^i \partial \tilde{\psi}^j\right) \tag{4.82}$$

The fermion terms contribute only contact terms to $\langle \mathcal{O}^{ij}(z,\bar{z})\mathcal{O}^{kl}(0,0)\rangle$, so (4.66) is unchanged. The discussion leading to (4.67) is also unchanged. Series expansions show that

$$c = \frac{3}{2}(D+1) - \frac{3}{2}D(D+1)g - \frac{9}{16}\zeta(3)D(D^2-1)g^4 + O(g^5). \tag{4.83}$$

To match this onto a spacetime action for non-critical type II superstrings, we require the form

$$S = \frac{1}{2\kappa_D^2}\int d^D x\,\sqrt{G}e^{-2\Phi}\left[-\frac{2(c+c_{\text{ghost}})}{3\alpha'} + R + 4(\partial\Phi)^2 + \ldots\right]. \tag{4.84}$$

Then, up to an overall factor and the ghost contribution, the first two terms of (4.83) match the first two terms in square brackets of (4.84). We note that (4.84) is of exactly the same form as (4.69) to the order shown.

There seem to be some conflicting claims in the literature[12] about the normalization of the potential term for non-critical superstrings. This normalization is tied to the factor in

[12]For instance, in [87, 88], a potential is quoted which is 2/3 of the one we claim, and in [89], the result is 1/2 of the one we claim. But we find consistency with the results of [90].

(4.79), so it is crucial for our discussion of central charges to get it right. Let us therefore consider an alternative to the straightforward free-field worldsheet calculation discussed after (4.82). Namely, in the NS5-brane background of type II string theory, $c = 9$ comes from the $\mathbf{R}^{5,1}$ portion of the CFT; $c = 9/2 - 6/k$ comes from the supersymmetrized WZW theory describing the S^3 with k units of H_3 flux (so that there are k coincident NS5-branes); and $c = 3/2+6/k$ is supposed to come from a linear dilaton background, for a total of $c = 15$ (see for example [91]). The geometrical description of the throat geometry is

$$ds^2 = -dt^2 + d\vec{x}^2 + dr^2 + k\alpha' d\Omega_3^2 \qquad \phi = -r/\sqrt{k\alpha'} \qquad H_3 = -k\alpha' \,\mathrm{vol}_{S^3}\,, \tag{4.85}$$

where $\vec{x}$ is a vector in $\mathbf{R}^5$. Consider now a spacetime treatment of the radial direction only. The string frame action (consistent with (4.84)) is

$$S = \int dr\, e^{-2\Phi} \left[-\frac{2\delta c}{3\alpha'} + 4(\partial\Phi)^2 \right], \tag{4.86}$$

where $\delta c = -6/k$ is the central charge deficit from the supersymmetrized WZW theory that forces a dilaton flow upon us. The radial equation of motion for the dilaton derived from (4.86) indeed possesses the solution $\phi = -r/\sqrt{k\alpha'}$, providing a check on the normalization of the potential term.

4.5 Applications to AdS/CFT and model building

In sections 4.3 and 4.4, we have laid out the evidence that AdS_{D+1} NLσM's, both supersymmetric and non-supersymmetric, have zeroes at finite coupling, at least for large enough D. We have also explained how this evidence could be misleading: see in particular the discussion following (4.8) and in section 4.4.5. While cautioning once more that we have not shown that our calculations rest upon a controlled approximation scheme, we will in this section assume what seems to us the likeliest alternative: that there are indeed non-trivial fixed points. What then are the consequences?

First and foremost, there may be vacua of string theory which incorporate an AdS_{D+1} NLσM in the worldvolume theory. In section 4.5.1 we focus on possible implications of an

AdS_5 vacuum, and in section 4.5.2 we turn to vacua with an AdS_3 factor. Aspects of these discussions will be quite speculative. In section 4.5.3 we comment on a sort of no-go theorem for de Sitter vacua arising from competition between different powers of the curvature. And in section 4.5.4 we remark on a prescription for including the effects of string loops in the spacetime effective action.

4.5.1 A dual for pure Yang-Mills theory?

The many existing examples of anti-de Sitter string vacua involve matter fields whose stress-energy supports the negatively curved geometry. In terms of the NLσM, there are additional couplings of the scalar fields (and possibly the fermions in the supersymmetric case) that modify the one-loop beta function in such a way that there is fixed point—usually, in fact, a fixed line. Actually, this is an over-simplification in most cases: the matter fields are usually Ramond-Ramond fields, and including them in the action leads to technical difficulties; see for example [92]. In any case, a string vacuum based on an AdS_{D+1} NLσM of the unadorned type that we have described would be quite different from most previously studied cases, for example in that the scale of curvature is necessarily close to the string scale. More precisely, $|\kappa| = \alpha' D/L^2 \approx 1$, so the radius of curvature of AdS_{D+1} is $L \approx \sqrt{\alpha' D}$. Because the construction we have given makes no reference to D-branes, it is not obvious what the dual field theories in D dimensions should be. In this respect our story is similar to [93]; see also [94] for more recent developments.

But a two-dimensional worldsheet CFT is not enough to guarantee the existence of a string vacuum. One must also cancel the Weyl anomaly by arriving at net zero central charge and define physical state conditions in a consistent way. In general, one must impose a GSO projection to eliminate any undesirable states that simultaneously leads to a self-contained spectrum of string states, and finally one must show that one-loop string diagrams are invariant under an appropriate set of torus transformations to ensure that one-loop divergences do not appear as described in the introduction.

The results for the central charge listed in table 4.1 are not particularly encouraging

at first sight: c is always non-integer. But we are always free to add a spatial dilaton gradient to continuously adjust the central charge. This is best understood in free field theory (the linear dilaton vacuum) but based on the spacetime effective action, it seems obviously to remain true in curved backgrounds. As long as we focus on Euclidean theories, decreasing the central charge with a timelike dilaton gradient is not an option. Referring to table 4.1, we see that we can cancel the Weyl anomaly in the type II case with a dilaton gradient for AdS_3, AdS_4, and AdS_5, but not AdS_6 and higher. A natural choice is for the dilaton gradient to be chosen in the radial direction in a Poincaré patch description of the geometry. The resulting geometry is an obvious candidate for a holographic dual of a gauge theory undergoing renormalization group flow. It is pleasing to see this construction work in the dimensions that it does because it is in dimensions 4 and lower that gauge theory interactions are renormalizable.

But wouldn't it be lovely if the Weyl anomaly canceled exactly in AdS_5, without any dilaton gradient? That would mean that there is no potential for the dilaton. Turning on a dilaton gradient would still be allowed, just as in $AdS_5 \times S^5$ [95]. Presumably, it would be a gentler flow, at least when Φ is large and negative. This would correspond to the fact that gauge couplings in four dimensions experience logarithmic flow, which is qualitatively gentler than the power law flow in lower dimensions.

As things stand in table 4.1, the critical dimension for the string theory construction seems to be about halfway between $D = 4$ and $D = 5$ (a precise computation gives $D = 4.517$). Everything would fit together a bit better if the critical dimension for the string theory construction coincided precisely with the upper critical dimension for gauge interactions in the AdS/CFT duals. If only (4.81) were an equality rather than an inequality! Recall that in deriving (4.81), we combined rather precise knowledge of $\beta(g)$ with a less precise computation of the metric on the space of couplings. Perhaps then there is enough wiggle room to wind up with $c = 3(D+1)$ for the non-trivial fixed point. Or perhaps we are engaging in wishful thinking: after all, our calculations were accurate enough so that the series expansion (4.83) avoided $O(g^2)$ and $O(g^3)$ terms, which was necessary to match

onto the absence of R^2 and R^3 terms in the type II effective action.

It is particularly attractive to suppose that the critical background is AdS_5—probably with a slight dilaton gradient—rather than a product of AdS_5 and some other geometry. The dual field theory may then be expected to be comparably simple, without (for example) any flavor symmetries. Perhaps a definite understanding of what theory it is would come from studying the dynamics of open strings on some version of D3-branes appropriate to the AdS_5 NLσM. Absent such a discussion, let us assume that it is pure Yang-Mills theory, with coupling $g_{YM} = e^{\Phi}$. Because of our limited understanding of the spacetime effective action and the lack of a D-brane construction, we cannot presently determine the central charge or the gauge group. But because the geometry is at string scale and the dilaton can flow to large negative values, we may hope that it embraces the asymptotic freedom and confinement of pure glue in a single holographic description. For example, confinement of external electric charges and screening of magnetic ones might be accounted for in terms of the radial variation of the tensions (as measured in Einstein frame) of fundamental strings and D1-branes, as in [95].

Before getting carried away with the idea that the type II AdS_5 construction should be critical, let us note another possibility that fits much better with the current numerical results: $AdS_5 \times S^1$ may be a critical background. The worldsheet boson parametrizing S^1 and its superpartner together contribute $c = 3/2$, so using the value for AdS_5 from table 4.1 leads to a total central charge of 14.99.[13] The dual four-dimensional theory should have a $U(1)$ symmetry. Pure $\mathcal{N} = 1$ Yang-Mills theory is an obvious candidate. If it is indeed the dual theory, then a fuller treatment should reveal a dilaton gradient, a dynamical breaking of the $U(1)$ symmetry, and (most fundamentally) a GSO projection that leads to spacetime supersymmetry. Indeed, an understanding of the GSO projection seems crucial to the entire discussion of AdS_{D+1} string vacua, since we have to find some way to get rid of the negative dimension operator or otherwise ensure stability.

[13]It may seem striking that $AdS_5 \times S^1$ is the bosonic part of $\frac{SU(2,2|2)}{SO(5)\times SU(2)}$, which was argued in [93] to support a NLσM. But the reasoning in [93] hinged on the inclusion of a fermionic version of a Wess-Zumino term whose presence combined with kappa symmetry forbade a non-zero beta function. This is rather different from our analysis. Moreover, $\frac{SU(2,2|2)}{SO(5)\times SU(2)}$ was stated in [93] to be a non-critical background.

4.5.2 Model building with quotients of AdS_3

Having articulated the hope that $c = 3(D+1)$ in a full calculation of the type II AdS_{D+1} NLσM's, let us note another striking consequence of this conjectured equality: AdS_3 has $c = 9$, the same value as a six-dimensional Calabi-Yau construction (CY_3). We are thus led to suggest a new class of type II string vacua: $\mathbf{R}^{3,1} \times AdS_3/\Gamma$, where $\Gamma \subset SO(3,1)$ is a discrete group such that AdS_3/Γ has finite volume.

There is an obvious candidate for a heterotic generalization, inspired by the familiar story of the standard embedding [96].[14] Let the fields $X^\mu(z,\bar{z})$ and $\tilde{\psi}^\mu(\bar{z})$ form the usual free $\mathbf{R}^{3,1}$ portion of the theory, with $c = 4$ and $\tilde{c} = 6$. Let the AdS_3 NLσM be constructed in a symmetric fashion, so that $c = \tilde{c} = 9$ (we assume). The anti-holomorphic part of the Weyl anomaly is now canceled. To cancel the holomorphic part, an additional holomorphic CFT is required with $c = 13$. This is easily big enough for model-building: for example, a Kac-Moody current algebra based on $E_8 \times SO(10)$ at level 1 has $c = 13$. But we have no definite proposal for how an appropriately chiral spectrum of fermions might emerge in such a construction, nor for how to make an appropriate GSO projection in such a way as to get rid of tachyons and/or negative dimension operators and be left with a phenomenologically attractive gauge group.

The total size of AdS_3/Γ is fixed in string units, once Γ is chosen, because the non-trivial zero of $\beta(g)$ is isolated. We must of course assume that GSO has gotten rid of operators of dimension less than 2. A very attractive feature of the finite volume spaces AdS_3/Γ is that they have no massless shape moduli [97]. There is however a large discrete class of these manifolds, and their number grows rapidly with their volume. It is known that finite volume AdS_3/Γ can never have Killing spinors [98, 99], so perhaps it is impossible to get $\mathcal{N} = 1$ supersymmetric vacua in four dimensions.

Another notable feature of manifolds AdS_3/Γ is that their volume scales exponentially with their linear size. This has been exploited in the context of brane-world scenarios [99, 100] to give an account of the hierarchy between the four-dimensional Planck scale

[14] We thank G. Michalogiorgakis for a discussion on this point.

and the weak scale without extensive tuning the size of the extra dimensions. We also note that the implications for compact hyperbolic manifolds in cosmology has been the subject of many studies [101, 102, 103, 104, 105, 106], and considerations for particle physics were discussed in [107]. And we note that we evade the objections of [108] because our construction is near the string scale. But we cannot claim to have demonstrated stability until a satisfactory GSO projection is formulated.

The framework we have suggested so far seems to depend strongly on having $c = 9$ exactly for the type II AdS_3 NLσM. This value is surely within "theoretical errors" of the results listed in table 4.1: large D methods cannot be expected to be terribly accurate for $D = 2$![15] But there might be some interest in this type of construction even if this is not true. Perhaps some flux of H_3 can be used to adjust the central charge. Perhaps, in a case where AdS_3/Γ has finite volume but is not compact, a dilaton gradient might be added. If the value $c = 7.732$ is a slight *over-estimate* of the true value, then perhaps a compactification to five dimensions (possibly with a slight dilaton gradient) would be possible.

In any case, the large discrete freedom in the choice of AdS_3/Γ could result in an interesting range of four-dimensional models, as in [109]. Most finite volume hyperbolic manifolds are not simply connected, and the minimal length of the various homotopy cycles are fixed in string units. This suggests interesting possibilities for the spectrum of wrapped strings. For example: could they provide generations of chiral fermions?

We should also consider the possibility that type II on $\mathbf{R}^{3,1} \times AdS_4$ is a critical background. Although this is almost as close to being realized in table 4.1 as criticality of $\mathbf{R}^{3,1} \times AdS_3$, it doesn't fit with the attractive hypothesis that AdS_5 is critical (which works if the values for c in table 4.1 are under-estimates); nor does it fit particularly well with the supposition that $AdS_5 \times S^1$ is critical, since this hypothesis works nearly perfectly when the values in table 4.1 are assumed to be highly accurate. Clearly, it would be highly desirable to determine the central charges more precisely. Absent this, a more quantitative

[15] Indeed, we should admit the possibility that the fixed point exists for larger D, but not $D = 2$. Certainly it doesn't exist for $D = 1$: see the discussion preceding (4.77).

estimate of the theoretical uncertainties in the determinations in table 4.1 would help bring the current discussion into better focus.

4.5.3 Positive curvature spacetimes

It is well-accepted that there cannot be a conformal NLσM on a sphere S^{N-1} in $d = 2$ without some participation of matter fields (i.e. couplings other than the target space metric): such a NLσM would be associated with a finite-temperature phase transition for the $O(N)$ model, which the Coleman-Mermin-Wagner theorem prohibits [110, 111]. This theorem states (more or less) that a compact, continuous symmetry cannot exhibit spontaneous symmetry breaking in two dimensions.[16]

It is only a small step from this to claim that there cannot be a conformal NLσM on de Sitter space, dS_{D+1}, without the participation of some matter fields. The reason, simply, is that the beta function is indifferent to signature. If competition between different powers of curvature gave rise to a dS_{D+1} fixed point, there would be a S^{N-1} fixed point too (with $N = D + 2$ as always). Previous claims that de Sitter vacua *do* arise in this way [112] rely upon a $SL(2, \mathbf{Z})$-covariantization of the type IIB spacetime effective action. This takes us outside our current scope (see however section 4.5.4), but we believe a careful analysis of signs still indicates AdS_{D+1} rather than dS_{D+1} solutions.

It is possible to check that the expressions (4.19) and (4.78) that we have given for the bosonic and type II NLσM's are consistent with the expectation that there are no positive curvature conformal points. But there is a subtlety: for $d \geq 4$, the scalar field interactions of our model become irrelevant, and hence do not affect the renormalization group flow. Thus for $d \geq 4$, we find the mean-field theory result $\lambda = 1$, to all orders in $1/D$, in both the bosonic and supersymmetric cases. A check on the expressions (4.40), (4.53), and (4.70) for the λ_i is that $\lambda_0 = 1$ and $\lambda_1 = \lambda_2 = 0$ for $d = 4$, so that $\lambda = 1$. In short, the large D results match smoothly onto mean field theory expectations, order by order in $1/D$. If this matching were not accounted for, then $\beta(g)$ would oscillate wildly for $\kappa > 2$, resulting in

[16] Reasons are noted in [64] why the CMW theorem does not extend to the non-compact symmetry group $SO(D + 1, 1)$ acting on AdS_{D+1}.

multiple zeroes. When it is, $\beta(g)$ has no zeroes at all for $\kappa > 0$.

4.5.4 Including string loops

Although our focus has been on non-trivial fixed points of AdS_{D+1} NLσM's, it is interesting to note that a series expansion of the beta functions calculated in section 4.4 can be translated into information about the low-energy effective action, or equations of motion, in ordinary type II superstring theory in ten nearly flat dimensions. We will focus on type IIB and show how to arrange $SL(2,\mathbf{Z})$ invariance.

The tree-level effective action in string frame has the schematic form

$$S = \frac{1}{2\kappa^2}\int d^{10}x\,\sqrt{G}e^{-2\Phi}\left[R + a_4R^4 + a_5R^5 + \cdots\right], \tag{4.87}$$

neglecting terms which involve derivatives of curvature. The coefficients a_i are closely related to the coefficients in a power series expansion of $\beta(g)$ in g. In Einstein frame, $g_{MN} = e^{-\Phi/2}G_{MN}$, and the term at order R^k will pick up a dilaton dependence of $e^{(1-k)\Phi/2}$. The Einstein-Hilbert term is then evidently $SL(2,\mathbf{Z})$-invariant, but the higher powers of curvatures are not. An algorithm for rendering them $SL(2,\mathbf{Z})$-invariant has been discussed by several authors [113, 114, 115]: briefly, one makes the replacement

$$2\zeta(q)e^{-q\Phi/2} \to \sum_{(m,n)\neq(0,0)}\left|\frac{\sqrt{\mathrm{Im}\,\tau}}{m+n\tau}\right|^q \to \sum_{(m,n)\neq(0,0)}\frac{e^{-q\Phi/2}}{(m^2+n^2e^{-2\Phi})^{q/2}} \tag{4.88}$$

in all the coefficients a_k. The replacement (4.88) leads to an effective action with information at all orders in string loops. For (4.88) to make sense, a highly non-trivial property is required of the a_k: they must be polynomials in $\zeta(q)$ such that every term is some multiple of a product $\zeta(q_1)\zeta(q_2)\cdots\zeta(q_r)$ such that $\sum_s q_s = k-1$. Then, in Einstein frame, all the dependence of the coefficients of R^k on the dilaton and on transcendental numbers can be factored into products of the form on the first expression in (4.88). The middle expression in (4.88) is $SL(2,\mathbf{Z})$-invariant: $\tau = C_0 + ie^{-\Phi}$ is the usual complexified dilaton. In the last step, we specialize to configurations with $C_0 = 0$.

As we noted in (4.72) and the discussion following it, the coefficient of $D^{k-2}g^{k+1}$ in $\beta(g)$ satisfies precisely the zeta function property required for (4.88) to make sense. It is

an interesting, qualitative, all-orders consistency check on the tree-level equation of motion $\beta(g) = 0$ that one can straightforwardly render it $SL(2, \mathbf{Z})$-invariant.

It is tempting to speculate that some version of $SL(2, \mathbf{Z})$-invariance can be arranged in AdS_5 (or perhaps $AdS_5 \times S^1$), where, according to our earlier speculations, the Weyl anomaly cancels just as in ten-dimensional flat space. If so, then in the same spirit as [112], it should be possible to solve the $SL(2, \mathbf{Z})$-covariant equation of motion for the complexified dilaton by setting $\tau = i$, i.e. $\Phi = C_0 = 0$. The reason is that $\tau = i$ is necessarily an extremum of an $SL(2, \mathbf{Z})$-invariant function. The upshot is that by making the replacement (4.88) and then setting $\Phi = 0$, one obtains from $\beta(g) = 0$ a modified equation which still has an AdS_5 solution. The radius is slightly larger: $\kappa_c \approx -0.72$ rather than the tree-level value -0.8696.

We are attracted to the idea that $SL(2, \mathbf{Z})$-invariance can be realized at some level for type II strings on AdS_5, because in the conjectured dual, pure Yang-Mills theory, the action possesses an $SL(2, \mathbf{Z})$ invariance. This does not imply that there is a conformal fixed point for this theory, but rather that renormalization group flows should have images under $SL(2, \mathbf{Z})$. Whether the AdS_5 vacuum with $\Phi = 0$ suggested in the previous paragraph is physically significant for pure Yang-Mills theory seems doubtful; more plausible is the idea that some dilaton gradient is required. But we remind the reader that we are at the end of a long chain of conjectures.

4.6 Summary

The absence of a zero of $\beta(g)$ for positive g—that is, for the $O(N)$ model—is well accepted because it is consistent with the known perturbative results, the large N results, the Coleman-Mermin-Wagner theorem, and, in the bosonic case, the non-perturbative results of [116]. The situation for the AdS_{D+1} NLσM is much less certain. The evidence from four-loop perturbative calculations and from the large D expansion through order $1/D^2$ points to the following picture:

1. There is indeed a zero of $\beta(g)$ for negative g, of order $-1/D$. This is true both for

the bosonic case and the supersymmetric case, at least for large enough D. In the supersymmetric case, $\beta(g)$ cannot have a zero for $D = 1$ (i.e. AdS_2), but for $D \geq 2$ it may. See equations (4.29), (4.40), (4.53), (4.70), (4.71), and (4.78); figures 4.1 and 4.4; and table 4.1.

2. The non-trivial fixed point has the peculiar property that the leading corrections to short-distance scaling are controlled by an operator of negative dimension. In section 4.4.5 we have outlined a heuristic physical picture that could account for this peculiarity: it hinges on the idea that infrared fluctuations are quite wild in an AdS_{D+1} target space, and that these large, non-Gaussian fluctuations make it possible for two point correlators to have power-law growth rather than power-law fall-off.

3. The central charge of the non-trivial fixed point has $c \lesssim \frac{5}{2}(D+1)$ in the bosonic case, and $c \lesssim 3(D+1)$ in the supersymmetric case. The dominant uncertainty in determining c is from the metric on the space of couplings, which we have computed at the level of free field theory on the worldsheet rather than in a systematic expansion. In the supersymmetric case, we have suggested that $c = 3(D+1)$ exactly because it makes sense for the critical dimension for strings in AdS_{D+1} to coincide with the upper critical dimension of gauge interactions in $\mathbf{R}^D$. This conjectured equality has the striking consequence that AdS_3 and quotients of it have the same central charge as six-dimensional Calabi-Yau manifolds.

Of these claims, surely the oddest is the second. But because the dimension of the operator is related to the slope of $\beta(g)$ at the fixed point, it is more sensitive to the nearly singular behavior of $\beta(g)$ there than the position g_c of the fixed point is. Thus one might hope that this "problem" goes away on its own. The determination of the central charge is also less sensitive to the precise form of $\beta(g)$ near the fixed point than $\beta'(g_c)$. If the values in table 4.1 are fairly accurate, then $AdS_5 \times S^1$ rather than AdS_5 is the leading candidate for a critical type II background. As we have noted in section 4.5.1, modifying our string-scale AdS_{D+1} backgrounds with a dilaton gradient for $D \leq 4$ leads to appealing candidates for

holographic duals of simple gauge theories, such as pure Yang-Mills theory, with no flavor symmetries.

We have been careful all along to point out the potential pitfalls of our calculations, but let us reiterate the main one: we are not calculating in a controlled approximation scheme. This is well illustrated for fixed order computations in figure 4.1, where successive terms alternate up to the fourth loop order. The alternating signs problem is fixed in the large D treatment: all powers of g except the first few contribute with the same sign to $\beta(g)$ for $g < 0$. But then the issue becomes the radius of convergence in $\kappa = gD$ of higher $1/D$ corrections. It would clearly be desirable to gain better control over these corrections. Perhaps the class of graphs at $O(D^{-3})$ that contributes to the leading singular behavior of $b_3(\kappa)$ is small enough for explicit calculations to be tractable. It is also clearly worthwhile to try to approach the same broad class of NLσM's in different ways, such as algebraic methods, lattice simulations, or (for $g > 0$) high temperature expansions. Explorations of D-branes in these NLσM's is clearly called for, as is an understanding of the possible GSO projections and their implications for stability.

Even the most conservative reading of these results strongly suggests that there is interesting structure in the beta function for the AdS_{D+1} NLσM which is not reliably visible at low loop orders. While we admit the possibility that all the strange behavior—including singularities and an apparent zero—could be artifacts of the minimal subtraction scheme we chose, or of a zero radius of convergence for $\beta(g)$, we think it more likely that these features signal interesting physics. A fixed point of RG is the simplest and most attractive possibility. If this fixed point is where we think it is; if it leads to a dual at string scale to four-dimensional gauge theory at moderate coupling; if it provides an alternative route to four-dimensional models—then these NLσM's and variants of them could become a central part of string theory.

Chapter 5

Conclusions

We have argued that though tests of stringy corrections to gravitational measurements may be difficult if not impossible, tests of string theory as it describes strong interactions is at a minimum substantially more plausible, and perhaps even likely with today's experiments. The presence of a strongly-coupled Quark-Gluon Plasma at the RHIC experiment provides hope for experimental tests of string theory, since the bulk physics can be described by the gravitational dynamics of an anti-de Sitter background in the presence of a horizon.

In particular, the strongly-coupled nature of the Quark-Gluon Plasma combined with the dynamic nature of jet quenching makes it difficult to study the phenomenon using standard methods, such as perturbative quantum field theory or lattice simulations. Ideal hydrodynamics comes close, however it is best applied in the far infrared region of parameter space and can not easily access the region of momenta that is most experimentally relevant, when the momentum is on the order of the plasma temperature. Indeed, the one remaining calculational tool that we are aware of is string theory via the AdS/CFT correspondence.

We have proceeded to compute the jet quenching efficiency from a simple gravity dual description, based on a string hanging near the boundary of AdS, with the bulk of the string trailing behind the "quark" endpoint in the bulk of AdS. Previous authors have shown that string theory indeed predicts that the quark momentum is exponentially damped, and we have extended their analysis to address the question of where the energy goes after it is

dissipated into the thermal medium by the relativistic quark. We have shown that the behavior of the outgoing energy density as a function of the angle between the outgoing particles from the quenched jet and the near-side jet that escapes the plasma quickly is qualitatively very similar to the string theory prediction.

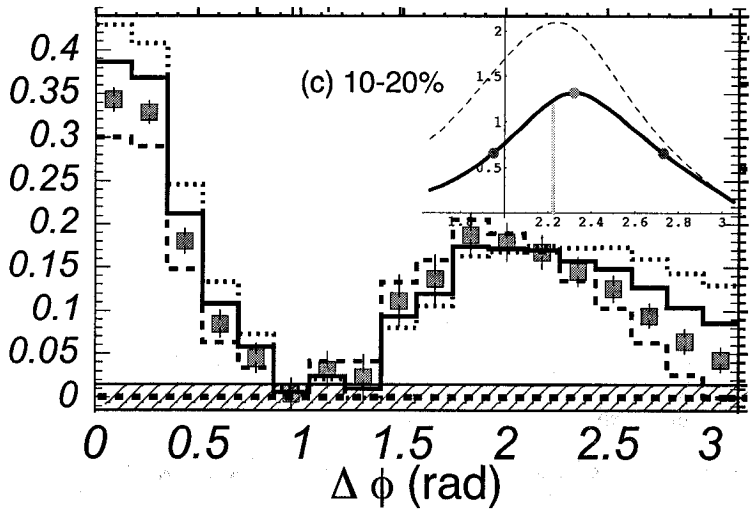

Figure 5.1: Figure 1.4 revisited. The vertical axis is proportional to the number of outgoing particles observed in each angular bin, where the angle is the separation between the near-side jet and the outgoing particle from the quenched jet.

We benefit further from the fact that though the RHIC data plots are consistent with a Mach-like sonic-boom, they do not imply this physics directly, and further directional measurements are required to say for certain that a sonic boom occurs. Therefore, to this extent, the presence of a sonic boom is a *prediction* from string theory regarding what should be seen at RHIC.

Strictly speaking, our calculations were carried out within the gravity dual to $\mathcal{N} = 4$ SYM in the limit of a large number of colors N, which is quite different from QCD. However, we remind the reader that lattice simulations of QCD tell us that at RHIC temperatures, the physics of QCD can be well-approximated by a conformal field theory, which is one of the essential properties of $\mathcal{N} = 4$ SYM. Furthermore, since our calculations deal only with the AdS_5 portion of the spacetime, which should be a generic component of any gravity dual to a four-dimensional gauge theory, one might also expect our essential findings—the

presence of a sonic boom in particular—to be generic to jet quenching physics in *any* gauge theory with a gravity dual, QCD perhaps included. Indeed, the S^5 portion of the spacetime, which contains the geometric encoding of the supersymmetry properties of the theory, was barely relevant to our calculations. Appropriate modifications to the setup to account for real-world deviations from conformality would certainly enhance the story.

Of course, our calculations are valid only at the leading order in the 't Hooft coupling and number of colors, and corrections will be on the order of $\lambda_t^{-3/2}$ and $1/N^2$, each about 10%. Though 10% may mean that our calculations receive large corrections, the fact that this number is reasonably large gives hope that physical effects that are uniquely stringy could be experimentally observed in strong interactions. To this end, we have presented a method for computing the higher order corrections to supergravity that arise from consideration of the beta function for the string worldsheet couplings. We have argued that by including an effectively infinite number of higher curvature corrections to supergravity, one can find solutions to string theory that have large curvatures. Though we have presented the reasons to doubt the existence of these solutions—in particular, the fact that our conclusions rely on approximations that strictly speaking are uncontrolled—we do know that their dual field theories, if the backgrounds exist in the first place, should have 't Hooft couplings that are order unity, as opposed to the infinite 't Hooft coupling of the standard $AdS_5 \times S^5$ limit. Furthermore the gauge theory duals will have minimal (if any) supersymmetry, and may exhibit important phenomena like confinement and asymptotic freedom in a unified framework. Clearly it would be interesting to understand how these backgrounds can contribute to an improved understanding of RHIC physics.

We have clearly emphasized the ability to test string theory as it applies to strong interactions. However, it is extremely important to note that this perspective on string theory is very closely related to string theory as it applies to quantum gravity. Indeed, many formulations of models of particle physics plus quantum gravity that come from string theory rely on AdS/CFT-like components in their setups [117, 118], and particle physicists have for years keyed in on so-called "warped geometries", *i.e.*, anti-de Sitter space, as a means

of explaining the large hierarchy between the electroweak and gravitational energy scales [119]. On the other hand, if we understand AdS/CFT as a duality between a theory that is purely *gravitational*, and another theory that is purely a theory of gluons, then the quantum gravity corrections to supergravity that one might calculate for AdS/CFT purposes are the *exact* same quantum gravity calculations that would be unobservable $\mathcal{O}(10^{-15})$ effects at, say, the LHC. Yet when viewed through the lens of the AdS/CFT correspondence, these corrections become $\mathcal{O}(g_{\rm str}^2 \sim 1/N^2 = 1/9 \simeq 10\%)$ contributions to gauge theory observables, and hence are significantly more likely to be testable. Therefore, although we are primarily concerned with the use of string theory as a description of strong interactions, if we are able to test string theory in that vein, then we are simultaneously testing string theory as it applies to quantum gravity. Clearly, the importance of RHIC to string theory can not be underestimated.

References

[1] N. Arkani-Hamed, S. Dimopoulos, and G. R. Dvali, "The hierarchy problem and new dimensions at a millimeter," *Phys. Lett.* **B429** (1998) 263–272, hep-ph/9803315.

[2] B. Greene, K. Schalm, J. P. van der Schaar, and G. Shiu, "Extracting new physics from the CMB," *ECONF* **C041213** (2004) 0001, astro-ph/0503458.

[3] N. Kaloper, M. Kleban, A. E. Lawrence, and S. Shenker, "Signatures of short distance physics in the cosmic microwave background," *Phys. Rev.* **D66** (2002) 123510, hep-th/0201158.

[4] J. M. Maldacena, "The large N limit of superconformal field theories and supergravity," *Adv. Theor. Math. Phys.* **2** (1998) 231–252, hep-th/9711200.

[5] S. S. Gubser, I. R. Klebanov, and A. M. Polyakov, "Gauge theory correlators from non-critical string theory," *Phys. Lett.* **B428** (1998) 105–114, hep-th/9802109.

[6] E. Witten, "Anti-de Sitter space and holography," *Adv. Theor. Math. Phys.* **2** (1998) 253–291, hep-th/9802150.

[7] O. Aharony, S. S. Gubser, J. M. Maldacena, H. Ooguri, and Y. Oz, "Large N field theories, string theory and gravity," *Phys. Rept.* **323** (2000) 183–386, hep-th/9905111.

[8] B. Muller and J. L. Nagle, "Results from the Relativistic Heavy Ion Collider," nucl-th/0602029.

[9] **PHENIX** Collaboration, K. Adcox *et. al.*, "Formation of dense partonic matter in relativistic nucleus nucleus collisions at RHIC: Experimental evaluation by the PHENIX collaboration," *Nucl. Phys.* **A757** (2005) 184–283, nucl-ex/0410003.

[10] **BRAHMS** Collaboration, I. Arsene *et. al.*, "Quark gluon plasma and color glass condensate at RHIC? The perspective from the BRAHMS experiment," *Nucl. Phys.* **A757** (2005) 1–27, nucl-ex/0410020.

[11] B. B. Back *et. al.*, "The PHOBOS perspective on discoveries at RHIC," *Nucl. Phys.* **A757** (2005) 28–101, nucl-ex/0410022.

[12] **STAR** Collaboration, J. Adams *et. al.*, "Experimental and theoretical challenges in the search for the quark gluon plasma: The STAR collaboration's critical assessment of the evidence from RHIC collisions," *Nucl. Phys.* **A757** (2005) 102–183, nucl-ex/0501009.

[13] The full MPEG can be found at http://www.bnl.gov/RHIC/images/movies/Au-Au_200GeV.mpeg, where it is attributed to the UrQMD group at Frankfurt, see http://www.physik.uni-frankfurt.de/ ~urqmd/.

[14] M. Kaneta and N. Xu, "Centrality dependence of chemical freeze-out in Au + Au collisions at RHIC," nucl-th/0405068.

[15] F. Karsch, "Lattice QCD at high temperature and density," *Lect. Notes Phys.* **583** (2002) 209–249, hep-lat/0106019.

[16] M. Cheng *et. al.*, "The transition temperature in QCD," *Phys. Rev.* **D74** (2006) 054507, hep-lat/0608013.

[17] **BRAHMS** Collaboration, I. G. Bearden *et. al.*, "Nuclear stopping in Au + Au collisions at $\sqrt{s(NN)} = 200$GeV," *Phys. Rev. Lett.* **93** (2004) 102301, nucl-ex/0312023.

[18] W. Zajc, private communication.

[19] M. D. Baker, "The latest Results from PHOBOS: Systematics of Charged Particle Production through $\sqrt{s_{NN}} = 200\,\mathrm{GeV}$," 2001. PowerPoint talk, available at http://www.phobos.bnl.gov/Presentations/paris01/.

[20] G. 't Hooft, "A Planar Diagram Theory for Strong Interactions," *Nucl. Phys.* **B72** (1974) 461.

[21] J. Polchinski, "Dirichlet-Branes and Ramond-Ramond Charges," *Phys. Rev. Lett.* **75** (1995) 4724–4727, hep-th/9510017.

[22] G. T. Horowitz and A. Strominger, "Black strings and P-branes," *Nucl. Phys.* **B360** (1991) 197–209.

[23] I. R. Klebanov, "TASI lectures: Introduction to the AdS/CFT correspondence," hep-th/0009139.

[24] J. Polchinski, "String theory. Vol. 2: Superstring theory and beyond,". Cambridge, UK: Univ. Pr. (1998) 531 p.

[25] S. S. Gubser, I. R. Klebanov, and A. W. Peet, "Entropy and Temperature of Black 3-Branes," *Phys. Rev.* **D54** (1996) 3915–3919, hep-th/9602135.

[26] S. S. Gubser, "Einstein manifolds and conformal field theories," *Phys. Rev.* **D59** (1999) 025006, hep-th/9807164.

[27] C. P. Herzog, A. Karch, P. Kovtun, C. Kozcaz, and L. G. Yaffe, "Energy loss of a heavy quark moving through N = 4 supersymmetric Yang-Mills plasma," hep-th/0605158.

[28] S. S. Gubser, "Drag force in AdS/CFT," hep-th/0605182.

[29] H. Liu, K. Rajagopal, and U. A. Wiedemann, "Calculating the jet quenching parameter from AdS/CFT," hep-ph/0605178.

[30] J. Casalderrey-Solana and D. Teaney, "Heavy quark diffusion in strongly coupled N = 4 Yang Mills," *Phys. Rev.* **D74** (2006) 085012, hep-ph/0605199.

[31] S.-J. Sin and I. Zahed, "Holography of radiation and jet quenching," *Phys. Lett.* **B608** (2005) 265–273, hep-th/0407215.

[32] A. Buchel, "On jet quenching parameters in strongly coupled non- conformal gauge theories," hep-th/0605178.

[33] C. P. Herzog, "Energy Loss of Heavy Quarks from Asymptotically AdS Geometries," hep-th/0605191.

[34] E. Caceres and A. Guijosa, "Drag Force in Charged N=4 SYM Plasma," hep-th/0605235.

[35] J. J. Friess, S. S. Gubser, and G. Michalogiorgakis, "Dissipation from a heavy quark moving through N = 4 super- Yang-Mills plasma," hep-th/0605292.

[36] S.-J. Sin and I. Zahed, "Ampere's Law and Energy Loss in AdS/CFT Duality," hep-ph/0606049.

[37] Y.-h. Gao, W.-s. Xu, and D.-f. Zeng, "Wake of color fileds in charged N = 4 SYM plasmas," hep-th/0606266.

[38] N. Armesto, J. D. Edelstein, and J. Mas, "Jet quenching at finite 't Hooft coupling and chemical potential from AdS/CFT," hep-ph/0606245.

[39] K. Peeters, J. Sonnenschein, and M. Zamaklar, "Holographic melting and related properties of mesons in a quark gluon plasma," hep-th/0606195.

[40] S. D. Avramis and K. Sfetsos, "Supergravity and the jet quenching parameter in the presence of R-charge densities," hep-th/0606190.

[41] F.-L. Lin and T. Matsuo, "Jet quenching parameter in medium with chemical potential from AdS/CFT," hep-th/0606136.

[42] E. Caceres and A. Guijosa, "On drag forces and jet quenching in strongly coupled plasmas," hep-th/0606134.

[43] J. F. Vazquez-Poritz, "Enhancing the jet quenching parameter from marginal deformations," hep-th/0605296.

[44] J. J. Friess, S. S. Gubser, G. Michalogiorgakis, and S. S. Pufu, "The stress tensor of a quark moving through N = 4 thermal plasma," hep-th/0607022.

[45] V. Balasubramanian and P. Kraus, "A stress tensor for anti-de Sitter gravity," *Commun. Math. Phys.* **208** (1999) 413–428, hep-th/9902121.

[46] D. Teaney, "Finite temperature spectral densities of momentum and R- charge correlators in N = 4 Yang Mills theory," hep-ph/0602044.

[47] U. H. Danielsson, E. Keski-Vakkuri, and M. Kruczenski, "Vacua, propagators, and holographic probes in AdS/CFT," *JHEP* **01** (1999) 002, hep-th/9812007.

[48] http://wwwphy.princeton.edu/~ssgubser/papers/stress/index.html.

[49] B. Jacak, private communication.

[50] **STAR** Collaboration, F. Wang, "Measurement of jet modification at RHIC," *J. Phys.* **G30** (2004) S1299–S1304, nucl-ex/0404010.

[51] **PHENIX** Collaboration, S. S. Adler *et. al.*, "Modifications to di-jet hadron pair correlations in Au + Au collisions at $\sqrt{s(NN)} = 200$GeV," nucl-ex/0507004.

[52] J. Casalderrey-Solana, E. V. Shuryak, and D. Teaney, "Conical flow induced by quenched QCD jets," *J. Phys. Conf. Ser.* **27** (2005) 22–31, hep-ph/0411315.

[53] I. Vitev, "Large angle hadron correlations from medium-induced gluon radiation," *Phys. Lett.* **B630** (2005) 78–84, hep-ph/0501255.

[54] A. Majumder and X.-N. Wang, "LPM interference and Cherenkov-like gluon bremsstrahlung in dense matter," *Phys. Rev.* **C73** (2006) 051901, nucl-th/0507062.

[55] V. Koch, A. Majumder, and X.-N. Wang, "Cherenkov radiation from jets in heavy-ion collisions," *Phys. Rev. Lett.* **96** (2006) 172302, `nucl-th/0507063`.

[56] A. K. Chaudhuri and U. Heinz, "Effect of jet quenching on the hydrodynamical evolution of QGP," `nucl-th/0503028`.

[57] J. Ruppert and B. Muller, "Waking the colored plasma," *Phys. Lett.* **B618** (2005) 123–130, `hep-ph/0503158`.

[58] J. J. Friess and S. S. Gubser, "Non-linear sigma models with anti-de Sitter target spaces," *Nucl. Phys.* **B750** (2006) 111–141, `hep-th/0512355`.

[59] J. Polchinski, "String theory. Vol. 1: An introduction to the bosonic string,". Cambridge, UK: Univ. Pr. (1998) 402 p.

[60] D. Friedan, "Nonlinear Models in $2+\epsilon$ Dimensions," *Phys. Rev. Lett.* **45** (1980) 1057.

[61] F. Wegner, "Four loop order β function of nonlinear sigma models in symmetric spaces," *Nucl. Phys.* **B316** (1989) 663–678.

[62] I. Jack, D. R. T. Jones, and N. Mohammedi, "A four loop calculation of the metric beta function for the bosonic sigma model and the string effective action," *Nucl. Phys.* **B322** (1989) 431.

[63] I. Jack, D. R. T. Jones, and N. Mohammedi, "The four loop string effective action from the bosonic sigma model," *Nucl. Phys.* **B332** (1990) 333.

[64] A. Duncan, M. Niedermaier, and E. Seiler, "Vacuum orbit and spontaneous symmetry breaking in hyperbolic sigma models," `hep-th/0405163`.

[65] E. Brezin and J. Zinn-Justin, "Spontaneous breakdown of continuous symmetries near two-dimensions," *Phys. Rev.* **B14** (1976) 3110.

[66] J. A. Gracey, "On the Beta function for sigma models with N=1 supersymmetry," *Phys. Lett.* **B246** (1990) 114–118.

[67] J. A. Gracey, "Critical exponents for the supersymmetric sigma model," *J. Phys.* **A23** (1990) 2183–2194.

[68] D. Friedan, "Non-linear models in $2+\epsilon$ dimensions," *Phys. Rev. Lett.* **45** (1980) 1057.

[69] L. Alvarez-Gaume, D. Z. Freedman, and S. Mukhi, "The background field method and the ultraviolet structure of the supersymmetric nonlinear sigma model," *Ann. Phys.* **134** (1981) 85.

[70] D. J. Gross and E. Witten, "Superstring modifications of Einstein's equations," *Nucl. Phys.* **B277** (1986) 1.

[71] M. T. Grisaru, A. E. M. van de Ven, and D. Zanon, "Four loop divergences for the $\mathcal{N}=1$ supersymmetric nonlinear sigma models in two-dimensions," *Nucl. Phys.* **B277** (1986) 409.

[72] M. T. Grisaru, A. E. M. van de Ven, and D. Zanon, "Four loop β function for the $N=1$ and $N=2$ supersymmetric nonlinear sigma model in two-dimensions," *Phys. Lett.* **B173** (1986) 423.

[73] C. G. Callan, E. J. Martinec, M. J. Perry, and D. Friedan, "String in background fields," *Nucl. Phys.* **B262** (1985) 593.

[74] A. N. Vasiliev, Y. M. Pismak, and Y. R. Khonkonen, "1/N expansion: Calculation of the exponents η and ν in the order $1/N^2$ for arbitrary number of dimensions," *Theor. Math. Phys.* **47** (1981) 465–475.

[75] A. N. Vasiliev, M. Pismak, Yu, and Y. R. Khonkonen, "Simple method of calculating the critical indices in the $1/N$ expansion," *Theor. Math. Phys.* **46** (1981) 104–113.

[76] G. Michalogiorgakis and S. S. Gubser, "Heterotic non-linear sigma models with anti-de Sitter target spaces," `hep-th/0605102`.

[77] D. J. Gross and J. H. Sloan, "The quartic effective action for the heterotic string," *Nucl. Phys.* **B291** (1987) 41.

[78] P. S. Howe and P. C. West, "The complete $\mathcal{N} = 2$, $d = 10$ supergravity," *Nucl. Phys.* **B238** (1984) 181.

[79] A. N. Vasilev, "The field theoretic renormalization group in critical behavior theory and stochastic dynamics,". Boca Raton, USA: Chapman & Hall/CRC (2004) 681 p.

[80] Y. Okabe and M. Oku, "1/N expansion up to order $1/N^2$. 3. Critical exponents γ and ν for $d = 3$,".

[81] T. Banks and A. Zaks, "On the phase structure of vector-like gauge theories with massless fermions," *Nucl. Phys.* **B196** (1982) 189.

[82] A. A. Tseytlin, "Conditions of Weyl invariance of two-dimensional sigma model from equations of stationarity of 'central charge' action," *Phys. Lett.* **B194** (1987) 63.

[83] J. A. Gracey, "Probing the supersymmetric O(N) sigma model to $\mathcal{O}(1/N^2)$: Critical exponent η," *Nucl. Phys.* **B348** (1991) 737–756.

[84] J. A. Gracey, "Probing the supersymmetric O(N) sigma model to $\mathcal{O}(1/N^2)$: Critical exponent ν," *Nucl. Phys.* **B352** (1991) 183–214.

[85] A. Y. Morozov, A. M. Perelomov, and M. A. Shifman, "Exact Gell-Mann-Low function of supersymmetric Kahler sigma models," *Nucl. Phys.* **B248** (1984) 279.

[86] V. A. Novikov, M. A. Shifman, A. I. Vainshtein, and V. I. Zakharov, "Instantons and exact Gell-Mann-Low function of supersymmetric $O(3)$ sigma model," *Phys. Lett.* **B139** (1984) 389.

[87] E. Silverstein, "(A)dS backgrounds from asymmetric orientifolds," `hep-th/0106209`.

[88] A. Maloney, E. Silverstein, and A. Strominger, "De Sitter space in noncritical string theory," `hep-th/0205316`.

[89] S. P. de Alwis, J. Polchinski, and R. Schimmrigk, "Heterotic strings with tree level cosmological constant," *Phys. Lett.* **B218** (1989) 449.

[90] R. C. Myers, "New dimensions for old strings," *Phys. Lett.* **B199** (1987) 371.

[91] J. Callan, Curtis G., J. A. Harvey, and A. Strominger, "Supersymmetric string solitons," `hep-th/9112030`.

[92] N. Berkovits, C. Vafa, and E. Witten, "Conformal field theory of AdS background with Ramond-Ramond flux," *JHEP* **03** (1999) 018, `hep-th/9902098`.

[93] A. M. Polyakov, "Conformal fixed points of unidentified gauge theories," *Mod. Phys. Lett.* **A19** (2004) 1649–1660, `hep-th/0405106`.

[94] A. M. Polyakov, "Supermagnets and sigma models," `hep-th/0512310`.

[95] S. S. Gubser, "Dilaton-driven confinement," `hep-th/9902155`.

[96] P. Candelas, G. T. Horowitz, A. Strominger, and E. Witten, "Vacuum configurations for superstrings," *Nucl. Phys.* **B258** (1985) 46–74.

[97] G. Mostow, "Strong Rigidity of Locally Symmetric Spaces," *Ann. Math. Stud.78* (1973).

[98] A. Kehagias and J. G. Russo, "Hyperbolic spaces in string and M-theory," *JHEP* **07** (2000) 027, `hep-th/0003281`.

[99] S. Nasri, P. J. Silva, G. D. Starkman, and M. Trodden, "Radion stabilization in compact hyperbolic extra dimensions," *Phys. Rev.* **D66** (2002) 045029, `hep-th/0201063`.

[100] M. Trodden, "Diluting gravity with compact hyperboloids," `hep-th/0010032`.

[101] N. Kaloper, J. March-Russell, G. D. Starkman, and M. Trodden, "Compact hyperbolic extra dimensions: Branes, Kaluza-Klein modes and cosmology," *Phys. Rev. Lett.* **85** (2000) 928–931, `hep-ph/0002001`.

[102] G. D. Starkman, D. Stojkovic, and M. Trodden, "Large extra dimensions and cosmological problems," *Phys. Rev.* **D63** (2001) 103511, hep-th/0012226.

[103] G. D. Starkman, D. Stojkovic, and M. Trodden, "Homogeneity, flatness and 'large' extra dimensions," *Phys. Rev. Lett.* **87** (2001) 231303, hep-th/0106143.

[104] P. K. Townsend and M. N. R. Wohlfarth, "Accelerating cosmologies from compactification," *Phys. Rev. Lett.* **91** (2003) 061302, hep-th/0303097.

[105] R. Emparan and J. Garriga, "A note on accelerating cosmologies from compactifications and S-branes," *JHEP* **05** (2003) 028, hep-th/0304124.

[106] C.-M. Chen, P.-M. Ho, I. P. Neupane, N. Ohta, and J. E. Wang, "Hyperbolic space cosmologies," *JHEP* **10** (2003) 058, hep-th/0306291.

[107] D. A. Demir and M. Shifman, "Flavor dynamics with conformal matter and gauge theories on compact hyperbolic manifolds in extra dimensions," *Phys. Rev.* **D65** (2002) 104002, hep-ph/0112090.

[108] S. M. Carroll, J. Geddes, M. B. Hoffman, and R. M. Wald, "Classical stabilization of homogeneous extra dimensions," *Phys. Rev.* **D66** (2002) 024036, hep-th/0110149.

[109] R. Bousso and J. Polchinski, "Quantization of four-form fluxes and dynamical neutralization of the cosmological constant," *JHEP* **06** (2000) 006, hep-th/0004134.

[110] S. R. Coleman, "There are no Goldstone bosons in two-dimensions," *Commun. Math. Phys.* **31** (1973) 259–264.

[111] N. D. Mermin and H. Wagner, "Absence of ferromagnetism or antiferromagnetism in one- dimensional or two-dimensional isotropic Heisenberg models," *Phys. Rev. Lett.* **17** (1966) 1133–1136.

[112] M. C. Bento, "Maximally symmetric cosmological solutions of type II superstrings," gr-qc/9902058.

[113] M. B. Green and M. Gutperle, "Effects of D-instantons," *Nucl. Phys.* **B498** (1997) 195–227, hep-th/9701093.

[114] I. Antoniadis, B. Pioline, and T. R. Taylor, "Calculable $e^{-1/\Lambda}$ effects," *Nucl. Phys.* **B512** (1998) 61–78, hep-th/9707222.

[115] G. Russo, Jorge, "An ansatz for a non-perturbative four-graviton amplitude in type IIB superstring theory," *Phys. Lett.* **B417** (1998) 253–258, hep-th/9707241.

[116] A. M. Polyakov and P. B. Wiegmann, "Theory of nonabelian Goldstone bosons in two dimensions," *Phys. Lett.* **B131** (1983) 121–126.

[117] M. Buican, D. Malyshev, D. R. Morrison, M. Wijnholt, and H. Verlinde, "D-branes at singularities, compactification, and hypercharge," hep-th/0610007.

[118] H. Verlinde and M. Wijnholt, "Building the standard model on a D3-brane," hep-th/0508089.

[119] L. Randall and R. Sundrum, "A large mass hierarchy from a small extra dimension," *Phys. Rev. Lett.* **83** (1999) 3370–3373, hep-ph/9905221.